Calixarene-based Langmuir monolayers: from crystallization templates to metal organic networks

Inauguraldissertation

zur

Erlangung der Würde eines Doktors der Philosophie

vorgelegt der

Philosophisch-Naturwissenschaftlichen Fakultät

der Universität Basel

von

Ludovico Giuseppe Tulli

aus Italien

Basel 2016

Genehmigt von der Philosophisch-Naturwissenschaftlichen Fakultät
auf Antrag von

Prof. Dr. Wolfgang Meier
Prof. Dr. Patrick Shahgaldian
Prof. Dr. Scott John Dalgarno

Basel, den 8. Dezember 2015

Prof. Dr. Jörg Schibler
Dekan

TABLE OF CONTENT

Abbreviations

AFM	atomic force microscopy
API	active pharmaceutical ingredient
ASU	asymmetric unit
ATR	attenuated total reflectance
BAM	Brewster angle microscopy
CA	contact angle
CoTCPP	5,10,15,20-tetrakis(4-carboxyphenyl)porphirinato-cobalt(II)
DNB	dinitrobenzene
DRC	dendron-rod-coil
FDA	food and drug administration
FWHM	full width at half maximum
GBP	gabapentin
GIXD	grazing incidence X-ray diffraction
GQ	guanosine quadruplex
IR	infrared spectroscopy
LB	Langmuir-Blodgett
LMWG	low-molecular-weight gelator
LS	Langmuir-Schaefer
MEK	methyl ethyl ketone
MOF	metal organic framework

NBS	N-bromosuccinimide
NMP	N-methyl-2-pyrrolidone
NN	nearest neighbor
NNN	next nearest neighbor
OTS	octadecyltrichlorosilane
PA	peptide-based amphiphile
PDMS-*b*-PMOXA	poly(dimethylsiloxane)-*block*-poly(2-methyloxazoline)
PYR	pyrene
R	reflectivity
R_F	Fresnel reflectivity
SAM	self-assembled monolayer
S_N2	substitution nucleophilic (bi-molecular)
TFA	trifluoroacetic acid
XNTRF	X-ray near-total-reflection fluorescence
XRR	X-ray reflectivity

Abstract

Molecular self-assembly plays a pivotal role in biological processes and living organisms can be considered as the result of the self-assembly of discrete molecular building blocks into sophisticated functional structures. Biology provides countless examples of complex and functional hierarchical self-assembled structures ranging from protein and nucleic acid biosynthesis to biological membranes self-assembly. Although Nature may produce such structures with an extreme efficieny, man-made chemical strategies to produce large covalent architectures are typically more complex and tedious. Due to the difficulty to precisely control the formation of large macromolecular architecture through covalent synthetic strategies, the self-assembly approach has been extensively exploited for the creation of supramolecular entities.

Amphiphiles are compounds able to self-assemble in myriad supramolecular structures such as micelles, vesicles, nanosheets, nanorods, nanotubes and nanofibers, to name but a few. The shape of the resulting supramolecular assembly is dependent on the structure of the amphiphilic building block and type of solvent. Among all kinds of natural and synthetic amphiphiles, macrocyclic amphiphiles are of particular interest due to the possibility to conveniently control the hydrophilic/lipophilic balance of the final amphiphilic structure. The basket-like rigid conformation of calix[4]arenes, and the possibility to selectively functionalize both the upper and lower rim, make these molecules attractive building blocks for the design of amphiphilic compounds.

Amphiphilic calix[4]arenes that are essentially insoluble in water self-assemble as monomolecular films at the air-water interface, forming Langmuir monolayers, where the aliphatic chains point into air while the polar functions are immerged into the subphase. Langmuir monolayers of amphiphilic calix[4]arene derivatives have been demonstrated to interact with a wide range of solutes, ranging from ions to macromolecules. In addition to this,

calix[4]arene-based monolayers have been shown to induce the interfacial crystallization of inorganic and organic solids. The polar heads of the macrocycles act as recognition units for the interfacial nucleation of the to-be-crystallized molecules. Electrostatic interactions, along with geometrical complementarity between the macrocycles polar functions and the solute are the determining factors for the interfacial crystal growth. In this thesis, the ability of Langmuir monolayers of a *p*-carboxycalix[4]arene derivative to act as templates for the crystallization of gabapentin (GBP), an active pharmaceutical ingredient used to relieve neuropathic pain, with a control over its polymorphism is reported.

The suitable chemical modification of the upper and lower rim of calix[4]arenes allows producing stable amphiphilic macrocycles able to form stable Langmuir monolayers at the air-water interface with strong affinities towards ions. The affinity of calix[4]arene-based Langmuir monolayers towards ions is mainly owing to the presence of a cavity that allows for the encapsulation of the ions, coupled with multiple polar ligating functions at the *p*-positions that strongly interact with the solute. In this thesis, the recognition properties of Langmuir monolayers of a series of *p*-carboxy- and *p*-aminocalix[4]arene derivatives towards strong, i.e. $CuCl_2$, $CoCl_2$, $NiCl_2$ and $MnCl_2$, and weak, i.e. $HgCl_2$, electrolytes are reported. The effect of the inorganic compounds on the self-assembly properties of the calix[4]arene-based Langmuir monolayers is investigated by means of surface pressure-area compression isotherms, Brewster angle microscopy (BAM) and synchrotron-based X-ray diffraction techniques. Notably, it has been demonstrated that the structure of the macrocycle has a crucial effect on its interfacial organization. Upon interaction of a long chain, i.e. C_{12}, *p*-carboxycalix[4]arene derivative with Cu^{2+} ions at the air-water interface, the corresponding calix[4]arene-based monolayer is mainly amorphous. On the other hand, Langmuir monolayers of the short chain (C_3), structural analogue on aqueous Cu^{2+} ions subphases possess significantly large and highly ordered structures. It is assumed that the interfacial self-assembly of the long chain *p*-carboxycalix[4]arene derivative is mainly driven by van der Waals interactions among the

aliphatic chains, which contribute to the partial disordered monolayer structure. On the contrary, the self-assembly of the short chain *p*-carboxycalix[4]arene derivative is driven by π-π interactions among aromatic rings of neighboring amphiphiles, which contribute to the highly ordered structure of the monomolecular film.

1 Introduction

1.1 Supramolecular chemistry

Supramolecular chemistry has been defined as "the chemistry beyond the molecule".[1] Although the term supramolecular chemistry was coined by Jean-Marie Lehn in 1978,[2] early work in the field was carried out by Charles Pedersen in the late 1960s.[3] The Nobel Prize in Chemistry was awarded to Jean-Marie Lehn, Charles J. Pedersen and Donald J. Cram in 1987 for their pioneering contributions to supramolecular chemistry.

First reports in the field of supramolecular chemistry describe the formation of discrete two components, i.e. the host and the guest, complexes through noncovalent interactions. The host is typically a large molecule that possesses a sizeable cavity, e.g. synthetic macrocycles. The guest may be an ion or a more complex molecule. As a matter of fact, the host-guest concept is much older than the work of Pedersen as it traces back to the second half of the 18th century. In 1778, the chemist Joseph Priestley prepared the first clathrate hydrate, also known as "anomalous ice".[4]

Modern host-guest chemistry is based on the core concept of the lock-and-key mechanism formulated by Emil Fischer in 1894.[5] The lock-and-key mechanism was initially developed to explain the binding of enzymes towards their substrates in a selective fashion. This high selectivity of binding was attributed to a complementarity in shape and size between hosts and guests, where the binding site of the receptor is well pre-organized to specifically recognize the substrate (Figure 1.1).

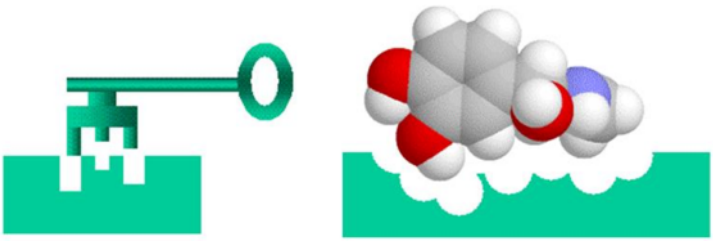

Figure 1.1. Graphical representation of the lock-and-key mechanism. Enzyme binding to the substrate is analogous to a key fitting into a lock.

In 1958, the lock-and-key mechanism was overcome by the induced-fit mechanism.[1] The induced-fit mechanism, developed by Koshland, postulates that the substrate, interacting with the enzyme, causes a conformational change of the structure of the enzyme binding site. The induced-fit mechanism, along with the concept of biological receptors introduced by Paul Ehrlich in 1906 and the theory of coordination chemistry by Alfred Werner in 1893, laid the foundation of modern supramolecular chemistry.[6] During the past 5 decades, supramolecular chemistry evolved from the mere concept of host-guest chemistry to the formation of supermolecules from complementary building blocks in which there is no host and guest. In 2002, Jean-Marie Lehn stated that "supramolecular chemistry aims at developing highly complex chemical systems from components interacting by noncovalent intermolecular forces".[7] The building blocks that take part in the formation of supramolecules are not restricted to the host-guest types. Large aggregates can be built from their smaller building blocks that show complementarity, without the presence of a binding site for the encapsulation of a guest. This approach allows for the construction of more complex and sophisticated supramolecular assemblies and embraces all aspects of self-assembly. For example, large supramolecular coordination networks with a variety of geometries can be conveniently constructed in one, two and three dimensions by noncovalent interactions between metal ions, that function as nodes and organic ligands as bridges.

1.2 Molecular self-assembly

Self-assembly is the spontaneous and reversible organization of complementary building blocks into supramolecular entities.[8,9] The shape and size of the building blocks as well as types of noncovalent interactions have crucial roles in the order and complexity of the final supramolecular structure.[10] Nature provides myriad examples of discrete and functional supramolecular assemblies.[11] For example, in the tobacco mosaic virus, more than 2000 identical proteins self-assemble in the form of a cylinder around a single strand of RNA to yield a ca. 300 nm long rod structure.[12] The high level of complexity showed by various supramolecular structures is hardly accessible through traditional synthetic strategies. Therefore, in the last 3 decades, the noncovalent approach played a central role in the construction of nano- and macro-scale structures with a precise control over their shape and size.[13]

Self-assembly encompasses different levels of complexity, from dimerization of two small building blocks to more sophisticated and larger supramolecules. Rebek produced tennis ball-shaped structures as example of dimeric assemblies (Figure 1.2).[14-16] Two identical self-complementary building blocks formed by two glycouril units and separated by an aromatic spacer self-assemble to generate dimeric structures. The intrinsic curvature of the glycouril derivatives allows for the molecular recognition event with the two units held together by eight pairs of hydrogen bonds.[17] Larger spherical assemblies have been produced by Atwood through the assembly of six calix[4]resorcinarenes and eight water molecules (Figure 1.2). This chiral spherical supramolecule possesses an internal volume of ca. 1375 $Å^3$ and the building blocks are held together by 60 hydrogen bonds.[18,19] Examples of functional supramolecular assemblies are well represented by g-quadruplexes (GQs). GQs are planar structures formed by four self-complementary guanosine derivatives that self-assemble through Hoogsten base pairing. These tetrameric structures further self-assemble into larger assemblies in the presence of metal cations.[20,21] However, the substituents attached to the guanosine units typically prevent the

assembly of structures larger than the octamer. A 8-aryl-2'-deoxyguanosine derivative developed by Rivera compensates the unfavorable steric repulsion and allows for the stabilization of the supramolecule in the form of a dodecamer (Figure 1.2).[22] The control over the structure and dimension of self-assembled entities remains one of the biggest challenges in supramolecular chemistry. An elegant example of control over molecular self-assembly has been reported by Stupp. The synthesized modular building block named dendron-rod-coil (DRC) consists of three distinct parts: a dendron-like moiety, a biphenyl unit as spacer and a branched 2-octyl-dodecyl coil. DRC self-assembles into uniform and well-defined nanoribbons via hydrogen bonds and π-π interactions (Figure 1.2). Minor chemical modifications of the DRC dendritic and biphenyl moieties allows to finely tune its self-assembly properties while the coil unit considerably affects its solubility.[23,24]

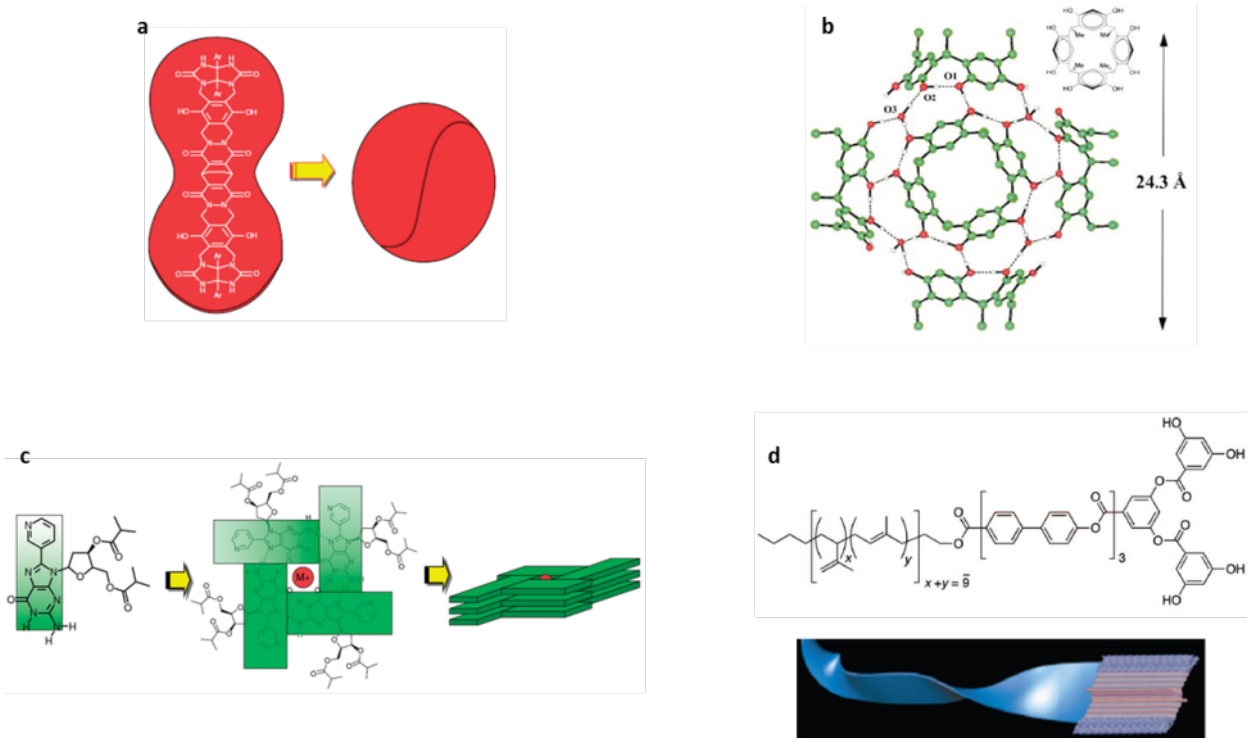

Figure 1.2. Examples of molecular self-assemblies. **a**: Rebek's tennis ball-shaped dimeric structure (Reproduced with permission from ref. 10, Copyright 2012, John Wiley & Sons, Ltd.); **b**: Atwood's chiral

spherical molecular assembly (Reproduced with permission from ref. 19, Copyright 1997, Nature Publishing Group); **c**: Guanine-based planar tetramer self-assembly into dodecamer G-quadruplex (Reproduced with permission from ref. 22, Copyright 2009, American Chemical Society); **d**: Chemical structure of DRC and graphical representation of its nanoribbon structure (Reproduced with permission from ref. 23, Copyright 2008, American Chemical Society).

1.3 Amphiphilic self-assembly

Amphiphiles are compounds that consist of at least one hydrophilic part covalently linked to at least one hydrophobic part. The use of amphiphiles traces back to 2200 B.C. when Babylonians regularly made soap-like materials by boiling fats with ashes.[25] According to the *Ebers Papyrus*, a medical document from ca. 1500 B.C., Egyptians used to commonly bath in a mixture of vegetable and animal oils and alkaline salts.[26] Nowadays, the understanding of self-assembly behavior of amphiphiles is of particular interest due to the pivotal role of amphiphilic self-assembly in biology, e.g. lipid bilayers formation in cell membranes, and in chemistry, e.g. micelles and vesicles formation.[27]

Amphiphiles are powerful building blocks for the construction of supramolecular assemblies. The size and the shape of the supramolecular assembly are dependent on the geometrical shape of the surfactants building blocks. For example, amphiphiles with a cone-like shape, where the cross-section of the headgroup is larger than that of the tail, are amenable to self-assemble into micelles. Kellermann et al. produced micelles from cone-like shaped calix[4]arenes bearing dendritic moieties as polar functions.[28] It has been demonstrated that the micelle consists of seven molecules of calix[4]arene; this study represents the first example of micelle structural characterization on the molecular scale. When the cross section of the surfactant tail is bigger than that of the headgroup, reversed micelles are formed. Surfactants with a cylindrical or rod shape, where the cross section of the headgroup is similar to that of the aliphatic chain, preferably self-assemble into bilayer structures, cf. Figure 1.3.[29]

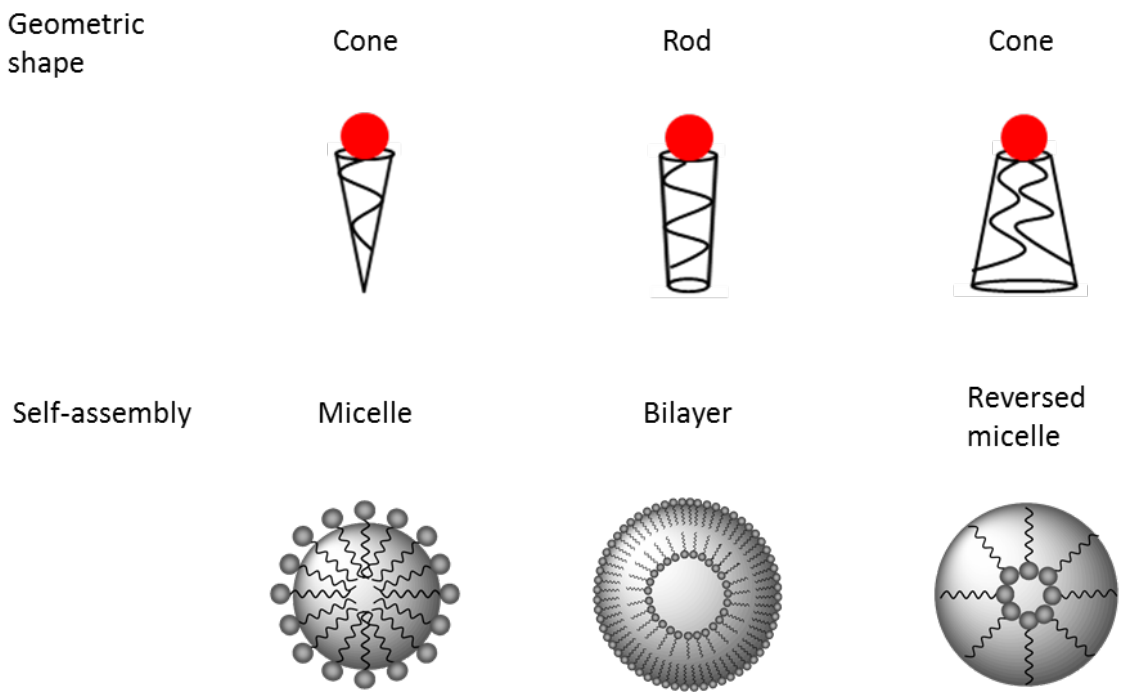

Figure 1.3. Representation of the relationship between the shape of the supramolecular assembly and the structure of the surfactant (Partially reproduced with permission from ref. 29, Copyright 2012, John Wiley & Sons, Ltd.).

Natural glycero-phospholipids, a class of amphiphiles that consists of one polar head covalently linked through a glycerol molecule to two hydrophobic chains are a major component of cell membranes. In vitro, phospholipids form bilayer structures that are similar to those that constitute cell membranes.

The self-assembly of amphiphiles generates supermolecules that may possess high levels of complexity. Peptide-based amphiphiles (PAs) are oligo-peptides functionalized with hydrophobic alkyl chains that can self-assemble in a variety of mono-dimensional structures.[30-33] Stupp demonstrated that subtle modifications in the structure of two PAs composed of a single surfactant molecule with a short peptide unit as a spacer drastically influence their self-assembly process. Molecules **1** and **2** have highly similar chemical structures and only differ for

two methyl groups attached to the end of one alkyl chain of **2**. Atomic force microscopy (AFM) showed that, while **1** self-assembles in the form of cylindrical fibers, the aggregation of **2** results in left-handed helices, therefore suggesting that the bulkier substituents at the terminus of the alkyl unit cause the twisting of the cylindrical assemblies of **2** (Figure 1.4).[34] The amphiphiles **1** and **2** show chirality. Despite the fact that the amphiphiles are chiral, the authors could not establish a general link between molecular chirality and the observed helical supermolecule.

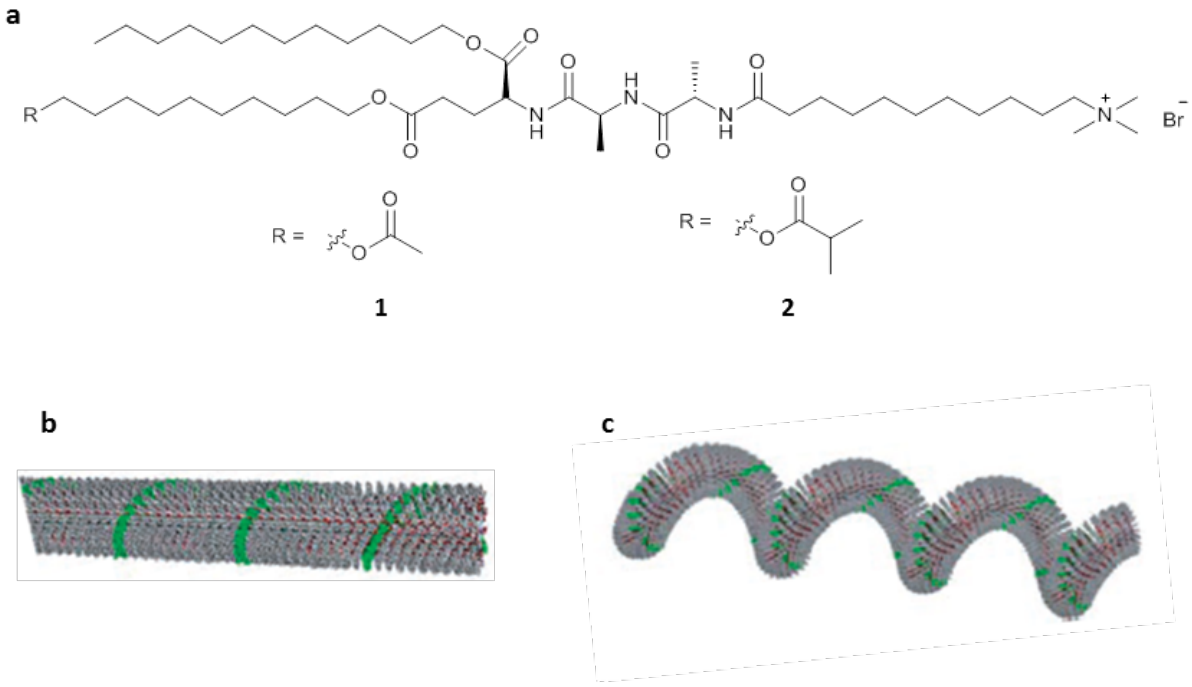

Figure 1.4. Chemical structures of **1** and **2** (**a**) and graphical representations of **1** shaped as a cylindrical nanofiber (**b**) and **2** self-assembled in a left-handed helix (**c**) [Reproduced with permission from ref. 34, Copyright 2007, John Wiley & Sons, Inc.].

Meier reported on the synthesis of superamphiphiles.[35] The authors synthesized amphiphilic poly(dimethylsiloxane)-*block*-poly(2-methyloxazoline) (PDMS-*b*-PMOXA) diblock copolymers functionalized with hydroxyl or piperazyl functions at the hydrophilic terminus. PDMS-*b*-PMOXA diblock copolymers were demonstrated to self-assemble in the form of polymersomes with

surface-exposed amino groups. The polymersomes, after covalent attachment to biomolecules such as antibodies, showed specific targeting towards biotin-patterned surfaces and breast cancer cells.

Giant surfactants, produced by linking a polymeric chain to a specific site of a protein or enzyme, are building blocks that self-assemble into highly sophisticated structures. The predefined protein-polymer ratio and the known position of the binding site allow discriminating giant amphiphiles from other protein-polymer conjugates.[36-38] The development of such large biohybrid supermolecules may open the way for the design of functional self-assembled systems that possess high levels of structural complexity.[39] Nolte produced giant amphiphiles through the binding of two molecules of monobiotinylated polystyrene, self-assembled as Langmuir monolayers at the air-water interface, to streptavidin. Compression isotherms, BAM and AFM measurements revealed that one side of streptavidin binds two biotinylated polymers, therefore proving the 2D noncovalent synthesis of giant surfactants.[40]

An emerging class of amphiphilic molecules is represented by supra-amphiphiles; the target amphiphile is assembled through noncovalent interactions.[41-44] The dynamic nature of such interactions facilitates the introduction of functional moieties in the amphiphiles and, as a consequence, the construction of highly functional supramolecular assemblies, e.g. external-stimuli responsive materials. In addition to this, the rational design of supra-amphiphiles allows for their hierarchical self-assembly into highly ordered structures.[45] For example, Zhang reported on the synthesis of a supra-amphiphile driven by charge transfer between an electron-rich pyrene derivative (PYR) and two electron-poor dinitrobenzene moieties of a linker unit (DNB). While PYR self-assembles in the form of tubular structures, the supra-amphiphile organizes into vesicles (Figure 1.5).[46]

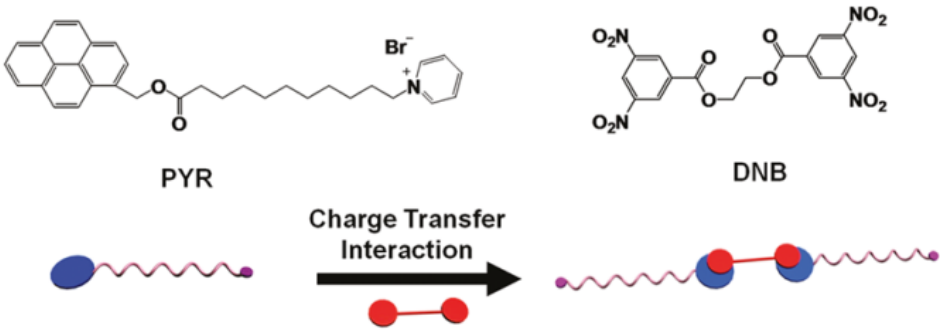

Figure 1.5. Formation of the DNB-PYR supra-amphiphile driven by charge-transfer interactions (Reproduced with permission from ref. 46, Copyright 2008, John Wiley & Sons, Inc.).

1.4 Amphiphilic calixarenes

Calixarenes are cyclic oligomers produced by the condensation of *p-tert*-butylphenol with formaldehyde. Gutsche coined the name calixarene in 1978; it derives from the Greek word *calix* that means chalice, and *arene*, which refers to the presence of aryl moieties in the molecular skeleton.[47,48] Gutsche chose this name because of the similarity of the structure of the cyclic tetramer, when all of the aryl moieties are oriented in the same direction, with the shape of a Greek chalice (Figure 1.6). The same name has been also extended to cyclic oligomers larger than the tetramer, where a bracketed number between the terms calix and arene specifies the number of aryl moieties.

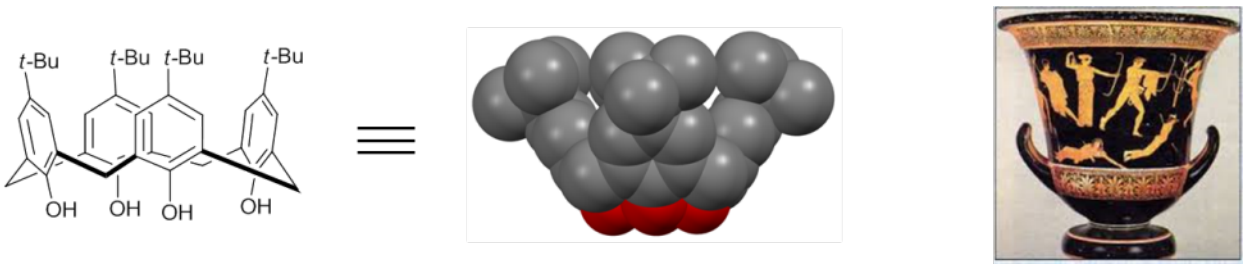

Figure 1.6. Chemical structure and space-filling model of *p-tert*-butylcalix[4]arene and its similarity with the Greek chalice.

Calixarenes are typically produced by the one-step base-catalyzed reaction of *p-tert*-butylphenol and formaldehyde. The size of the macrocycle is dependent on the type of base and reaction temperature. While the cyclic tetramer and octamer are formed in the presence of NaOH as base, the highest yield of the cyclic hexamer is obtained by using KOH, thus indicating a templating effect of the cations during the cyclization step.[47] Unlike the calix[6]arene and calix[8]arene, the cyclic tetramer shows only four main conformations, i.e. cone, partial cone, 1,2 and 1,3 alternate. The conformational interconversion of the calix[4]arene-25,26,27,28-tetrol can occur by the rotation of the OH groups through the macrocyclic ring. The tetramethoxy- (R = CH_3) and tetraethoxy- (R = CH_2CH_3) calix[4]arenes are also conformationally

mobile while bulkier alkyl groups hinder the interconversion. Therefore, the conformational behavior of calix[4]arenes can be controlled by the size and length of the substituents introduced at the lower rim.[49-52]

Calix[4]arenes in the cone conformation are promising building blocks for the synthesis of amphiphilic molecules. A large variety of suitable chemical modifications can be conducted on the lower and upper rims of calix[4]arenes. Polar groups, as well as lipophilic functions, can be anchored on both sides of the macrocycles, therefore making the synthesis of a wide range of amphiphilic macrocycles possible. The degree of substitution on both rims can be finely tuned so as to control the hydrophilic/lipophilic balance of the resulting amphiphiles. In addition to this, the fairly rigid skeleton of the cyclic tetramer allows for a control over the shape and conformation of the final amphiphilic structure. From a synthetic point of view, the presence of a rigid macrocycle dictates the orientation of the polar and hydrophobic groups introduced.[53]

The synthesis of amphiphilic calix[4]arenes is typically accomplished by first introducing the aliphatic chains on the lower rim of the calixarene skeleton and by further attaching the suitable polar functions at the *p*-position. As an alternative, amphiphilic *p*-acyl calix[4]arenes can be readily synthesized by introducing the corresponding acyl group at the *p*-positions of the ring in the presence of a Lewis acid such as aluminum trichloride.[54]

Etherification is the most extensively used reaction for the lower rim functionalization of calix[4]arenes.[55] Complete alkylation is usually performed in the presence of a strong base, e.g. NaH, with an excess of an alkylating agent (Figure 1.7).[56] By varying the type of base and amount of alkylating agent, partial alkylation can be achieved. For example, distal dialkylation of *p-tert*-butylcalix[4]arene is favored using a weak base such as K_2CO_3 with a limiting amount of the alkylating agent[57] while proximal dialkylation is favored in the presence of NaH with an excess of the alkylating agent.[58]

A large variety of electrophilic aromatic substitutions can be carried out at the *p*-positions of the calix[4]arene skeleton, e.g. sulfonation,[59] halogenation,[55] acylation,[60] chloromethylation,[61,62] (Figure 1.7). The functional groups introduced by these routes can be further functionalized so as to allow the insertion of the desired polar functions at the *p*-position of the macrocycles.

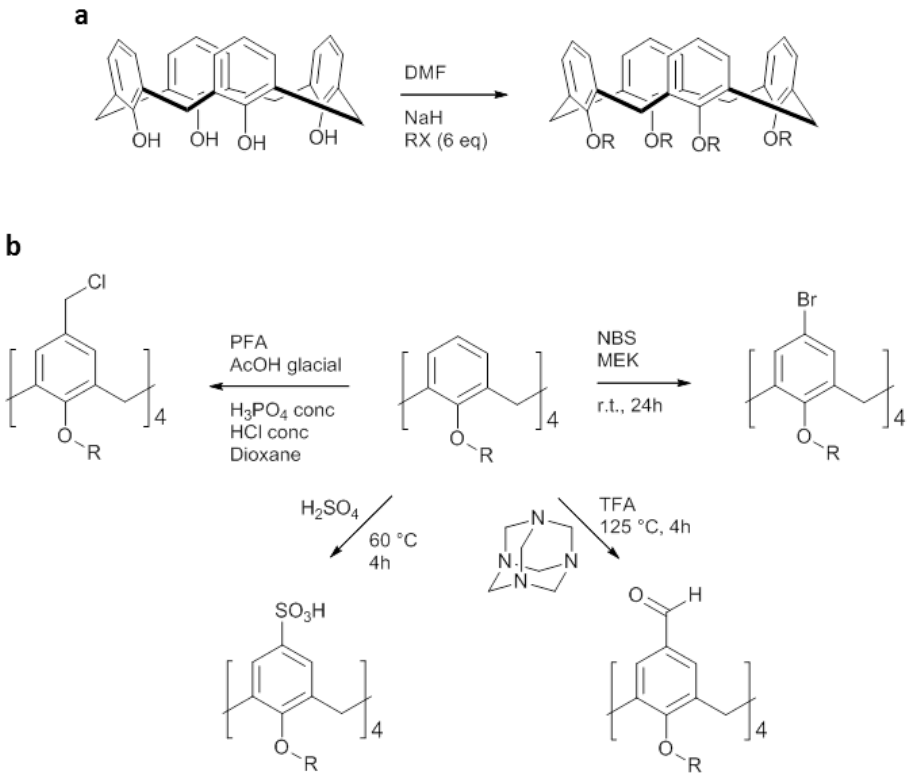

Figure 1.7. Tetraalkylation reaction of calix[4]arene-25,26,27,28-tetrol with the alkylating agent RX in the presence of NaH as base (**a**) and some examples of upper rim electrophilic aromatic substitutions (**b**) of alkylated calix[4]arenes.

1.5 Langmuir monolayers of amphiphilic calixarenes

In the past 4 decades, the self-assembly behavior of amphiphilic calixarenes at the air-water interface has been thoroughly investigated. A large number of calixarenes self-assemble as stable monomolecular films at the air-water interface, where the polar moieties are immerged into water while the hydrophobic groups point toward air, forming Langmuir monolayers.[63-69] This interfacial self-assembly is driven by van der Waals interactions among aliphatic chains and electrostatic interactions (e.g. H-bonding) between the polar functions of the macrocycle and water molecules. The self-assembly process of amphiphilic calixarenes at the air-water interface is also driven by π-π interactions among aromatic rings of neighboring amphiphiles. Shahgaldian demonstrated that an amphiphilic *p*-amido-phenol calix[4]arene derivative forms stable Langmuir monolayers at the air-water interface.[70] On the other hand, the corresponding monomer does not self-assemble as a monomolecular film at the interface. Therefore, the cyclic structure of amphiphilic calixarene derivatives favors the interfacial aggregation process when compared to the corresponding monomers.

Shahgaldian et al. investigated the self-assembly behavior of a series of *p*-acyl calix[4]arenes at the air-water interface. It was demonstrated that the self-assembly properties of the amphiphiles are dependent on the length of the aliphatic chains. The longer are the aliphatic chains, the more stable are the resulting monomolecular films. On the other hand, no variations of the collapse areas, i.e. apparent molecular area values at the collapse of the monolayer, have been observed by varying the length of the alkyl chains. These results indicate that the hydrophobic chains are oriented parallel with one another and that the molecular packing is dictated by the size of the macrocycle ring.[71]

In addition to their excellent self-assembly properties, amphiphilic calixarenes can act as receptors or ligands to bind several neutral and charged molecules. The presence of an apolar cavity, along with multiple polar moieties at the *p*-positions, makes calixarenes suitable

molecular receptors for a large variety of guests. The interaction properties of Langmuir monolayers of amphiphilic calix[4]arenes with ions,[72-76] amino acids,[77,78] nucleosides and nucleotides,[79,80] catecholamines,[81] proteins[82,83] and DNA[84,85] have been therefore extensively investigated.

Langmuir monolayers of amphiphilic calixarenes have been also exploited as supramolecular templates for the crystallization of inorganic and organic molecules at the air-water interface. The polar groups of the macrocycles act as nucleating agents through structural complementarity with the to-be-crystallized molecule, thus lowering the activation barrier for the nucleation process.

1.5.1 Langmuir monolayers as templates for the interfacial crystallization of inorganic and organic molecules

Solid-state polymorphism is defined as the ability of a substance to exist as two or more crystalline phases.[86] Polymorphism of active pharmaceutical ingredients (APIs) can drastically affect the formulation process of solid drugs. Indeed, the arrangement of molecules affects the physical and chemical properties of the crystal, such as melting point, mechanical properties, vapor pressure, density, dissolution rate, solubility. The physicochemical properties of the crystal have a crucial influence on the bioavailability and pharmacokinetics of the produced drug.[87] As a result, the Food and Drug Administration (FDA) acknowledges each API polymorph as a patentable entity.[88]

A remarkable example that emphasizes the importance of polymorphism in APIs formulation is represented by ranitidine hydrochloride, trade name ®Zantac. Ranitidine is a drug used to treat peptic ulcer and gastroesophageal reflux diseases. This API was produced by Glaxo, which issued a patent in 1978 and due to expire in 1995. In 1981, a new polymorphic form was unexpectedly produced during the scaling up process. The new polymorph was named form II (the original

polymorph was named form I). After this event, repetitions of the procedure did not longer yield the pure original form I. Due to superior filtering and drying characteristics of form II with respect to form I, Glaxo issued the patent for form II four years later its discovery, in 1985, so as to maintain the patent for a longer time. The patent for form II was due to expire in 2002. Generic companies tried to produce form I few years before its patent expiration (1995) without succeeding; they could only produce form II. Therefore, Glaxo could protect its invention for other additional seven years so as to maintain the yearly revenue of nearly $3.5 billion.[89]

The control over the polymorphism of APIs is typically achieved by modulating the physical (e.g. pressure, temperature, evaporation) and chemical (e.g. solvent, anti-solvent) conditions of the crystallization process.[90] In addition to this, heterogeneous crystallization may represent a valid alternative for the crystal growth and polymorphism control of pharmaceuticals. For example, Steed demonstrated that low-molecular-weight gelators (LMWGs) act as seeds for the crystal growth of pharmaceuticals with a control over their polymorphism.[91] A series of bis(urea) derivatives with different spacers and functional groups at their ends were demonstrated to form gels in several solvents ranging from aqueous systems to toluene. This class of molecules may be used as basis for the creation of a library of gelators employed for the crystallization of a wide range of compounds. The bis(urea) derivative shown in Figure 1.8 was demonstrated to gelate the solvent mixture acetonitrile/toluene (1:9 v/v). This gel kicks off the crystallization of the needle-like shape polymorphic form II of piroxicam, an API that exists in four polymorphic forms. On the other hand, piroxicam crystallizes from the same solvent mixture acetonitrile/toluene (1:9 v/v) as block-shaped crystals form I. The same bis(urea) derivative was also demonstrated to form gels in a DMSO/water mixture (1:1 v/v). While the hydrate form of piroxicam grows in solution, the polymorphic form II crystallizes from the gel (Figure 1.8).

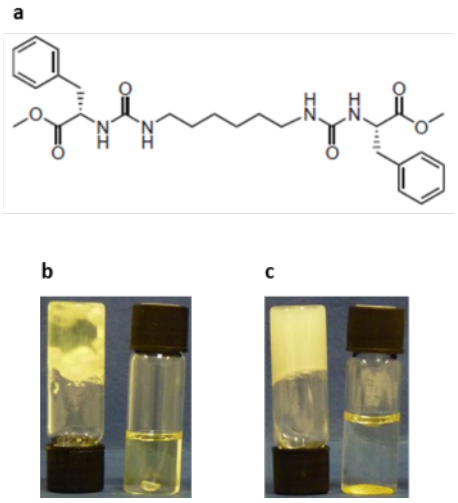

Figure 1.8. (**a**) Chemical structure of the bis(urea) derivative; (**b**) piroxicam crystals from the gel and the bulk of a mixture acetonitrile/toluene (1:9 v/v); (**c**) piroxicam crystals from the gel and the bulk of a mixture DMSO/water (1:1 v/v) [Reproduced with permission from ref. 91, Copyright 2010, Nature Publishing Group].

Langmuir monolayers of amphiphilic molecules at the air-water interface may also act as nucleation sites by structural complementarity between the polar heads of the surfactant and the to-be-crystallized molecule. Mann et al. demonstrated that Langmuir monolayers of stearic acid at the air-water interface initiate the crystallization of the vaterite polymorphic form of calcium carbonate.[92,93] In the absence of the monolayer, the calcite polymorph of $CaCO_3$ is formed. Compression isotherms of the stearic acid monolayer in the presence of $CaCO_3$ dissolved in the aqueous phase revealed that a Stern layer of Ca^{2+} ions is formed underneath the carboxylate film; the formation of the Stern layer allows for the nucleation of the vaterite face. Along with charge accumulation, the geometrical features of the carboxylate groups of stearic acid represent the determining factors for the controlled crystallization process. In calcite crystals, the carbonate ions are oriented parallel to the Stern layer. On the other hand, the anions are oriented perpendicular to the Stern layer in vaterite crystals. The orientation of the anions in vaterite crystals is equivalent to that of the carboxylate groups of stearic acid with

respect to the Stern layer. Therefore, the arrangements of the carboxylic groups of stearic acid, along with the binding of Ca^{2+} ions, favors the formation of a two-layer subunit cell motif of vaterite, cf. Figure 1.9.

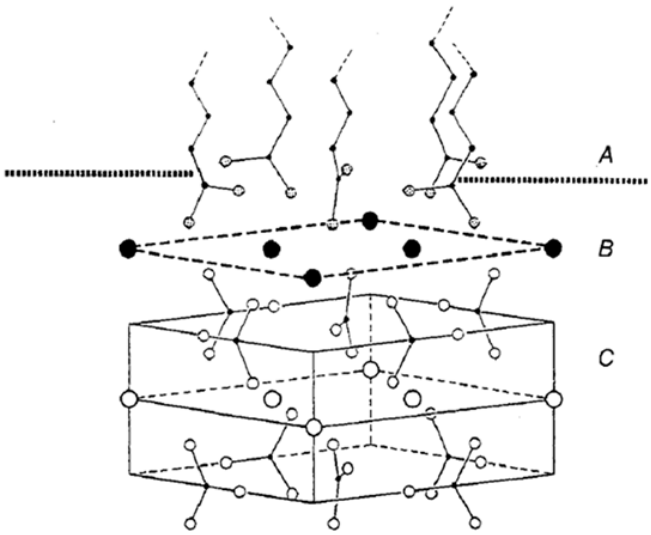

Figure 1.9. Graphical representation of the suggested interfacial organization of $CaCO_3$ molecules during nucleation. *A* is the stearic acid monolayer with the polar heads arranged perpendicular to the air-water interface; *B* is the Stern layer of headgroups-Ca^{2+} ions; *C* is the vaterite sub-cell with the carbonate ions organized perpendicular to the Stern layer (Reproduced with permission from ref. 92, Copyright 1988, Nature Publishing Group).

Langmuir monolayers of amphiphilic calixarenes have been also shown to kick off the crystallization of $CaCO_3$ at the air-water interface.[94] Volkmer et al. demonstrated that Langmuir monolayers of a carboxymethylcalix[4]resorcarene derivative trigger the crystallization of aragonite crystals at the air-water interface while Langmuir monolayers of a tetramethylbutyl-carboxymethoxycalix[8]arene derivative act as templates for the crystallization of calcite crystals.[95] Monolayers of tetramethylbutyl-carboxymethoxycalix[8]arene derivatives induce the crystallization of uniformly oriented calcite single crystals at low surface pressure values (π = 0.0-0.2 mN m^{-1}). At higher surface pressures, the crystals lose their preferred orientation. The

authors suggest that the template effect of such structurally mobile monomolecular films could not be explained by geometrical complementarity between the polar groups of the monolayer and the carbonate ions of the $CaCO_3$ double layer. Therefore, the crystal growth of $CaCO_3$ is dependent on non-specific electrostatic interactions such as the average charge density or the mean dipole moment of the monolayer. In 2011, Shahgaldian et al. reported on the ability of Langmuir monolayers of an amphiphilic amido-phenol modified calix[4]arene derivative to template the crystallization of acetaminophen, an API widely used as analgesic and antipyretic, at the air-water interface.[70] The calixarene monolayer triggers the nucleation of acetaminophen strictly at the interface generating crystals of centimeter size. It has been also demonstrated that the packing density of the monolayer has a relevant effect on the quantity of produced crystals. The template effect of the monolayer was attributed to the structural analogy between the headgroups of the amphiphile and the API (Figure 1.10).

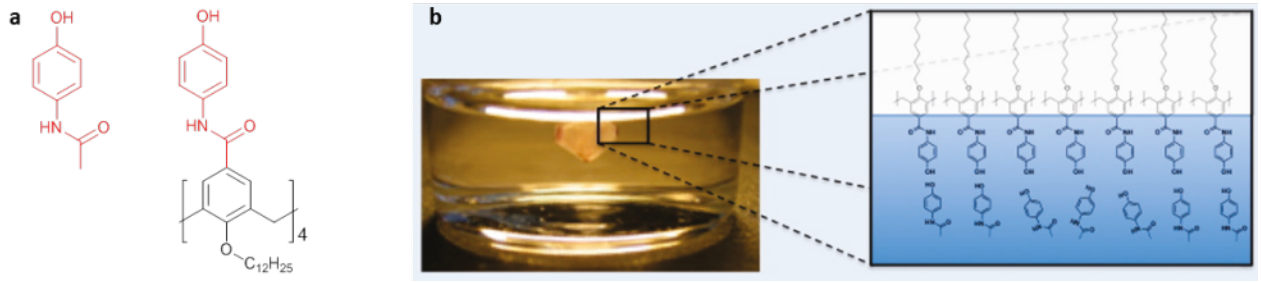

Figure 1.10. (**a**) Chemical structures of acetaminophen and *p*-amidophenol-modified calix[4]arene; (**b**) Snapshot of the interfacial crystallization of acetaminophen at the air-water interface (Reproduced with permission from ref. 70, Copyright 2011, American Chemical Society).

Even if acetaminophen exists as two polymorphic forms, no control over the polymorphism has been achieved; only the thermodynamically favored polymorphic form I has been crystallized.

1.5.2 Interfacial interaction of Langmuir monolayers with ions

The interfacial interaction of charged surfaces with electrolytes plays a crucial role in processes such as electrodeposition, biomineralization and ion transport through biological membranes. As Langmuir monolayers resemble to half a biological membrane, they are appropriate models to study such interactions with electrolytes.[96] These monomolecular films offer the advantage that variables such as amphiphile composition and packing density can be precisely controlled. In addition, synchrotron-based X-ray diffraction techniques, such as X-ray reflectivity (XR) and grazing incidence X-ray diffraction (GIXD), allows evaluating the monolayer structure at the molecular level.[97]

The structure of Langmuir monolayers of single chain amphiphiles is strongly affected by metal ions dissolved in the aqueous subphase. Metal ions typically increase the order of the monomolecular films, even at low surface pressure values.[98] Dutta demonstrated that nickel, barium, cobalt and copper ions induce the formation of a highly condensed phase of heneicosanoic acid Langmuir monolayers at zero surface pressure. GIXD measurements revealed that the molecular packing of the heneicosanoic acid monolayer on the ions subphase at zero surface pressure, i.e. before the isotherm takeoff, is similar to that of a fatty acid monolayer compressed to the solid-like phase on pure water.[99] In addition to this, some metal ions form crystalline layers beneath Langmuir monolayers of fatty acids. In 1991, Als-Nielsen reported on the structure of Langmuir monolayers of arachidic acid on aqueous cadmium (II) chloride solutions. GIXD measurements revealed that the ions in the subphase increase the order of the fatty acids self-assembled as a Langmuir monolayer at the air-water interface. In addition, GIXD analyses showed that a crystalline counterion layer of cadmium ions was formed beneath the arachidate monomolecular film.[100]

Metal ions are also known to improve the transfer of Langmuir monolayers onto solid substrates through the Langmuir-Blodgett (LB) transfer and deposition method. The deposition

process is carried out by compressing the monomolecular film to the desired surface pressure and by vertically dipping the substrate into the water subphase. When the substrate is removed from the subphase, a second layer is transferred. Schwartz et al. demonstrated that LB films of arachidic acid are highly stabilized by Cd^{2+} ions. AFM images revealed that the surface of the layer attached to the layer below via headgroups-headgroups interactions possesses a crystalline order while the surface of the layer attached to the layer below via aliphatic chain-aliphatic chain interactions is disordered. The stabilization effect was attributed to the electrostatic interactions between the headgroups of the amphiphile and the cations; cf. Figure 1.11.[101,102]

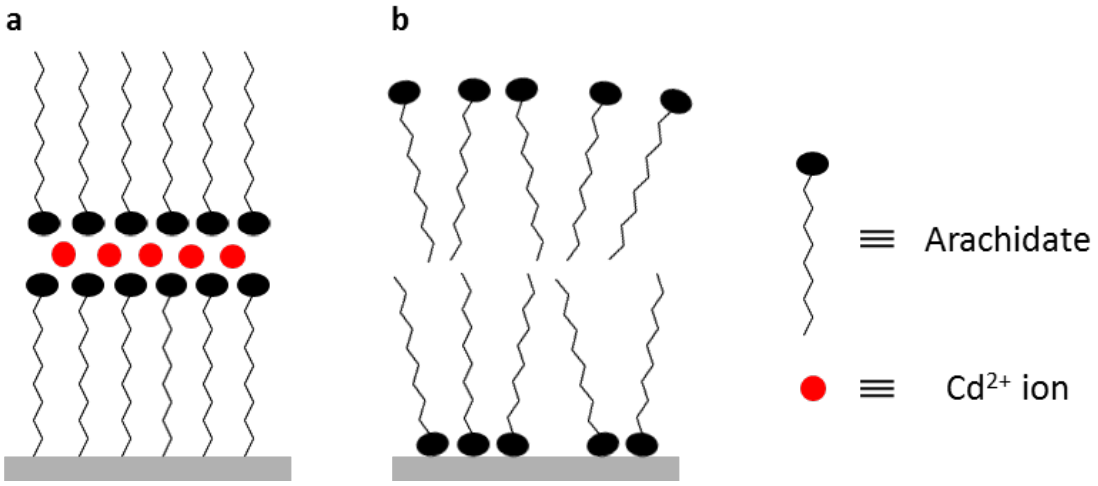

Figure 1.11. Graphical representation of the highly ordered (**a**) and disordered LB films (**b**). The crystallinity is ascribed to the interaction between the headgroups of arachidate molecules and Cd^{2+} ions.

The interaction of Langmuir monolayers of amphiphilic calixarenes with ions has been extensively investigated over the past 25 years.[72-76] The vase-like conformation of the macrocycles, along with the presence of multiple polar functions at the *p*-position, makes them suitable hosts for ion binding.

Shinkay first described the interactions of calixarenes Langmuir monolayers with ions at the air-water interface in 1989.[103] It was reported that Langmuir monolayers of a calix[4]arene ester derivative are selective to sodium ions while Langmuir monolayers of a calix[6]arene ester derivative mainly interact with potassium ions. The authors demonstrated that the calixarene films are selective toward cations binding. The selectivity of Langmuir monolayers of calixarenes is dependent on the size of the cavity of the macrocycles.

In 1996, Baglioni investigated the complexation properties of Langmuir monolayers of calix[6]arene derivatives towards cations.[104] Surface pressure-area compression isotherms revealed that *p-tert*-butylcalix[6]arene films are selective to Cs^+ while Langmuir monolayers of its hexamide structural analogue binds preferentially guanidinium ions. The results demonstrate that the polar moieties of the macrocycles contribute to their binding affinity towards cations.

Shahgaldian and Coleman reported in 2001 on the interaction of Langmuir monolayers of *p*-dodecanoylcalix[4]arene with a series of monovalent cations at the air-water interface, i.e. Li^+, Na^+, K^+, Rb^+ and Cs^+.[105] Surface pressure-area compression isotherms revealed that, despite the presence of the four-membered ring macrocycle, the monolayer is better stabilized by the large rubidium ions. These results suggest that the binding properties of the *p*-dodecanoylcalix[4]arene-based monolayers are affected not only by the structure of the macrocycle, but also by its self-assembly state. The effect of the counterion has been also investigated by using a series of anions, i.e. Cl^-, Br^-, I^-, NO_3^-, SO_4^{2-}, $H_2PO_4^-$, $CH_3CO_2^-$, BF_4^- and HCO_3^-, maintaining Na^+ constant. The monolayer is strongly stabilized by anions such as $CH_3CO_2^-$ and HCO_3^-.

In 2005, Baglioni investigated the interaction properties of *p-tert*-butylcalix[6] and [8]arene with a series of potassium salts.[72] The counterions effect on the monolayer structure was discussed in terms of the Hofmeister series. The cyclic octamer possesses a less rigid structure than the cyclic hexamer. The more flexible conformation of the cyclic octamer causes the aromatic rings

to be closer to the water surface. The authors postulated that the anions are in the proximity of a hydrophobic-water interface and show a different interfacial behavior with respect to that observed at the air-water interface. This would explain the opposite trend of the surface pressure values as a function of the different physicochemical parameters related to the Hofmeister phenomenon.

The high affinity of Langmuir monolayers of amphiphilic calixarenes towards ions is dependent on the macrocycle structure. The presence of a cavity chemically functionalized with the desired polar functions at the *p*-positions favors the formation of 1:1 complexes between the calixarene derivatives, self-assembled as Langmuir monolayers at the air-water interface, and the ions. At the same time, the multivalency of calixarene derivatives allows them potentially binding more than one ion at the air-water interface so as to form an extended organized array of noncovalent interactions, i.e. two-dimensional metal organic networks.

1.5.3 Langmuir monolayers as two-dimensional metal organic networks

Two-dimensional assemblies are structures that possess molecular thickness and submicro- or micrometer lateral size.[106] Self-assembled monolayers (SAMs) are highly ordered molecularly thin layers formed on solid surfaces. Molecules with different terminal functional groups at the extremity of the alkyl chains can be adsorbed on the surface of solids so as to produce a large variety of structures. The highly packed structure of SAMs makes them suitable materials for application in the fields of sensing and optics.[107,108]

The air-water interface represents an appropriate platform for the fabrication of well-organized 2D assemblies. Indeed, the water surface allows for the self-assembly of amphiphilic molecules at the air-water interface where the packing density of the organic building blocks can be precisely controlled. For example, Makiura reported on the fabrication of 2D molecularly thin

metal organic frameworks (MOFs) that consist of porphyrin units (CoTCPP) linked by Cu^{2+} ions, with the ring of the porphyrin that lies parallel to the air-water interface, e.g. Figure 1.12.[109,110]

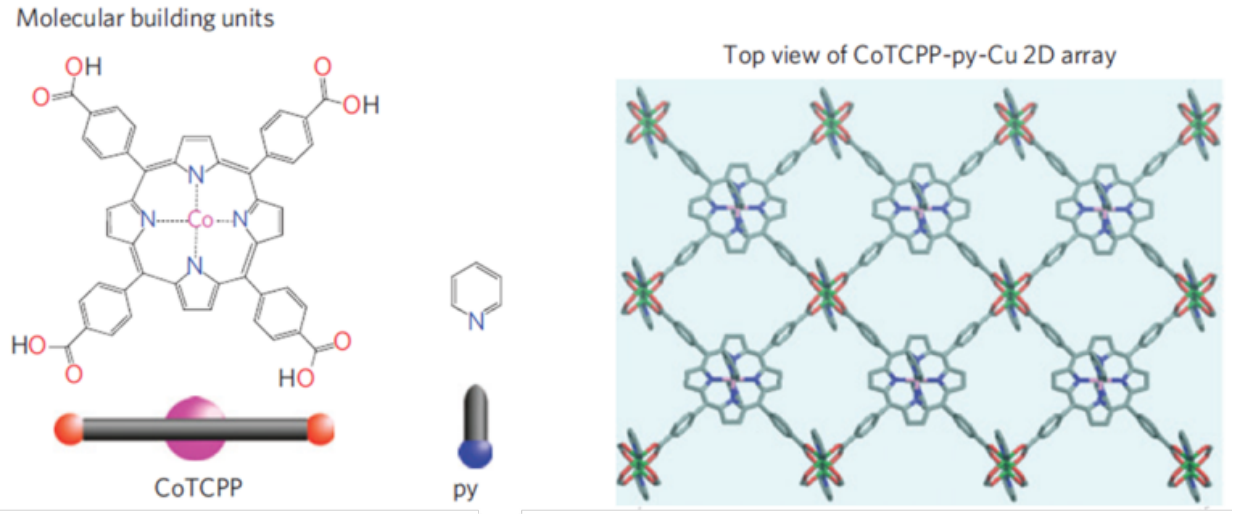

Figure 1.12. Molecular structure of CoTCPP and top view of the copper-mediated CoTCPP two-dimensional array at the air-water interface (Reproduced with permission from ref. 110, Copyright 2010, Nature Publishing Group).

The formation of crystalline domains of CoTCPP is driven by noncovalent interactions among the carboxylic functions attached at the periphery of the porphyrin ring and the metal ions. In addition, the size of the crystalline domains is increased by injecting the aqueous Cu^{2+} solution into the subphase right after spreading the porphyrin monolayer on the water surface. The authors assumed that, by spreading drops of the CoTCPP solution on the water, surface ripples are produced so as to partially disrupt the coordination event. This event was captured by BAM micrographs that showed the random movement of the monolayer domains prior to compression. The injection of the copper solution into the subphase after spreading the monolayer favors therefore the slow diffusion of the metal joints; crystalline domains with a lateral size of 200 nm are produced. Schlüter reported on the synthesis of freestanding highly

ordered 2D polymers at the air-water interface.[111] The nanosheets consist of hexafunctional terpyridine-based monomers held together by Fe^{2+} ions (Figure 1.13).

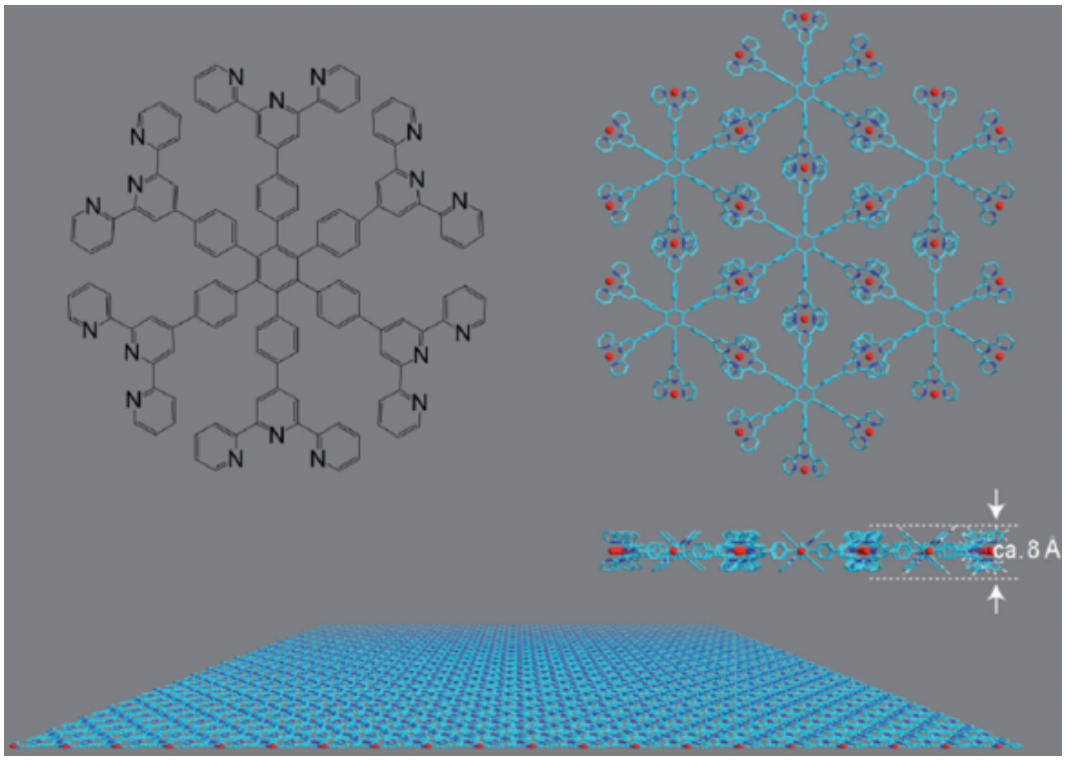

Figure 1.13. Chemical structure of the terpyridine-based monomer and small and large scale representation of the two-dimensional nanosheet at the air-water interface (Reproduced with permission from ref. 111, Copyright 2011, John Wiley & Sons, Inc.).

The interfacial polymerization of the terpyridine-based monomer is driven by the coordinative reaction among the terpyridine moieties and the metal ions. Large ordered nanosheets with a size bigger than 500 × 500 μm^2 have been demonstrated to be produced at the air-water interface. The highly ordered structure of the nanosheets is maintained after their transfer onto solid substrates by means of the LB technique.

2 Objective of the work

Langmuir monolayers of amphiphilic calixarenes have been demonstrated to show recognition properties towards a large variety of solutes, such as ions and small organic molecules, at the air-water interface. The interfacial affinity of calixarene-based Langmuir monolayers towards ions relies on the size, the nature of the polar headgroups and the self-assembly state of the macrocycle. Structural complementarity between the headgroups of the calixarene derivative, self-assembled as a Langmuir monolayer at the air-water interface, and the organic molecule dissolved in the aqueous subphase is at the basis of the interfacial molecular recognition process.

One of the appealing features of Langmuir monolayers is that the packing of the amphiphiles within the monomolecular film can be finely tuned. If the arrangement of the amphiphiles is dependent on the compression state of the film, different monolayer phases will be observed. Distinct monolayer structures may initiate the nucleation of different crystal faces of the to-be-crystallized molecule at the interface, for example via epitaxial growth or specific/non-specific electrostatic interactions. Previous experiments revealed that Langmuir monolayers of a *p*-carboxycalix[4]arene derivative at the air-water interface show a phase transition.[67,112] Such phase transition may be exploited for the control over the polymorphism of GBP. In the results and discussion chapter 3.1, the ability of Langmuir monolayers of an amphiphilic *p*-carboxycalix[4]arene derivative to act as templates for the crystallization of an API with a control over its polymorphism at the air-water interface is reported.

The recognition properties of Langmuir monolayers of amphiphilic calixarenes towards electrolytes are dependent on the nature of the polar moiety attached at the *p*-position of the macrocycle. In the results and discussion chapters 3.2 and 3.3, the self-assembly behavior of Langmuir monolayers of amphiphilic *p*-carboxy and *p*-aminocalix[4]arenes, at the air-water interface, in the presence of inorganic molecules dissolved in the aqueous solution is discussed.

Synchrotron-based X-ray diffraction techniques, i.e. X-ray near-total-reflection fluorescence (XNTRF), XRR and GIXD, along with compression isotherms and BAM measurements, shed light on the response of *p*-carboxycalix[4]arene monolayers towards divalent fourth-period transition metals and of a series of tetra and diamino-substituted calix[4]arenes towards $HgCl_2$ at the air-water interface.

Calix[4]arene derivatives are multivalent molecules that can potentially bind more than one ion when self-assembled as Langmuir monolayers at the air-water interface. The multivalency of these macrocycles, coupled with a fairly rigid conformation, could be exploited to generate highly ordered and extended arrays of noncovalent interactions with ions in the two dimensions. The common trait of Makiura and Schlüter's works described in chapter 1.5.3 is that the organic building blocks possess a planar geometry.[109,111] Both the porphyrin and the terpyridine derivatives lie at the air-water interface with their planes parallel to the water surface. The planar conformation of the ligands favors the coordination reaction with the metal joints. On the other hand, amphiphilic calix[4]arene molecules are intrinsically three-dimensional building blocks that self-assemble at the air-water interface with their C_4 pseudo-symmetry axis perpendicular to the water surface. Such arrangement seems to be a limiting factor for the fabrication of calixarene-based two-dimensional molecularly thin metal organic networks. Indeed the polar functions of the macrocycles would be geometrically constrained and therefore prevented from binding the metal joints in the most stable coordination geometry. Despite this apparent limitation, it is demonstrated in the results and discussion chapter 3.4 that the proper design of the molecular structure of the macrocycle allows for the fabrication of considerably large crystalline 2D calix[4]arene-based metal organic networks at the air-water interface. The ability of Langmuir monolayers of a short chain amphiphilic *p*-carboxycalix[4]arene to form 2D metal organic networks at the air-water interface is thus discussed.

3 Results and discussion

3.1 Polymorphism control of GBP beneath calix[4]arene-based Langmuir monolayers

3.1.1 Synthesis and crystal structure of 5,11,17,23-tetra-carboxy-25,26,27,28-tetradodecyloxycalix[4]arene (3)

The amphiphilic calix[4]arene **3** was synthesized in six synthetic steps as shown Figure 3.

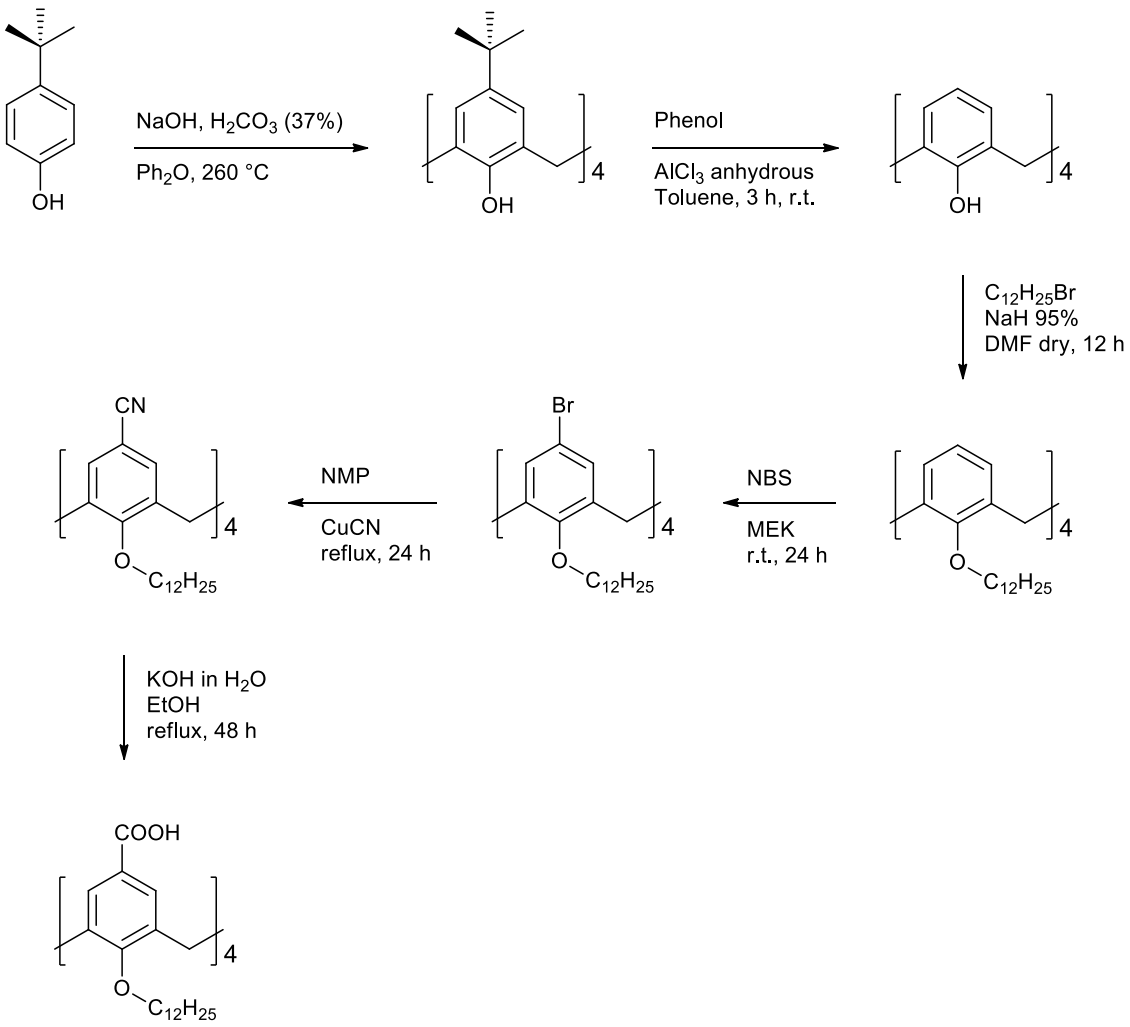

Figure 3. Synthetic route of **3**.

The synthesis of the 24,25,26,27-calix[4]arene tetrol was performed as described in the literature.[113,114] The introduction of the C_{12} alkyl chains on the lower rim of 25,26,27,28-calix[4]arene tetrol was conducted in the presence of NaH as base and 1-bromododecane as alkylating agent in dry DMF. Electrophilic aromatic substitution at the *p*-positions of 25,26,27,28-tetradodecyloxycalix[4]arene using N-bromosuccinimide (NBS) in methyl ethyl ketone (MEK), followed by nucleophilic aromatic substitution in the presence of copper (I) cyanide yielded the *p*-tetra-cyano-tetradodecyloxycalix[4]arene derivative. Hydrolysis of the nitrile groups with KOH in H_2O and recrystallization of the crude product in ethyl acetate yielded pure **3**.[115,116]

Colorless crystals of quality suitable for single crystal X-ray diffraction analysis were obtained by recrystallization of **3** from pyridine by the slow evaporation method. The structure of **3** was solved in the triclinic space group *P*-1 with one molecule of **3** and four molecules of pyridine in the asymmetric unit (ASU). The solid-state structure of **3** revealed that the amphiphile is in a pinched cone conformation where two opposite arenes are parallel to each other while the other two aromatic rings are splayed apart, cf. Figure 3.1. The pinched cone conformation of **3** is in agreement with the structure of the tetra-butoxy-tetra-*p*-carboxylatocalix[4]arene reported by Dalgarno.[117] The distance between the centroids of the two parallel arenes of **3** in the pinched cone conformation is 4.7 Å while the distance between the centroids of the other two aromatic rings is 10.2 Å. Pyridine molecules are organized in the structure so as to form H-bonding with the amphiphiles. Each of the four carboxylic groups of **3** forms hydrogen bond with one molecule of pyridine, as shown in Figure 3.1. The distances of the N···HO bonds are in the range of 1.96-1.77 Å.

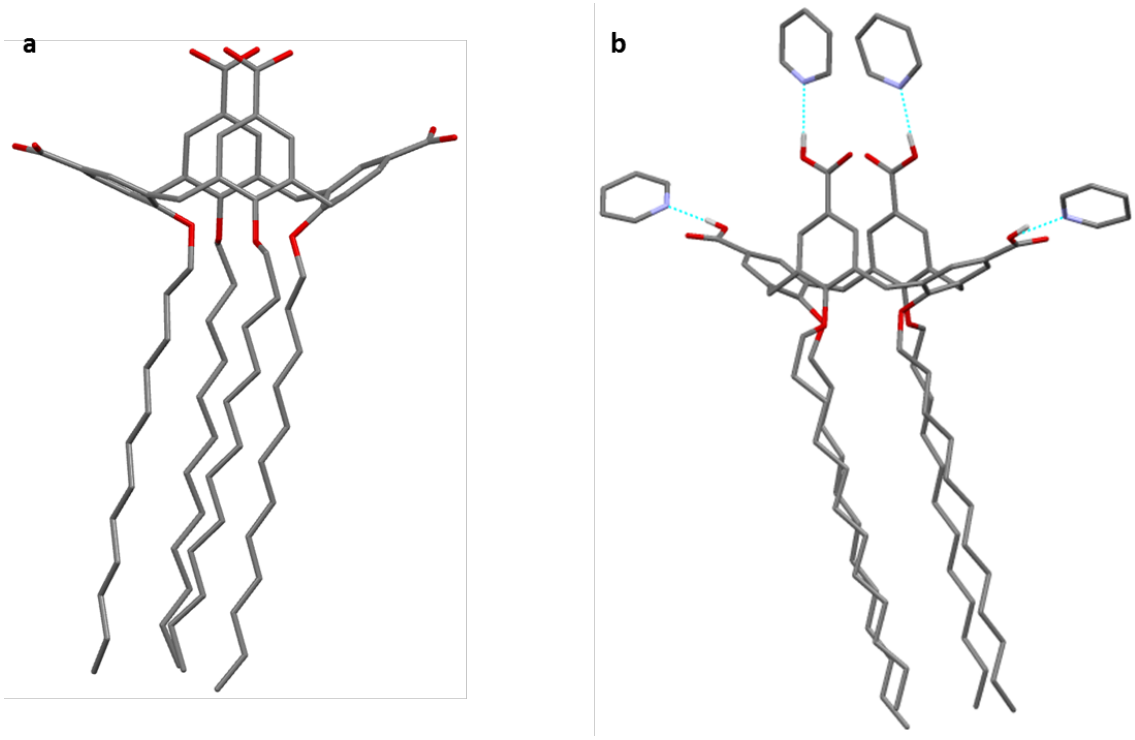

Figure 3.1. Single crystal X-ray structure of **3** (**a**) and H-bonding interactions (dashed light blue lines) of **3** with four molecules of pyridine (**b**). Hydrogen atoms are omitted for clarity (except those involved in H-bonding).

Examination of the expanded structure of **3** reveals that the amphiphiles self-assemble as a bilayer in the solid state (Figure 3.2). The formation of a bilayer array is consistent with that reported for the parent tetra-butoxy-tetra-*p*-carboxylatocalix[4]arene derivative.[117] The aliphatic chains of **3** in the solid state do not show interdigitation and are organized in an all-parallel fashion, with a tilt of 9.7° with respect to the axis of the bilayer.

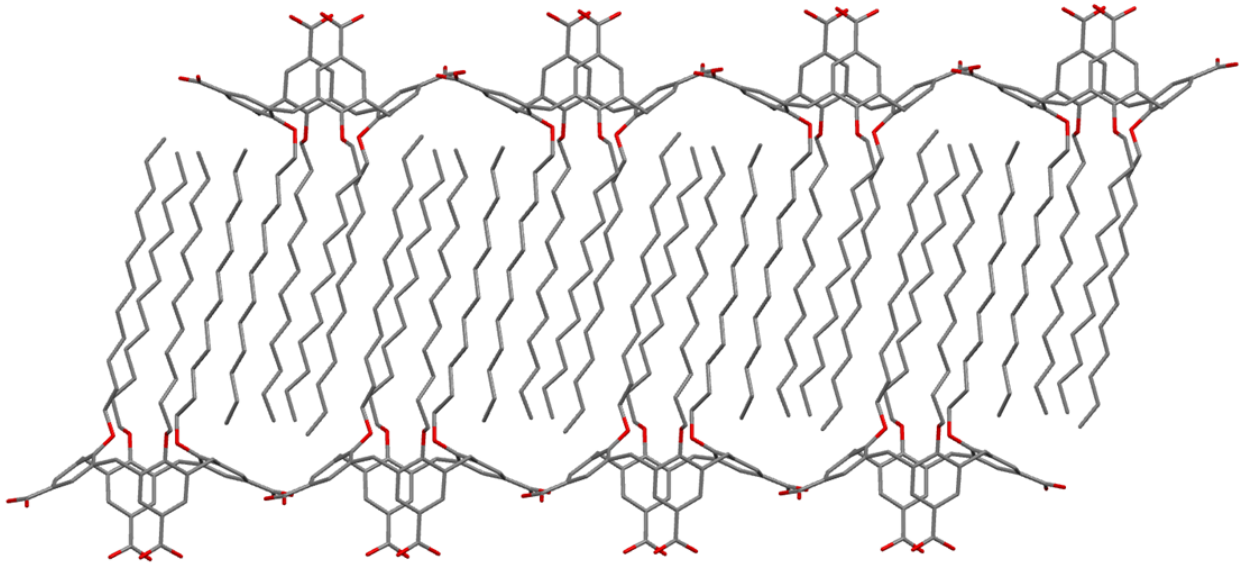

Figure 3.2. Packing arrangement of **3** in the solid state. Hydrogen atoms are omitted for clarity.

3.1.2 Interfacial self-assembly

The ability of **3** to self-assemble at the air-water interface as stable Langmuir monolayers was investigated by surface pressure-area compression isotherms using a Langmuir balance. The isotherm of **3** on pure water shows a collapse pressure (π_c) of 51 ± 0.5 mN m^{-1} and a collapse area (A_c) of 99 ± 1 $Å^2$ $molecule^{-1}$. In addition, a phase transition at 38 ± 0.5 mN m^{-1} is observed, in agreement with the results reported in the literature (Figure 3.3).[67,112]

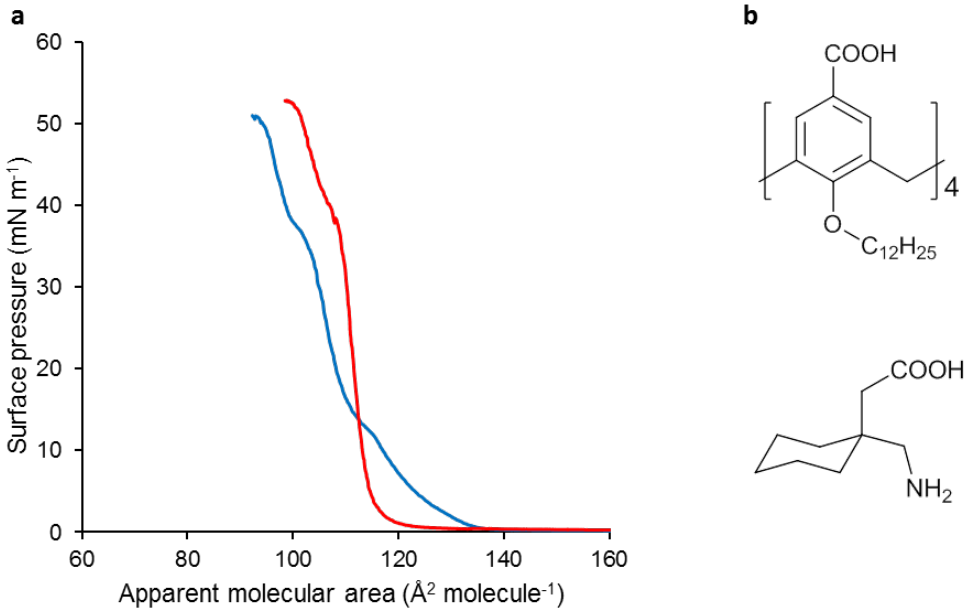

Figure 3.3. Surface pressure-area compression isotherms of **3** on pure water (–) and on a 5 g L^{-1} aqueous GBP subphase (–) (**a**) and chemical structures of **3** and GBP (**b**).

Unlike **3**, the corresponding monomer 4-(dodecyloxy)benzoic acid does not self-assemble as stable monolayers at the air-water interface. This highlights the importance of the macrocyclic backbone for the self-assembly process at the interface. The A_c value of 99 ± 1 $Å^2$ $molecule^{-1}$ is consistent with the presence of **3**, in the cone conformation, at the air-water interface with the pseudo C_4 symmetry axis orthogonal to the surface of the water. When GBP is dissolved in the aqueous subphase at a concentration of 5 g L^{-1}, the profile of the isotherm drastically changes, cf. Figure 3.3. The A_c value is shifted towards lower values, i.e. from 99 on pure water to 92 ± 1 $Å^2$ $molecule^{-1}$ on the GBP subphase, while the takeoff area (A_0) value is shifted towards higher values, from 122 on pure water to 136 ± 1 $Å^2$ $molecule^{-1}$ on the GBP subphase. In addition, a second phase transition at 12 ± 0.5 mN m^{-1} is observed. These results clearly demonstrate that the monolayer of **3** interacts with GBP at the air-water interface.

Surface ellipsometry was employed to determine the thickness of the monomolecular film of **3** on pure water and on a 5 g L^{-1} aqueous GBP subphase. Ellipsometry measurements of the monolayer on pure water showed that, before reaching an apparent molecular area value of 137 ± 1 $Å^2$ $molecule^{-1}$, no thickness could be measured, cf. Figure 3.4.

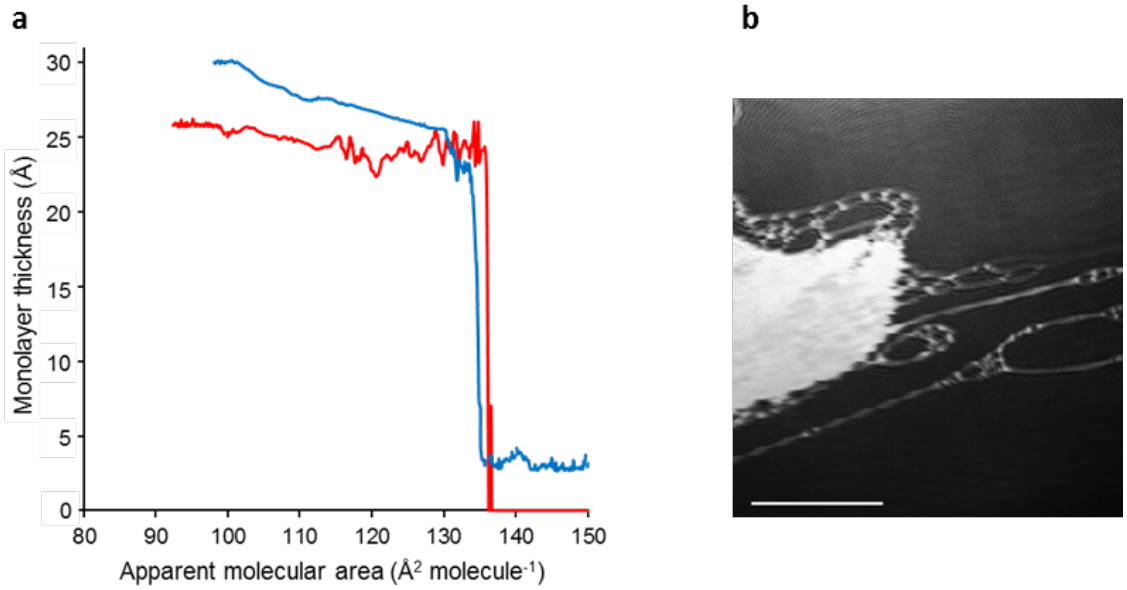

Figure 3.4. Monolayer thickness of **3** on pure water (–) and on a 5 g L^{-1} aqueous GBP subphase (–) (**a**) and BAM micrograph of the monolayer of **3** on a 5 g L^{-1} aqueous GBP subphase compressed at a surface pressure value of 0 mN m^{-1} (**b**). Scale bar = 100 µm (Reproduced with permission from ref. 121, Copyright 2014, Royal Society of Chemistry).

This result might be explained by the fact that **3** is in a gas-like phase and that no thickness can be measured. Despite that, BAM micrographs of the monomolecular film of **3** indicate that the amphiphiles, before the isotherm takeoff, self-assemble at the interface forming liquid-like domains (Figure 3.4). These results suggest that the surface coverage of **3** is too low to acquire a measurable thickness. By further compression of the monolayer, a thickness of 24 ± 1 Å is measured and this value remains constant until the phase transition. After the phase transition, the thickness slightly increases to 26 ± 1 Å (Figure 3.4). This value is in agreement with the

presence of **3**, self-assembled as a Langmuir monolayer at the air-water interface, with the pseudo C_4 symmetry axis perpendicular to the surface of the water, thus in agreement with the results obtained by compression isotherms experiments. In the presence of GBP dissolved in the aqueous subphase at a concentration of 5 g L^{-1}, a thickness value of 2 Å is measured before the isotherm takeoff (136 ± 1 $Å^2$ $molecule^{-1}$). This result suggests that relatively large liquid-like domains of **3** are formed and allow measuring a thickness of 2 Å. At the takeoff, the thickness rapidly increases to 24 ± 1 Å. After the takeoff, the thickness steadily increases up to a value of 26 ± 1 Å before the phase transition measured at 36 ± 0.5 mN m^{-1}. The value of 26 ± 1 Å measured on the aqueous GBP subphase is close to that measured on pure water (24 ± 1 Å), thus indicating that no clear difference in the monolayer thickness on pure water and on the aqueous GBP solution is observed. After the phase transition, the thickness of the monolayer of **3** considerably increases up to 30 ± 1 Å (Figure 3.4). The higher thickness measured after the phase transition is attributed to a partial layer of GBP in direct contact with the monomolecular layer of **3** at the air-water interface. These results suggest that the organization of **3**, after the phase transition, considerably favors the interaction of the monomolecular film with the API at the interface.

The structure of the monolayer of **3** on pure water and on a 5 g L^{-1} aqueous GBP solution was investigated by synchrotron-based grazing incidence X-ray diffraction. GIXD of the monolayer of **3** on pure water compressed below the phase transition, i.e. π = 25 mN m^{-1}, shows the presence of a broad peak (A1) centered at Q_{xy} = 1.40 $Å^{-1}$, where Q_{xy} represents the horizontal component of the scattering vector. This value has been already observed for short chain surfactants at the air-water interface and has been ascribed to bulk hydrocarbon chains in the liquid-like state.[118,119] The full width at half maximum (FWHM) of A1 is Q_{xy} = 0.2-0.3 $Å^{-1}$ (Figure 3.5), a value that corresponds to lateral short-range order of the hydrocarbon chains of the monolayer of **3**. The peak A1 is the result of aliphatic chains interference with nearest neighbor (NN) and at most with next nearest neighbor (NNN) chains. When the monolayer of **3** on pure water is

compressed to a surface pressure of 45 mN m^{-1}, that is above the phase transition, two additional sharp Bragg-reflections (C1 and C2) emerge at Q_{xy} = 1.51 and 1.67 $Å^{-1}$, with a peak height ratio of 2:1 (Figure 3.5).

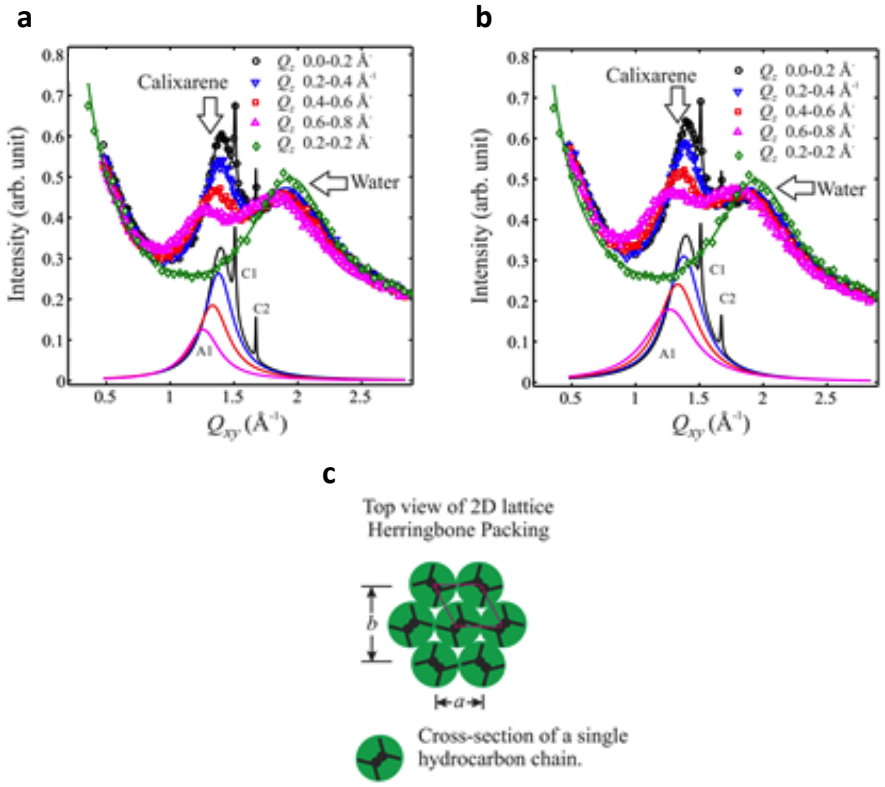

Figure 3.5. GIXD pattern of the monolayer of **3** on pure water (**a**) and on a 5 g L^{-1} aqueous GBP solution (**b**) at a compression of 45 mN m^{-1}. Schematic representation of 2D herringbone packing of hydrocarbon chains, in a rectangular unit cell (**c**) [Reproduced with permission from ref. 121, Copyright 2014, Royal Society of Chemistry].

By considering a rectangular unit cell with lengths *a* = 5.0 Å and *b* = 7.5 Å, the C1 and C2 peaks index as [11] and [02] crystalline planes, respectively, with d_{02} = 3.76 Å and d_{11} = 4.16 Å. Such a structure is in agreement with the herringbone acyl-chain packing typically observed in crystalline alkanes adsorbed on solid substrates and, more rarely, in Langmuir monolayers of

lipids.[97] These results demonstrate that the fully compressed monolayer of **3**, i.e. π = 45 mN m^{-1}, possesses a highly crystalline phase that coexists with an amorphous phase. The packing features of the monolayer of **3** on pure water, compressed above the phase transition, are similar to those shown by linear alkanes, even if the molecular structure of the macrocycle strongly differs from that of linear alkanes. When GBP is dissolved in the aqueous subphase at a concentration of 5 g L^{-1}, no relevant changes in the diffraction pattern of the monolayer of **3** are observed (Figure 3.5). These results strongly suggest that GBP molecules, interacting with **3** at the air-water interface, do not affect the arrangement of the aliphatic chains of the amphiphile.

3.1.3 Interfacial crystallization of GBP

The ability of the monolayers of **3** to act as templates for the crystallization of GBP at the air-water interface was investigated by spreading appropriate amounts of the macrocycle**,** corresponding to Langmuir monolayers compressed at surface pressures of 0, 1, 25 and 45 mN m^{-1}, on the surface of supersaturated aqueous solutions of GBP ([GBP] = 150 g L^{-1}). The control experiments included the supersaturated solutions of GBP in the absence of the monolayer of **3** and the supersaturated solutions of GBP with the pure solvent, i.e. $CHCl_3$, spread at the interface. The second control was performed because of the endothermic reaction caused by the evaporation of the solvent; the rapid cooling of the solution at the interface may trigger the crystallization of the API at the air-water interface. After 14 days, large centimeter-sized crystals were observed, strictly at the air-water interface, in the vials containing the monolayers of **3** compressed at surface pressure values of 0, 1, 25 and 45 mN m^{-1}. In the controls, crystals have grown only after one month, both at the interface and in the bulk solution. Infrared (IR) spectroscopy revealed that the crystals grown underneath the monolayers of **3** compressed at 0, 1, and 25 mN m^{-1}, i.e. below the phase transition shown by the compression isotherm, were the GBP polymorphic form γ, cf. Figure 3.6. On the other hand, the crystals grown underneath the monolayers of **3** compressed at 45 mN m^{-1}, i.e. above the phase transition shown by the

compression isotherm, were the polymorphic form α (Figure 3.6).[120] This is the first example that describes the control over the polymorphism of the crystallized organic molecule at the air-water interface by Langmuir monolayers of amphiphilic calixarenes.

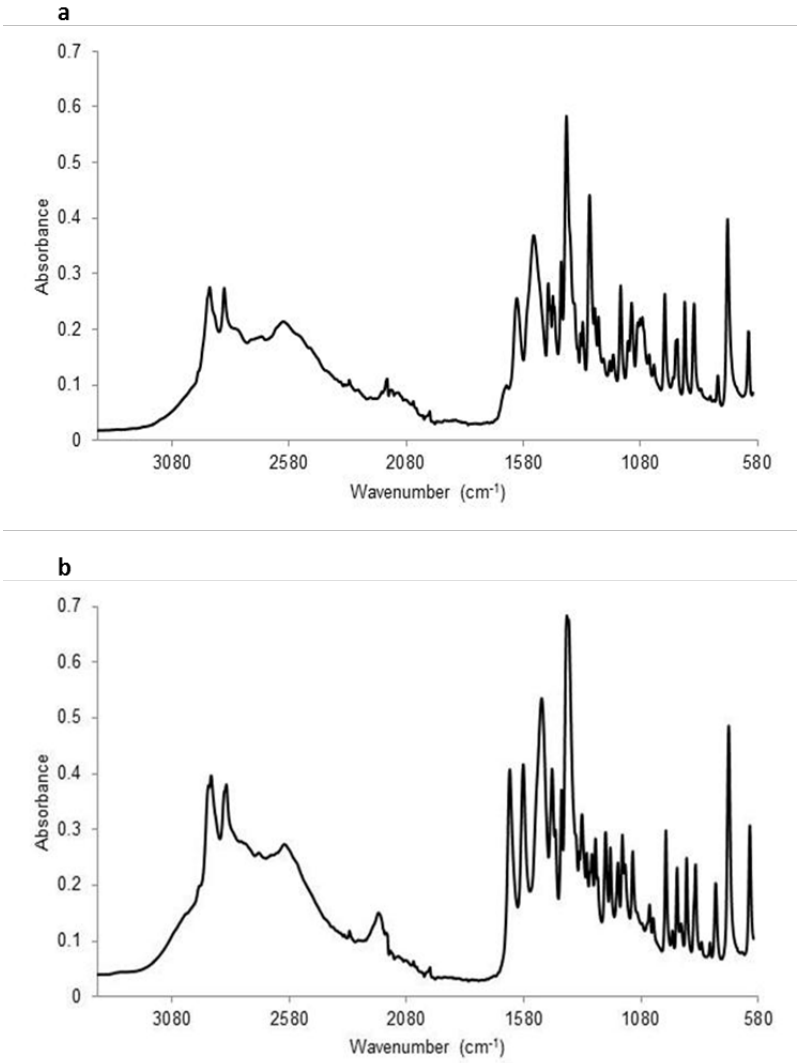

Figure 3.6. IR spectra of GBP polymorphic form α (**a**) and γ (**b**) [Reproduced with permission from ref. 121, Copyright 2014, Royal Society of Chemistry].

The hydrate polymorphic form of GBP was found to grow in the controls. Single crystal X-ray diffraction analysis confirmed that two distinct polymorphic forms of GBP were grown beneath Langmuir monolayers of **3** compressed at different packing densities. These results unambiguously demonstrate that the monolayer of **3** acts as "seed" for the interfacial crystallization of GBP and that the modulation of the packing density of the monomolecular film allows for the control over the polymorphism of the API. Face-indexing analysis of the crystals revealed that the polymorph γ nucleates with the (100) crystallographic plane parallel to the interface while the polymorph α crystallizes with the (001) crystallographic plane parallel to the interface. Both the polymorphs were shown to possess a bilayer structure with the plane of the bilayers parallel to the interface. The polymorphs γ and α nucleated with the polar functions of GBP oriented towards the headgroups of **3**, c.f. Figure 3.7.

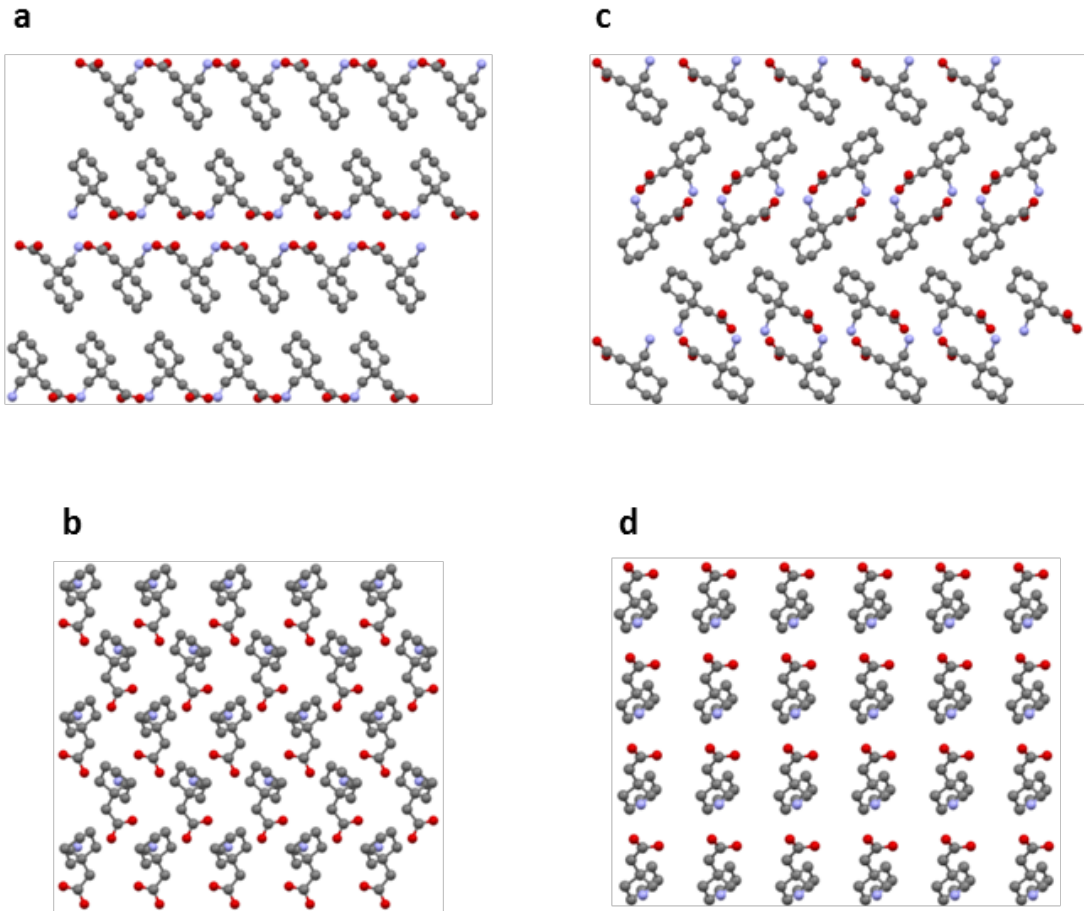

Figure 3.7. Packing arrangements of GBP polymorphs γ (**a**: side view; **b**: top view) and α (**c**: side view; **d**: top view).

This set of results confirms that the monolayers of **3** act as templates for the crystallization of GBP at the air-water interface, where the headgroups of the amphiphile act as molecular recognition units for the nucleation process. The template effect of the monolayer of **3** on the interfacial crystallization of GBP is ascribed to electrostatic interactions between the carboxylate functions of the macrocycle and the protonated amino moieties of the API. The difficulty in establishing the arrangement of the headgroups of **3** at the air-water interface prevented us so far from establishing potential epitaxial match between the amphiphiles and GBP molecules.[121]

3.1.4 Conclusions

The ability of **3** to interact with GBP at the air-water interface was investigated by means of Langmuir compression isotherms and surface ellipsometry. The profile of the isotherm of **3** on pure water is significantly different from that on a 10^{-5} M aqueous GBP subphase. The thickness measured for the fully compressed monolayer of **3**, i.e. π = 45 mN m^{-1}, on a 10^{-5} M aqueous GBP solution is higher than that on pure water. These results unambiguously demonstrate that the monomolecular film of **3** interacts with GBP at the air-water interface.

The structure of the monolayer of **3** on pure water and on a 10^{-5} M aqueous GBP subphase was investigated by GIXD. The measurements indicate that the partially compressed monolayer, i.e. π = 25 mN m^{-1}, on pure water is mostly amorphous. On the other hand, the fully compressed monolayer, i.e. π = 45 mN m^{-1}, on pure water possesses a highly crystalline phase that coexists with an amorphous phase. When GBP is added in the subphase, the structure of the monolayer is similar to that on pure water, suggesting that the interaction of the monolayer with the API does not affect the packing of the aliphatic chains of the macrocycle.

The ability of the monolayer of **3** to act as template for the crystallization of GBP at the air-water interface was further studied. It has been found that, in the presence of the monolayer of **3**, the anhydrous forms of GBP are crystallized while, in the absence of the monolayer of **3**, the hydrate form of GBP grows. This result demonstrates the templating effect of the monomolecular film of **3** on the nucleation of GBP at the air-water interface. For the first time, the modulation of the packing density of the macrocycles within the monolayer was demonstrated to exert a control over the polymorphism of GBP. Indeed, while the partially compressed monolayer kicks off the crystallization of the polymorphic form γ, the fully compressed monolayer acts as template for the crystallization of the polymorphic form α.

3.2 Interfacial binding of divalent cations to calix[4]arene-based Langmuir monolayers

3.2.1 Langmuir compression isotherms

The amphiphile **3** was synthesized as shown in chapter 3.1.1. The self-assembly properties of the monolayer of **3** on pure water were investigated by means of Langmuir compression isotherms. The compression isotherm of **3** on pure water shows a π_c value of 51 ± 1 mN m^{-1} and an A_0 value of 122 ± 1 $Å^2$ $molecule^{-1}$. Moreover, a phase transition at a surface pressure value of 39 ± 1 mN m^{-1} is observed, in perfect agreement with the results shown in chapter 3.1.2 (Figure 3.8).

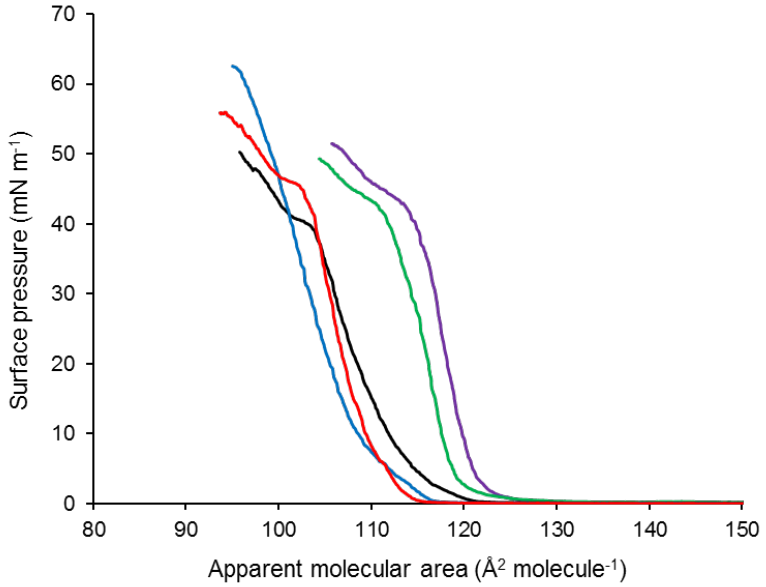

Figure 3.8. Compression isotherms of **3** on pure water (–) and on 10^{-5} M aqueous $CuCl_2$ (–), $CoCl_2$ (–), $NiCl_2$ (–) and $MnCl_2$ (–) subphases.

The self-assembly properties of the monolayer **3** on aqueous solutions of $CuCl_2$, $CoCl_2$, $NiCl_2$ and $MnCl_2$ were investigated by means of Langmuir compression isotherms. The experiments were performed at salts concentrations of 10^{-5} and 10^{-3} M. To avoid potential counterion effects, the

counterion Cl^- was kept constant through the all series of salts.[105] In the presence of $NiCl_2$ and $MnCl_2$ dissolved in the aqueous subphase at a concentration of 10^{-5} M, the A_0 (A_0 = 126 and 125 ± 1 Å^2 molecule^{-1}, respectively) and π_c (π_c = 51 ± 1 mN m^{-1}) values of the isotherms of **3** are similar to those on pure water (A_0 = 122 ± 1 Å^2 molecule^{-1}; π_c = 51 ± 1 mN m^{-1}), cf. Figure 3.8 and Table 1.

Table 1. Characteristic values of the isotherms of **3** on pure water and on 10^{-5} M aqueous $CuCl_2$, $CoCl_2$, $NiCl_2$ and $MnCl_2$ solutions.

Subphase	π_c	A_c	A_{lim}	A_0	$\delta\pi/\delta A$
Pure water	51 ± 1	95 ± 1	115 ± 1	122 ± 1	3.9 ± 0.2
$CuCl_2$	62 ± 1	96 ± 1	110 ± 1	116 ± 1	4.4 ± 0.2
$CoCl_2$	55 ± 1	97 ± 1	110 ± 1	113 ± 1	6.1 ± 0.2
$NiCl_2$	51 ± 1	104 ± 1	119 ± 1	126 ± 1	5.5 ± 0.2
$MnCl_2$	51 ± 1	105 ± 1	121 ± 1	125 ± 1	6.6 ± 0.2

Π_c and A_c represent the maximum values of pressure and area to which, after further compression of the monolayer, the amphiphile is forced out of the interface. A_{lim} is the extrapolation of the linear part of the isotherm on the x-axis. A_0 is the area occupied by one molecule at the isotherm takeoff. $|\delta\pi/\delta A|$ is the modulus of the slope on the steepest part of the monolayer.

On the other hand, the limiting area (A_{lim}) and A_c values of the isotherms of **3** on the aqueous $NiCl_2$ and $MnCl_2$ subphases at a concentration of 10^{-5} M (A_{lim} = 119 and 121 ± 1 Å^2 molecule^{-1}, respectively; A_c = 104 and 105 ± 1 Å^2 molecule^{-1}, respectively) are slightly higher than those on pure water (A_{lim} = 115 ± 1 Å^2 molecule^{-1}; A_c = 95 ± 1 Å^2 molecule^{-1}). These results indicate that the monolayer of **3** interacts with Ni^{2+} and Mn^{2+} ions at the air-water interface. When $CoCl_2$ was dissolved in the aqueous subphase at the same concentration of 10^{-5} M, the A_c value of the isotherm of **3** (A_c = 97 ± 1 Å^2 molecule^{-1}) is almost identical to that on pure water (A_c = 95 ± 1 Å^2 molecule^{-1}), cf. Figure 3.8. On the contrary, the A_{lim} and A_0 values (A_{lim} = 110 ± 1 Å^2 molecule^{-1}; A_0 = 113 ± 1 Å^2 molecule^{-1}) of the isotherm of **3** on the aqueous $CoCl_2$ solution (10^{-5} M) are lower

than those on pure water (A_{lim} = 115 ± 1 Å^2 molecule^{-1}; A_0 = 122 ± 1 Å^2 molecule^{-1}) while π_c (π_c = 55 ± 1 mN m^{-1}) is higher than that on pure water (π_c = 51 ± 1 mN m^{-1}). These data reveal that the self-assembly properties of the monolayer of **3** are affected by Co^{2+} ions dissolved in the aqueous solution. In addition, the modulus of the slope of the steepest portion of the isotherm values ($|\delta\pi/\delta A|$) for the monolayer of **3** on the aqueous Co^{2+}, Ni^{2+} and Mn^{2+} ions subphases (10^{-5} M) are higher ($|\delta\pi/\delta A|$ = 6.1, 5.5 and 6.6 ± 0.2 mN m^{-1}/Å^2 molecule^{-1}, respectively) than that measured on pure water ($|\delta\pi/\delta A|$ = 3.9 ± 0.2 mN m^{-1}/Å^2 molecule^{-1}), cf. Table 1. These results indicate that the binding of the monolayer of **3** with Co^{2+}, Ni^{2+} and Mn^{2+} ions at the air-water interface produces more rigid monomolecular films.

When $CuCl_2$ is added in the aqueous subphase at a concentration of 10^{-5} M, the A_c value of the isotherm of **3** (A_c = 96 ± 1 Å^2 molecule^{-1}) is essentially identical to that on pure water (A_c = 95 ± 1 Å^2 molecule^{-1}), cf. Figure 3.8. On the other hand, the $|\delta\pi/\delta A|$ increases from a value of 3.9 on pure water to 4.4 ± 0.2 mN m^{-1}/Å^2 molecule^{-1} while the A_0 and A_{lim} values decrease to 116 and 110 ± 1 Å^2 molecule^{-1} from 122 and 115 ± 1 Å^2 molecule^{-1} on pure water, respectively. Remarkably, the π_c value significantly increases from a value of 51 on pure water to 62 ± 1 mN m^{-1} on the aqueous $CuCl_2$ subphase; such a collapse pressure value is considerably high for a monolayer formed by a calixarene derivative. Moreover, the phase transition showed by the isotherm of **3** on pure water is not any longer observed on the aqueous $CuCl_2$ solution (Figure 3.8). This set of results clearly demonstrates that the monolayer of **3** binds the cations at the air-water interface at relatively low concentration of Cu^{2+} ions (10^{-5} M) in the aqueous subphase.

In chapter 3.1.1, it has been shown that **3** possesses a pinched cone conformation in the solid state, where two distal aromatic rings are parallel with one another while the other two are splayed outwards. The expansion of the ASU revealed that the amphiphiles are organized in a bilayer fashion with the carboxylic functions of adjacent molecules of **3** arranged side-by-side. In the present case, when the divalent ions are dissolved in the aqueous subphase, the carboxylic

moieties of adjacent macrocycles self-assembled as Langmuir monolayers at the air-water interface are presumably arranged head-by-head. As a result, the ions are expected to be bound by two carboxylic groups of adjacent amphiphiles and two water molecules, in cis position around the central ion, via a distorted octahedral coordination geometry. The geometric constraint of the macrocycle rules out the presence of a 1:1 complex between **3** and the ions. Such coordination geometry has been already observed for solid-state Cu (II), Co (II), Ni (II) and Mn (II)-carboxylate complexes.[122-125] Chen reported on the crystal structure of $[Cu_2$(biphenyl-4,4′-dicarboxylate$)_2$(1,10-phenanthroline$)_2(H_2O)]_2 \cdot 2H_2O$.[125] The distance between two adjacent carboxylates that bind Cu^{2+} is 3.2 Å; this distance is slightly higher than the sum of the van der Waals radii of the two oxygen atoms (3 Å). No shift towards higher A_0 values of the isotherm of **3** on a 10^{-5} M aqueous $CuCl_2$ subphase is expected when compared to that on pure water, thus in agreement with the Langmuir compression isotherms results.

In the presence of 10^{-3} M aqueous Ni^{2+}, Mn^{2+} and Co^{2+} ions subphases, the A_0 (A_0 = 120, 120 and 121 ± 1 Å^2 molecule^{-1}, respectively) and A_c (A_c = 97, 97 and 98 ± 1 Å^2 molecule^{-1}, respectively) values of the isotherms of **3** are highly similar to those on pure water (A_0 = 122 ± 1 Å^2 molecule^{-1}; A_c = 95 ± 1 Å^2 molecule^{-1}), cf. Figure 3.9 and Table 2.

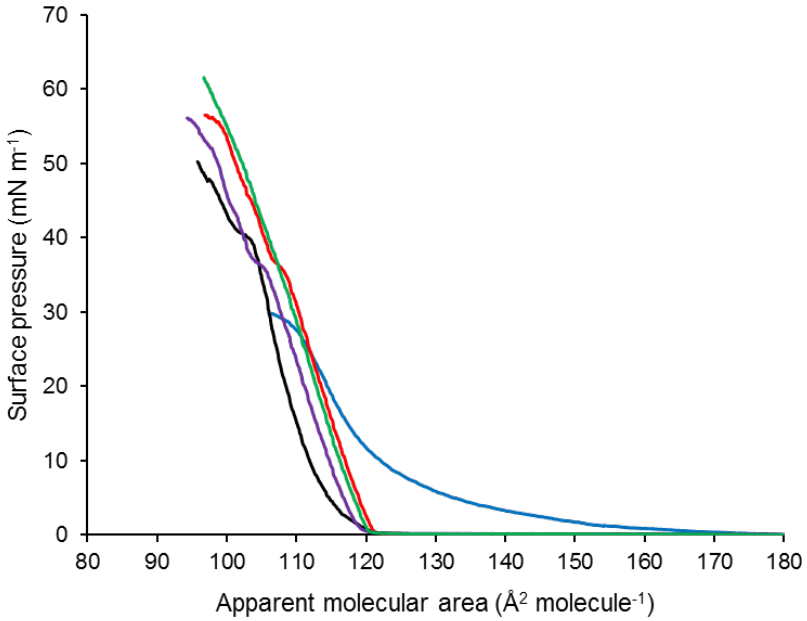

Figure 3.9. Compression isotherms of **3** on pure water (–) and on 10^{-3} M aqueous $CuCl_2$ (–), $CoCl_2$ (–), $NiCl_2$ (–) and $MnCl_2$ (–) subphases.

Table 2. Characteristic values of the isotherms of **3** on pure water and on 10^{-3} M aqueous $CuCl_2$, $CoCl_2$, $NiCl_2$ and $MnCl_2$ solutions.

Subphase	π_c	A_c	A_{lim}	A_0	$\delta\pi/\delta A$
Pure water	51 ± 1	95 ± 1	115 ± 1	122 ± 1	3.9 ± 0.2
$CuCl_2$	29 ± 1	109 ± 1	125 ± 1	174 ± 1	1.3 ± 0.2
$CoCl_2$	56 ± 1	98 ± 1	120 ± 1	121 ± 1	3 ± 0.2
$NiCl_2$	60 ± 1	97 ± 1	120 ± 1	121 ± 1	2.9 ± 0.2
$MnCl_2$	56 ± 1	97 ± 1	119 ± 1	120 ± 1	2.8 ± 0.2

Π_c and A_c represent the maximum values of pressure and area to which, after further compression of the monolayer, the amphiphile is forced out of the interface. A_{lim} is the extrapolation of the linear part of the isotherm on the x-axis. A_0 is the area occupied by one molecule at the isotherm takeoff. $|\delta\pi/\delta A|$ is the modulus of the slope on the steepest part of the monolayer.

On the contrary, the A_{lim} (A_{lim} = 120, 119 and 120 ± 1 Å^2 molecule^{-1} respectively) and π_c (π_c = 60, 56 and 56 mN m^{-1}, respectively) values of the isotherms of **3** on the aqueous Ni^{2+}, Mn^{2+} and Co^{2+} ions solutions (10^{-3} M) are higher than those observed on pure water (A_{lim} = 115 ± 1 Å^2 molecule^{-1}; π_c = 51 ± 1 Å^2 molecule^{-1}). In addition, the $|\delta\pi/\delta A|$ values of the isotherms of **3** on the aqueous Ni^{2+}, Mn^{2+} and Co^{2+} ions subphases (10^{-3} M) are lower ($|\delta\pi/\delta A|$ = 2.9, 2.8 and 3 ± 0.2 mN m^{-1}/Å^2 molecule^{-1} respectively) with respect to that measured on pure water ($|\delta\pi/\delta A|$ = 3.9 ± 0.2 mN m^{-1}/Å^2 molecule^{-1}), cf. Table 2. These results suggest that the interfacial interaction of **3** with the ions causes an expansion of the monomolecular film. Interestingly, the surface pressure of the isotherms of **3** on the aqueous 10^{-3} M Ni^{2+}, Mn^{2+} and Co^{2+} ions subphases rise steadily after the takeoff. This strongly suggests that the ions trigger the interfacial self-assembly of the amphiphiles prior to compression with the formation of relatively large liquid-like domains.

The isotherm profile of **3** on a 10^{-3} M aqueous $CuCl_2$ subphase drastically differs from that on pure water. The A_{lim} and A_c values of the isotherm of **3** on the aqueous Cu^{2+} ions subphase (10^{-3} M) increase up to 125 and 109 ± 1 Å^2 molecule^{-1}, respectively (A_{lim} = 115 and A_c = 95 ± 1 Å^2

molecule^{-1} on pure water), cf. Figure 3.9. Interestingly, the A_0 value of the isotherm of **3** on the aqueous Cu^{2+} ions subphase significantly increases to 174 ± 1 Å^2 molecule^{-1} (A_0 = 122 ± 1 Å^2 molecule^{-1} on pure water) while the π_c considerably decreases to 29 mN m^{-1} (π_c = 51 ± 1 mN m^{-1} on pure water). In addition, the $|\delta\pi/\delta A|$ value of the isotherm of **3** on the aqueous Cu^{2+} ions subphase (10^{-3} M) drops to 1.3 ± 0.2 mN m^{-1}/Å^2 molecule^{-1} ($|\delta\pi/\delta A|$ = 3.9 ± 0.2 mN m^{-1}/Å^2 molecule^{-1} on pure water), cf. Figure 3.9 and Table 2. The drastic difference in the isotherm profile of **3** on a 10^{-3} M aqueous Cu^{2+} ions solution in comparison with those on the aqueous Ni^{2+}, Mn^{2+} and Co^{2+} subphases, at the same concentration of 10^{-3} M, suggests that copper clusters are formed contiguous to the monolayer.

3.2.2 BAM measurements

The morphology of the monolayer of **3** on pure water and on aqueous $CuCl_2$, $CoCl_2$, $NiCl_2$ and $MnCl_2$ subphases at concentrations of 10^{-5} and 10^{-3} M was investigated by BAM. The micrographs revealed that **3** on pure water, before the isotherm takeoff, self-assembles in the form of relatively large liquid-like domains, cf. Figure 3.10. It is known that Langmuir monolayers of amphiphilic calixarenes, after the isotherm takeoff (π = 1 mN m^{-1}), typically show uniform texture with the absence of visible structuring.[126,127] In the present case, the monolayer of **3** lacks homogeneity. Indeed, for surface pressure values higher than 0.1 mN m^{-1}, the monolayer consists of domains of different contrasts. Such morphology is maintained until the collapse of the monomolecular film (Figure 3.10).

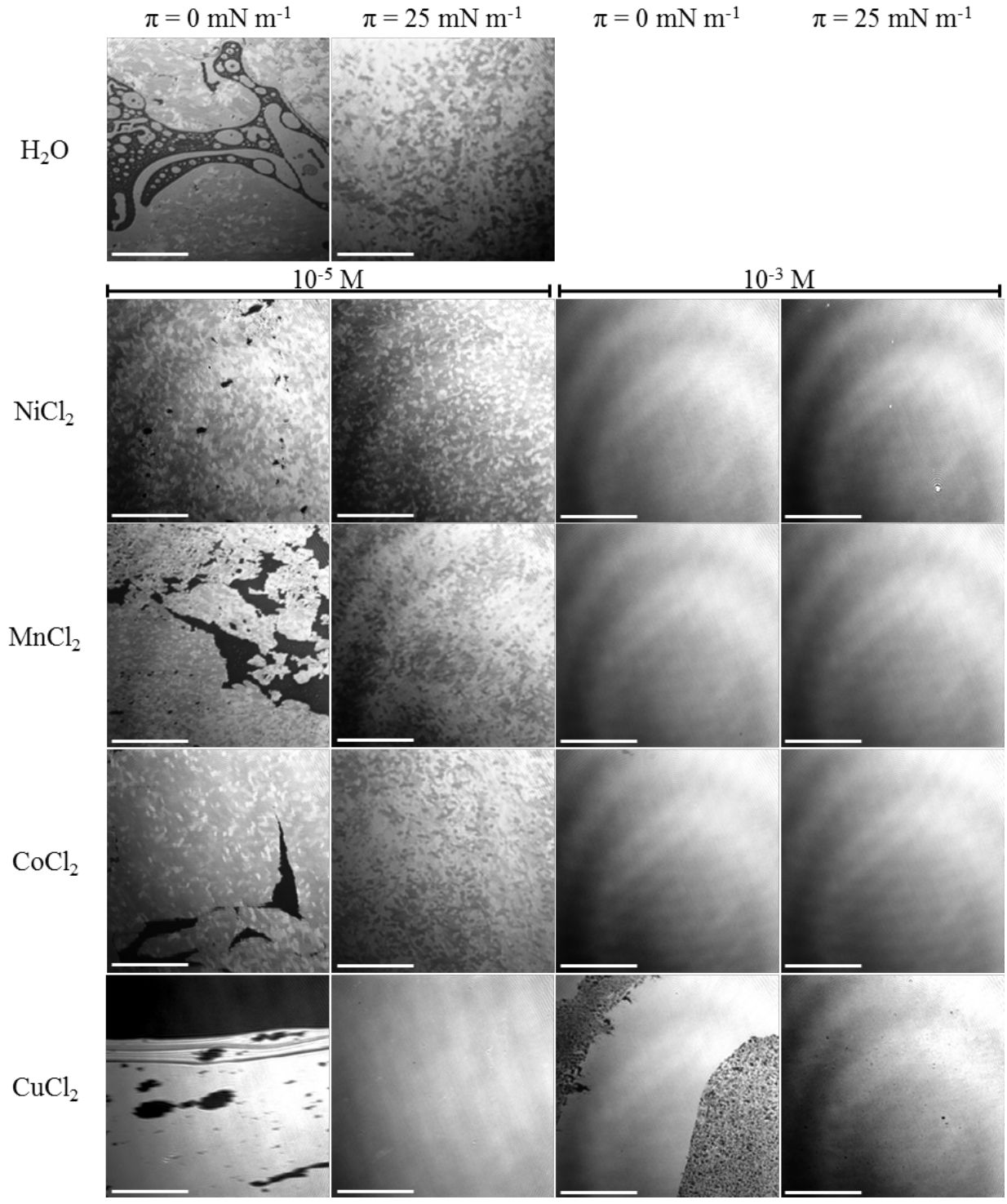
π = 0 mN m-1
π = 25 mN m-1
π = 0 mN m-1
π = 25 mN m-1
H2O
10-5 M
10-3 M
NiCl2
MnCl2
CoCl2
CuCl2

Figure 3.10. BAM micrographs of the monomolecular film of **3** on pure water and on aqueous $CuCl_2$, $CoCl_2$, $NiCl_2$ and $MnCl_2$ subphases at concentrations of 10^{-3} and 10^{-5} M. Scale bar = 100 μm (Reproduced with permission from ref. 128, Copyright 2015, American Chemical Society).

When $CoCl_2$, $NiCl_2$ and $MnCl_2$ are added in the aqueous subphase at a concentration of 10^{-5} M, the morphology of the monolayer of **3** appears similar to that on pure water (Figure 3.10). Domains of different contrast can be observed and are maintained until the collapse of the monolayer. These results indicate that the interactions of **3** with Co^{2+}, Ni^{2+} and Mn^{2+} ions at the air-water interface do not affect the morphology of the monolayer. On the contrary, in the presence of Cu^{2+} ions in the aqueous solution at the same concentration (10^{-5} M), the texture of the monomolecular film of **3** radically changes (Figure 3.10). Indeed, at the isotherm takeoff, the monolayer appears homogeneous and such texture is maintained until the collapse of the film. These data reveal that Cu^{2+} ions, added in the aqueous solution at a concentration of 10^{-5} M, significantly affect the microscopic properties of the monolayer of **3**.

At a higher concentration (10^{-3} M) of $CoCl_2$, $NiCl_2$ and $MnCl_2$ dissolved in the aqueous solution, the morphology of the monolayers of **3** is different from that on pure water (Figure 3.10). Indeed, the monolayers are highly homogeneous already before the takeoff of the isotherms. These results suggest that the studied ions favor the self-assembly process of the amphiphiles at the air-water interface so as to form dense domains prior to compression, therefore consistent with the Langmuir compression isotherms results. In the presence of an aqueous $CuCl_2$ subphase at a concentration of 10^{-3} M, the monolayer of **3** is not highly homogeneous, cf. Figure 3.10. The monolayer exhibits an irregular texture and turns highly homogeneous only at the monomolecular film collapse. These results confirm that the microscopic properties of the monolayer of **3** on the aqueous $CuCl_2$ subphases (10^{-5} M and 10^{-3} M) are significantly different from those on aqueous $CoCl_2$, $NiCl_2$ and $MnCl_2$ solutions at the same concentration values.

3.2.3 Synchrotron-based X-ray diffraction analyses

Synchrotron-based XNTRF, XRR and GIXD measurements of the monolayer of **3** on pure water and on aqueous $CuCl_2$ and $CoCl_2$ subphases were conducted in order to gain further insights into the interfacial behavior of the amphiphiles. XNTRF measurements show that, in the presence of 1.4×10^{-3} M aqueous $CuCl_2$ and 10^{-3} M aqueous $CoCl_2$ solutions in the absence of the monolayer of **3**, the emission lines of the cations are barely detectable, cf. Figure 3.11.

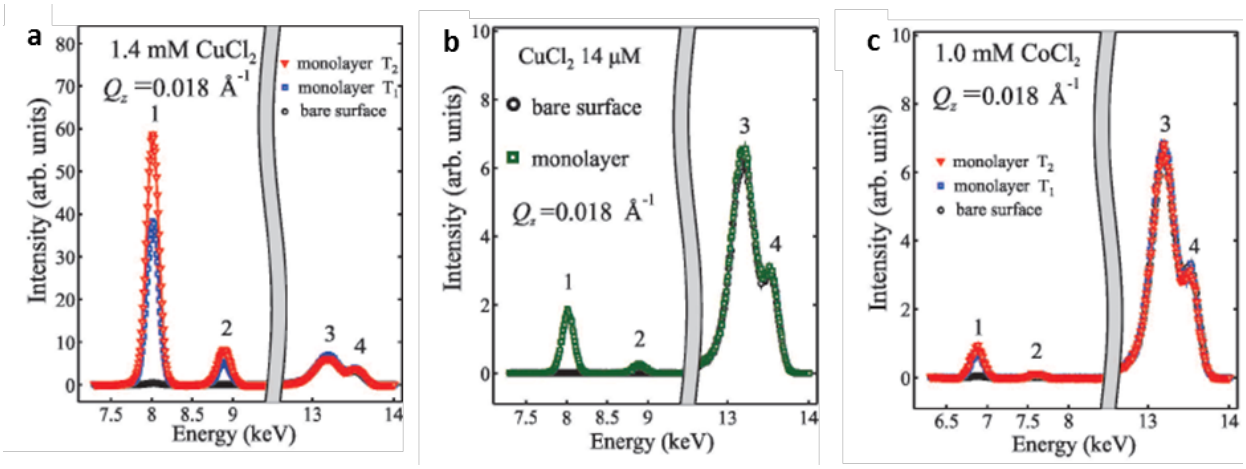

Figure 3.11. XNTRF spectra in the presence and absence of the monolayer of **3** for 1.4×10^{-3} M aqueous $CuCl_2$ (**a**), 1.4×10^{-5} M aqueous $CuCl_2$ (**b**) and 10^{-3} M aqueous $CoCl_2$ (**c**) subphases. The shaded bands in a-c block the unessential part of the spectra. In **a** and **c**, two measurements were sequentially conducted at time intervals T_1 and T_2, respectively, with a time interval $(T_2 - T_1) = 1$ hour. Numerical labels 1 and 2 denote the K_α and K_β emission lines, respectively, from Cu^{2+} and Co^{2+} surfaces. Label 3 represents the Compton scattering while label 4 the Thomson scattering. Label 3 and 4 are the result of the interaction of X-ray radiations, water and helium (Reproduced with permission from ref. 128, Copyright 2015, American Chemical Society).

In the absence of the monolayer of **3**, the intensities of the characteristic emission lines of Cu^{2+} and Co^{2+} ions are barely detectable as the density of the cations within the penetration depth close to the surface is lower than the detection limit of the instrument. On the contrary, when

the monolayer of **3** is spread at the air-water interface and compressed to a surface pressure value of 20 mN m^{-1} emission lines for both ions are visible as a consequence of Cu^{2+} and Co^{2+} ions surface enrichment (Figure 3.11). XNTRF experiments revealed that the intensity of the emission lines for Cu^{2+} ions are around 25-38 times higher than those for Co^{2+} ions. These results clearly demonstrate that the monolayer of **3** binds more to Cu^{2+} than Co^{2+} ions. In the presence of an aqueous $CuCl_2$ subphase at a concentration of 1.4×10^{-5} M, XNTRF measurements showed that the monomolecular film of **3** binds to Cu^{2+} ions, cf. Figure 3.11. The intensities of the emission lines for Cu^{2+} ions, added in the aqueous subphase at a concentration of 1.4×10^{-5} M, are ca. 20-30 times lower than those detected at higher concentration of the cations (1.4×10^{-3} M). In addition, the intensities of the emission lines for Cu^{2+} ions detected at a concentration of 1.4×10^{-5} M are comparable with those observed for Co^{2+} ions dissolved in the aqueous subphase at a concentration of 10^{-3} M. These results confirm the high interfacial affinity of the monolayer of **3** towards Cu^{2+} ions. The emission line intensities for Cu^{2+} ions increase over time, thus suggesting the constant aggregation of the cations beneath the monolayer of **3**. On the contrary, the interfacial binding of Co^{2+} ions was demonstrated to be time-independent. XNTRF provided a qualitative analysis of the Cu^{2+} and Co^{2+} ions surface enrichment underneath Langmuir monolayers of **3**. By using a molecular area value of 115 $Å^2$ $molecule^{-1}$ extrapolated from the compression isotherms, XNTRF measurements revealed that 4.6 ± 1.2 Cu^{2+} ions are bound to one molecule of **3**, corresponding to 1.2 ± 0.3 ions per carboxylic group of **3**. On the other hand, one molecule of **3** binds 0.15 Co^{2+} ions.

XRR measurements shows that the Q'_z value, i.e. the *z*-component (surface normal) of the scattering vector, of the monolayer of **3** on an aqueous $CoCl_2$ solution at a concentration of 10^{-3} M, compressed to a surface pressure value of 20 mN m^{-1}, barely changes with respect to that on pure water (Figure 3.12).

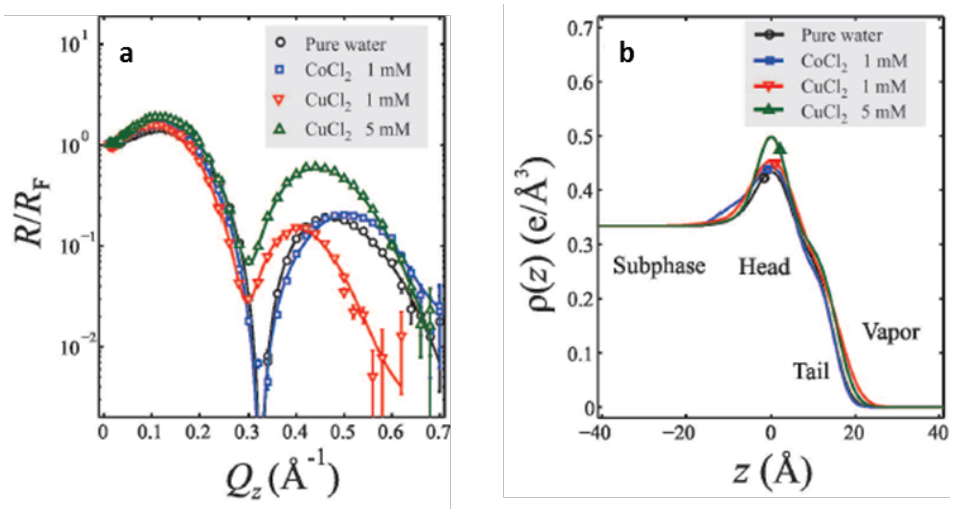

Figure 3.12. Reflectivity data (R) normalized to the Fresnel reflectivity (R_F), R/R_F, of the monomolecular film of **3** on pure water, on 10^{-3} M aqueous $CuCl_2$ and $CoCl_2$ subphases and on a 5×10^{-3} M aqueous $CuCl_2$ solution (**a**). Corresponding best-fit electron density profiles across the interfaces (**b**) [Reproduced with permission from ref. 128, Copyright 2015, American Chemical Society].

The fact that the Q'_z value for the monolayer of **3** on the aqueous $CoCl_2$ subphase is similar to that on pure water demonstrates that the amphiphiles are weakly bound to Co^{2+} ions. On the contrary, in the presence of a 10^{-3} M aqueous $CuCl_2$ subphase, the Q'_z value of the monolayer of **3** is shifted to a lower value of 0.3 $Å^{-1}$ (Figure 3.12). This result shows that the monolayer becomes thicker and therefore indicates that a strong interaction between the macrocycle and Cu^{2+} ions occurs at the air-water interface. For higher concentrations of $CuCl_2$, the thickness of the monolayer does not further increase, thus suggesting that the monomolecular film approaches Cu^{2+} ions binding saturation.

GIXD analyses were conducted in order to determine the structure of **3** on the aqueous Co^{2+} and Cu^{2+} ions solutions. The diffraction pattern of the monolayer of **3** compressed to a surface pressure value of 20 mN m^{-1} on pure water shows a broad peak at ca. Q_{xy} = 1.4 $Å^{-1}$, cf. Figure 3.13.

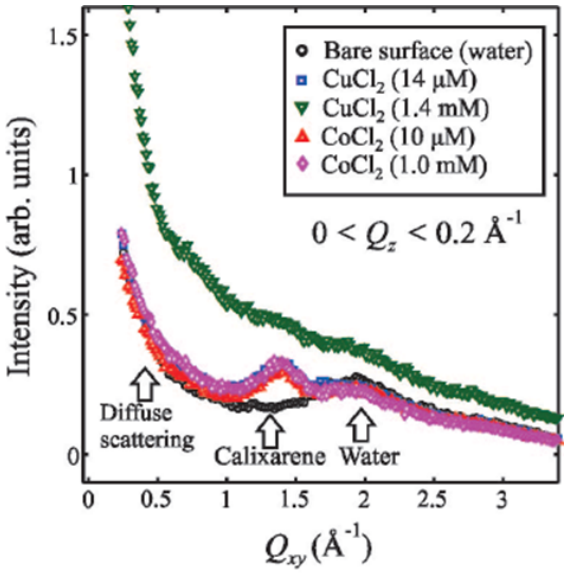

Figure 3.13. Integrated GIXD data over Q_z as a function of Q_{xy} for the monolayer of **3** on pure water, on 1.4×10^{-5} and 10^{-3} M aqueous $CuCl_2$ subphases and on 10^{-5} and 10^{-3} M aqueous $CoCl_2$ solutions, respectively (Reproduced with permission from ref. 128, Copyright 2015, American Chemical Society).

The broad peak shown by the diffraction spectrum of the monolayer of **3** on pure water is attributed to the presence of a liquid-like phase generated by the C_{12} chains of the macrocycle. These results are consistent with those previously discussed in chapter 3.1.2 for the structure of the same monomolecular film on pure water. On an aqueous subphase containing $CuCl_2$ at a concentration of 1.4×10^{-3} M, the GIXD pattern of the monolayer, compressed to a surface pressure value of 20 mN m^{-1}, drastically changes when compared with that on pure water (Fig 3.13). These results are ascribed to the formation of sporadic non-uniform clusters of Cu^{2+} ions contiguous to the monolayer of **3**. Such clusters increase the surface roughness and enhance the diffuse scattering from the surface. When $CoCl_2$ was added into the aqueous subphase at a concentration of 10^{-3} M, the diffraction pattern of the monomolecular film of **3** appears fairly similar to that observed on pure water, therefore suggesting that the interfacial interaction between the amphiphiles and Co^{2+} ions do not affect the order of the hydrocarbon chains

(Figure 3.13). These results indicate that the structure of the monolayer of **3** is significantly affected by Cu^{2+} ions at the air-water interface.[128]

3.2.4 Conclusions

The ability of the monolayer of **3** to interact with a series of divalent fourth-period transition metal ions at the air-water interface was investigated by means of Langmuir compression isotherms and BAM. Compression isotherms indicated that the monolayer of **3** interacts with Cu^{2+}, Co^{2+}, Ni^{2+} and Mn^{2+} ions at the air-water interface even at a relatively low concentration of the ions in the aqueous subphase, i.e. 10^{-5} M. At a higher concentration, i.e. 10^{-3} M, the isotherm profile of **3** on the aqueous Cu^{2+} solution is considerably different with respect to those measured on aqueous Co^{2+}, Ni^{2+} and Mn^{2+} subphases. This result is attributed to the formation of Cu^{2+} clusters contiguous to the monomolecular film of **3**.

BAM measurements revealed that the morphology of the monolayers of **3** on 10^{-5} M aqueous Co^{2+}, Ni^{2+} and Mn^{2+} solutions is highly similar to that on pure water. On the contrary, the texture of the monolayer of **3** on a 10^{-5} M aqueous Cu^{2+} subphase is drastically different from that on pure water. When the ions are dissolved in the aqueous subphase at a concentration of 10^{-3} M, the texture of the monolayer of **3** on the Cu^{2+} subphase appears different from that on Co^{2+}, Ni^{2+} and Mn^{2+} solutions. This set of results indicates that the microscopic properties of the monolayer of **3** are significantly affected by Cu^{2+} ions.

Synchrotron-based X-ray diffraction measurements were performed to shed light on the affinity of the monolayer of **3** towards Cu^{2+} and Co^{2+} ions. X-ray reflectivity revealed that the intensity of the emission lines for Cu^{2+} ions are 25-30 times higher than those for Co^{2+} ions. In addition, unlike Co^{2+} ions, the intensity of the emission lines for Cu^{2+} ions are time-dependent, therefore suggesting a constant aggregation of Cu^{2+} ions beneath the monolayer of **3**. GIXD measurements indicated that the diffraction pattern of the monolayer of **3** on a 1.4×10^{-3} M aqueous Cu^{2+} subphase is significantly different from that on pure water. This result is ascribed to the formation of non-uniform clusters of Cu^{2+} ions underneath the monomolecular film of **3**. On the other hand, no relevant changes are observed in the diffraction pattern of the monolayer of **3**

on a 10^{-3} M aqueous Co^{2+} ions subphase. These data unambiguously demonstrate the monomolecular film of **3** binds more to Cu^{2+} than Co^{2+} ions at the air-water interface.

3.3 Selective binding of mercury chloride to calix[4]arene-based Langmuir monolayers

3.3.1 Langmuir compression isotherms

A series of amphiphilic amino-substituted calix[4]arene derivatives bearing dodecyl alkyl chains on the lower rim, namely 5,11,17,23-tetraamino-tetrakis(dodecyloxy)-calix[4]arene (**4**), 5,11-diamino-tetrakis(dodecyloxy)-calix[4]arene (**5**) and 5,17diamino-tetrakis(dodecyloxy)-calix[4]arene (**6**) were synthesized by others in our group, cf. Figure 3.14.[129]

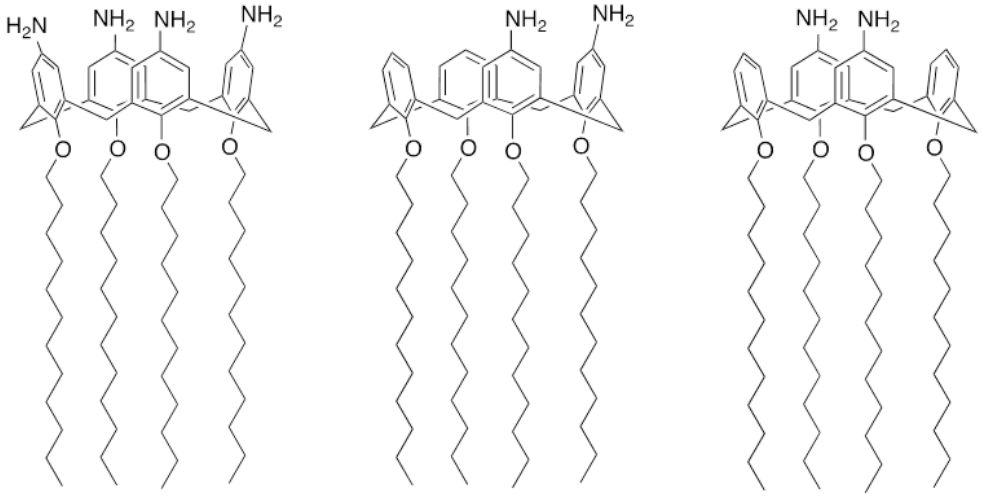

4 **5** **6**

Figure 3.14. Chemical structures of **4**, **5** and **6**.

The self-assembly properties of **4**, **5** and **6** on pure water and on a 10^{-3} M aqueous $HgCl_2$ solution were investigated by Langmuir compression isotherms. The π_c, A_c, A_{lim} and A_0 values of the isotherm of **4** on pure water are 44 mN m^{-1}, 94, 107 and 112 ± 1 $Å^2$ $molecule^{-1}$, respectively; these values are in agreement with those reported in the literature (Figure 3.15).[84]

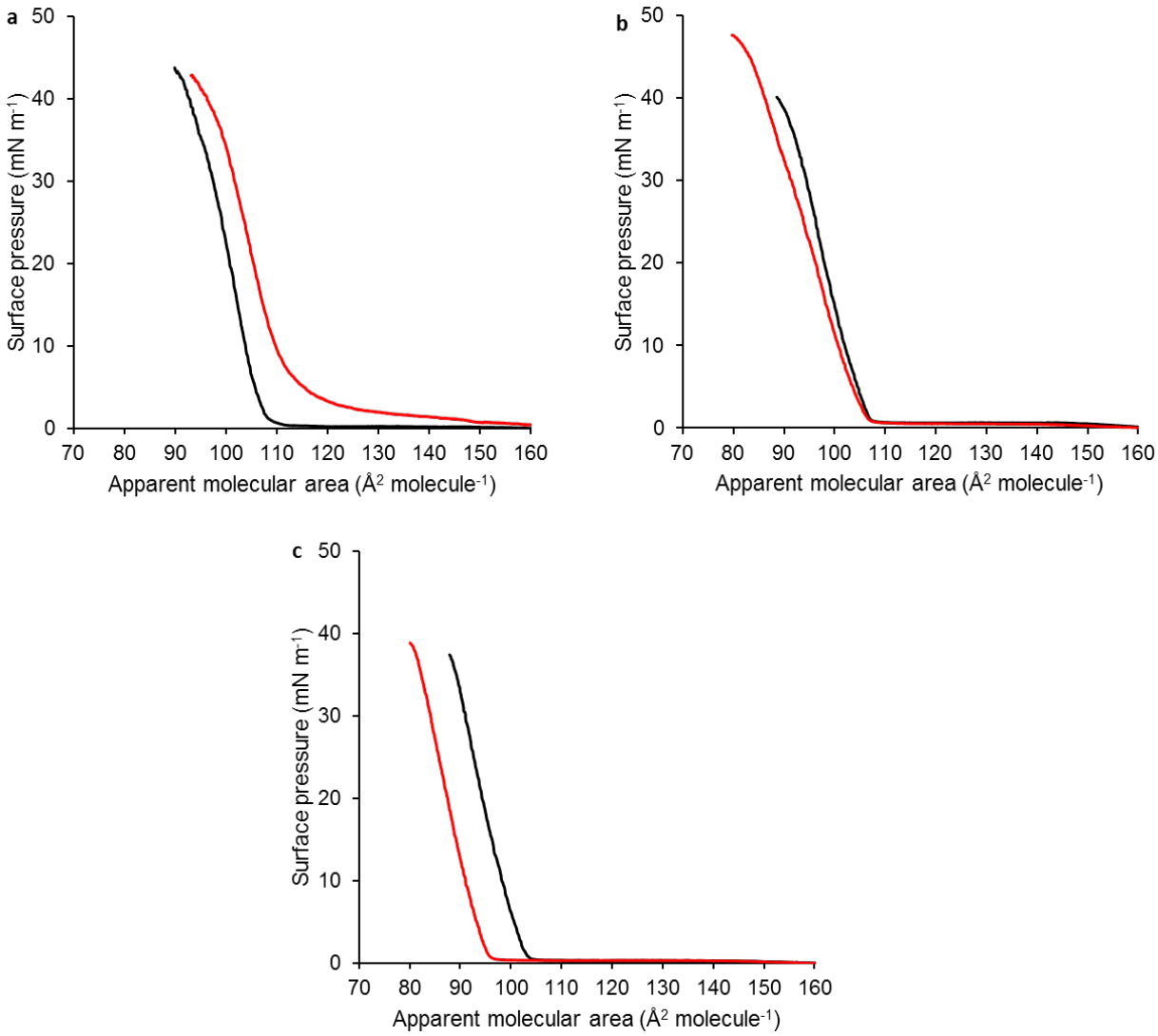

Figure 3.15. Surface pressure-area compression isotherms of **4** (**a**), **5** (**b**) and **6** (**c**) on pure water (–) and on a 10^{-3} M aqueous $HgCl_2$ solution (–).

The A_{lim} value of 107 ± 1 Å^2 molecule^{-1} is consistent with the presence of the calix[4]arene macrocycle, self-assembled as a Langmuir monolayer at the air-water interface, with the pseudo C_4 symmetry axis perpendicular to the interface. The isotherms of **5** and **6** on pure water reveal that, despite the presence of only two amino functions, both the amphiphiles self-assemble as stable monomolecular films at the air-water interface (Figure 3.15). The A_{lim} values of the

isotherms of **5** and **6** on pure water are 105 and 102 ± 1 $Å^2$ $molecule^{-1}$, respectively, similar to that of the isotherm of **4** on pure water (A_{lim} = 107 ± 1 $Å^2$ $molecule^{-1}$). These results indicate that **5** and **6** self-assemble as stable Langmuir monolayers at the air-water interface with the plane of the macrocycles, i.e. the plane that passes through the arene centroids, oriented parallel to the water surface, i.e. with the headgroups immersed into the water subphase and the aliphatic chains that point into air. The A_c and A_0 values of the isotherms of **5** (A_c = 91 ± 1 $Å^2$ $molecule^{-1}$; A_0 = 107 ± 1 $Å^2$ $molecule^{-1}$) and **6** (A_c = 90 ± 1 $Å^2$ $molecule^{-1}$; A_0 = 105 ± 1 $Å^2$ $molecule^{-1}$) on pure water are similar to those of **4** (A_c = 94 ± 1 $Å^2$ $molecule^{-1}$; A_0 = 112 ± 1 $Å^2$ $molecule^{-1}$), cf. Figure 3.15. On the contrary, the π_c values of **5** (π_c = 39 ± 1 mN m^{-1}) and **6** (π_c = 38 ± 1 mN m^{-1}) on pure water are considerably lower than that of **4** (π_c = 44 ± 1 mN m^{-1}), cf. Table 3.

Table 3. Characteristic values of the isotherms of **4**, **5** and **6** on pure water and on 10^{-3} M aqueous $HgCl_2$ solution.

	π_c	A_c	A_l	A_0
4 on water	43 ± 1	94 ± 1	107 ± 1	112 ± 1
4 on 10^{-3} M $HgCl_2$	42 ± 1	97 ± 1	113 ± 1	150 ± 1
5 on water	39 ± 1	91 ± 1	105 ± 1	107 ± 1
5 on 10^{-3} M HgCl2	46 ± 1	83 ± 1	106 ± 1	107 ± 1
6 on water	38 ± 1	90 ± 1	102 ± 1	105 ± 1
6 on 10^{-3} M HgCl2	38 ± 1	82 ± 1	94 ± 1	96 ± 1

Π_c and A_c represent the maximum values of pressure and area to which, after further compression of the monolayer, the amphiphile is forced out of the interface. A_{lim} is the extrapolation of the linear part of the isotherm on the x-axis. A_0 is the area occupied by one molecule at the isotherm takeoff.

The lower π_c values of **5** and **6** in comparison with that of **4** is attributed to the presence of only two polar functions at the *p*-positions of **5** and **6** with respect to the four headgroups of **4**. The reduced number of polar functions causes the decrease of the hydrophilic/lipophilic balance of the amphiphiles **5** and **6** and, as a consequence, a decrease in the stabilization of the monolayers of **5** and **6** in comparison with that of **4**.

When $HgCl_2$ is added in the aqueous subphase at a concentration of 10^{-3} M, the isotherm profile of **4** is different with regard to that measured on pure water, cf. Figure 3.15. The π_c value of the isotherm of **4** on the aqueous $HgCl_2$ subphase slightly decreases to 42 ± 1 mN m^{-1} in comparison with that on pure water (π_c = 44 ± 1 mN m^{-1}). The A_c and A_{lim} values of the isotherm of **4** on the aqueous $HgCl_2$ subphase (A_c = 97 ± 1 Å^2 $molecule^{-1}$; A_{lim} = 113 ± 1 Å^2 $molecule^{-1}$) are similar to those on pure water (A_c = 94 ± 1 Å^2 $molecule^{-1}$; A_{lim} = 107 ± 1 Å^2 $molecule^{-1}$). On the other hand, the A_0 of the isotherm of **4** on the aqueous $HgCl_2$ subphase (10^{-3} M) significantly increases to a value of 150 from that of 112 ± 1 Å^2 $molecule^{-1}$ measured on pure water (Figure 3.15). This result indicates that **4**, self-assembled as a Langmuir monolayer at the air-water interface, interacts with $HgCl_2$ at a relatively low compression state. The isotherm profile of the monolayers of **5** and **6** is considerably affected by $HgCl_2$ dissolved in the aqueous subphase at a concentration of 10^{-3} M, cf. Figure 3.15. While the A_{lim} and A_0 values of the isotherm of **5** on the aqueous $HgCl_2$ subphase (A_{lim} = 106 ± 1 Å^2 $molecule^{-1}$; A_0 = 107 ± 1 Å^2 $molecule^{-1}$) are almost identical to those on pure water (A_{lim} = 105 ± 1 Å^2 $molecule^{-1}$; A_0 = 107 ± 1 Å^2 $molecule^{-1}$), the A_c value (A_c = 83 ± 1 Å^2 $molecule^{-1}$) decreases with respect to that on pure water (A_c = 91 ± 1 Å^2 $molecule^{-1}$). In addition, the π_c value of the isotherm of **5** on the aqueous $HgCl_2$ subphase (10^{-3} M) significantly increases to 46 ± 1 mN m^{-1} with respect to that on pure water (π_c = 39 ± 1 mN m^{-1}). For the monolayer of **6** on the aqueous $HgCl_2$ subphase (10^{-3} M), the π_c value is identical to that measured on pure water (π_c = 38 ± 1 mN m^{-1}), cf. Figure 3.15. On the contrary, the A_c, A_{lim} and A_0 values of the isotherm of **6** decrease from values of 90, 102 and 105 ± 1 Å^2 $molecule^{-1}$ on pure water to 82, 94 and 96 ± 1 Å^2 $molecule^{-1}$ on the aqueous $HgCl_2$ solution, respectively. This set of results demonstrates that, even if the regioisomers **5** and **6** have highly similar structures, the corresponding monolayers possess significant differences in their binding properties towards $HgCl_2$ at the air-water interface. This may be attributed to the different coordination geometries of **5** and **6** with $HgCl_2$. The two distal amino groups of **6** are expected to form a partially distorted diagonal bond with one mercury atom so as to generate a 1:1 complex

between the macrocycle and Hg. Such coordination geometry has been previously described by Hosseini for the complex between tetramercapto *p-tert*-butylcalix[4]rene in the 1,3 alternate conformation and mercury ions.[130] On the other hand, the vicinal arrangement of the two amino groups of **5** is expected to prevent the formation of a 1:1 complex between the macrocycle and Hg. It is therefore anticipated that two amino groups of two adjacent amphiphiles interact with one mercury atom with the formation of 1:2 complex between **5** and mercury.

3.3.2 BAM measurements

The morphology of the monolayers of **4**, **5** and **6** on pure water and on a 10^{-3} M aqueous $HgCl_2$ solution was investigated by BAM. The micrographs reveal that **4** self-assembles in the form of liquid-expanded domains before the takeoff of the isotherm (π = 0 mN m^{-1}), Figure 3.16.

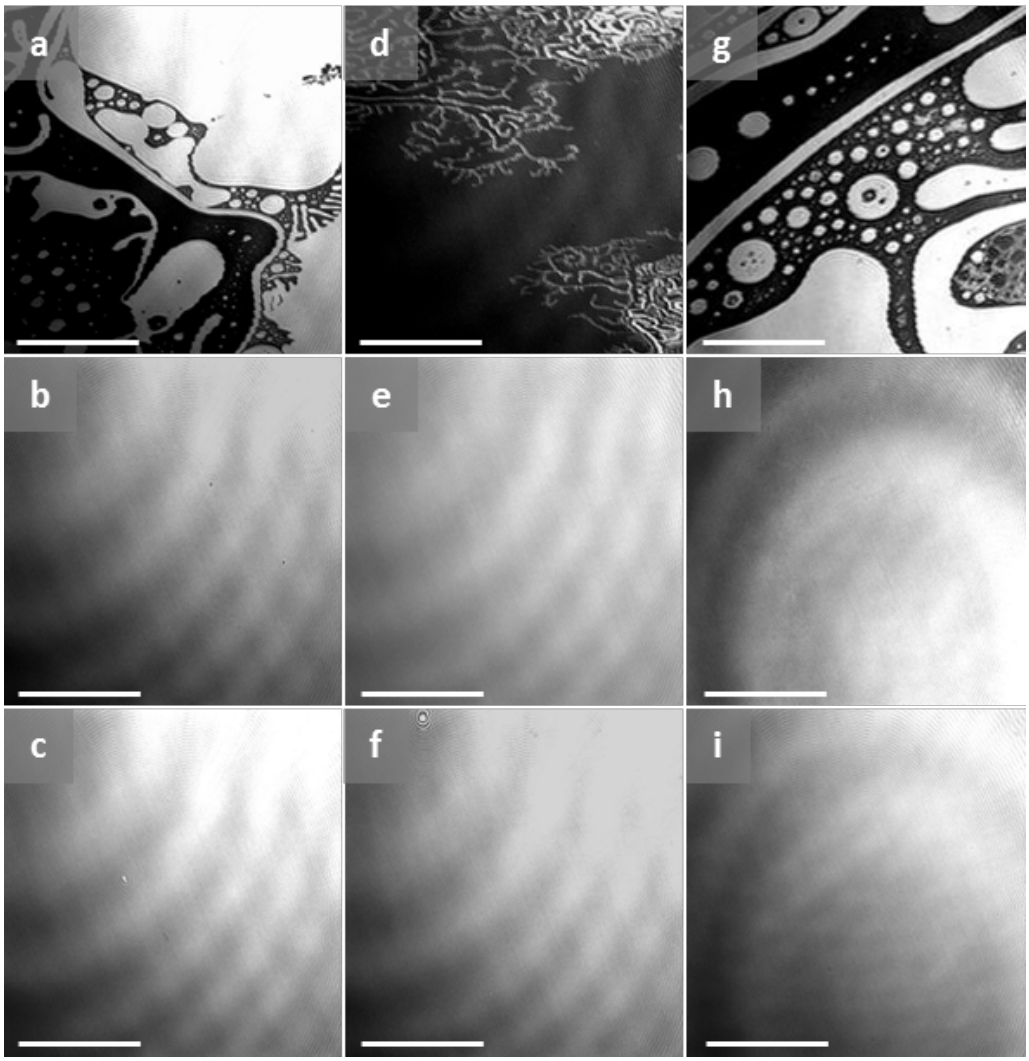

Figure 3.16. BAM micrographs of the monolayer of **4** on pure water (**a**: π = 0 mN m^{-1}; b: π = 1 mN m^{-1}) and on a 10^{-3} M aqueous $HgCl_2$ solution (**c**: π = 0 mN m^{-1}), of **5** on pure water (**d**: π = 0 mN m^{-1}; **e**:

π = 5 mN m^{-1}) and on a 10^{-3} M aqueous $HgCl_2$ solution (**f**: π = 1 mN m^{-1}) and of **6** on pure water (**g**: π = 0 mN m^{-1}; **h**: π = 5 mN m^{-1}) and on a 10^{-3} M aqueous $HgCl_2$ solution (**i**: π = 1 mN m^{-1}). Scale bars = 100 μm.

At the isotherm takeoff (π = 0.1 mN m^{-1}), the monolayer of **4** appears ideally homogeneous and this texture is maintained until the collapse of the monomolecular film. On an aqueous $HgCl_2$ solution at a concentration of 10^{-3} M, the monolayer of **4** appears highly homogeneous already before the isotherm takeoff, i.e. π = 0 mN m^{-1} (Figure 3.16). This result shows that the monolayer of **4** interacts with $HgCl_2$ at the air-water interface at a relatively low compression state, thus confirming the results obtained by Langmuir compression isotherms. The micrographs reveal that the monolayers of **5** and **6** on pure water form relatively large liquid-expanded domains already before the isotherm takeoff (π = 0 mN m^{-1}). Unlike the monolayer of **4**, the monomolecular films of **5** and **6** on pure water appear homogeneous at a surface pressure value of 5 mN m^{-1} (Figure 3.16). This result is explained by the fact that **4** possesses a more favorable hydrophilic/lipophilic balance for the self-assembly process at the air-water interface in comparison with that of **5** and **6**. When $HgCl_2$ is added in the aqueous subphase at a concentration of 10^{-3} M, the monolayers of **5** and **6** appear homogeneous at π = 1 mN m^{-1}, cf. Figure 3.16. These results indicate that an interaction between the monolayers of **5** and **6** and $HgCl_2$ takes place at the air-water interface.

3.3.3 Synchrotron-based X-ray diffraction analyses

Synchrotron-based XNTRF, XRR and GIXD measurements of the monolayers of **4**, **5** and **6** on pure water and on a 10^{-3} M aqueous $HgCl_2$ subphase were carried out in order to gain further information on their structures and binding affinities towards $HgCl_2$. XNTRF was performed to establish the surface excess of Hg atoms beneath Langmuir monolayers of **4**, **5** and **6**. The X-ray waves penetrate into a shallow depth in the water along the normal to the surface when the angle of incidence α_i is below the critical angle α_c for total reflection. On the other hand, the X-ray waves penetrate in the bulk with a scale-length in the order of micrometers, therefore

probing the bulk, when $\alpha_i > \alpha_c$. When $HgCl_2$ is dissolved in the water solution at a concentration of 10^{-3} M, for $\alpha_i > \alpha_c$ and in the absence of the monolayer, the characteristic emission lines of Hg atoms are readily observed as a consequence of the interaction of the X-ray waves with bulk Hg atoms (Figure 3.17).

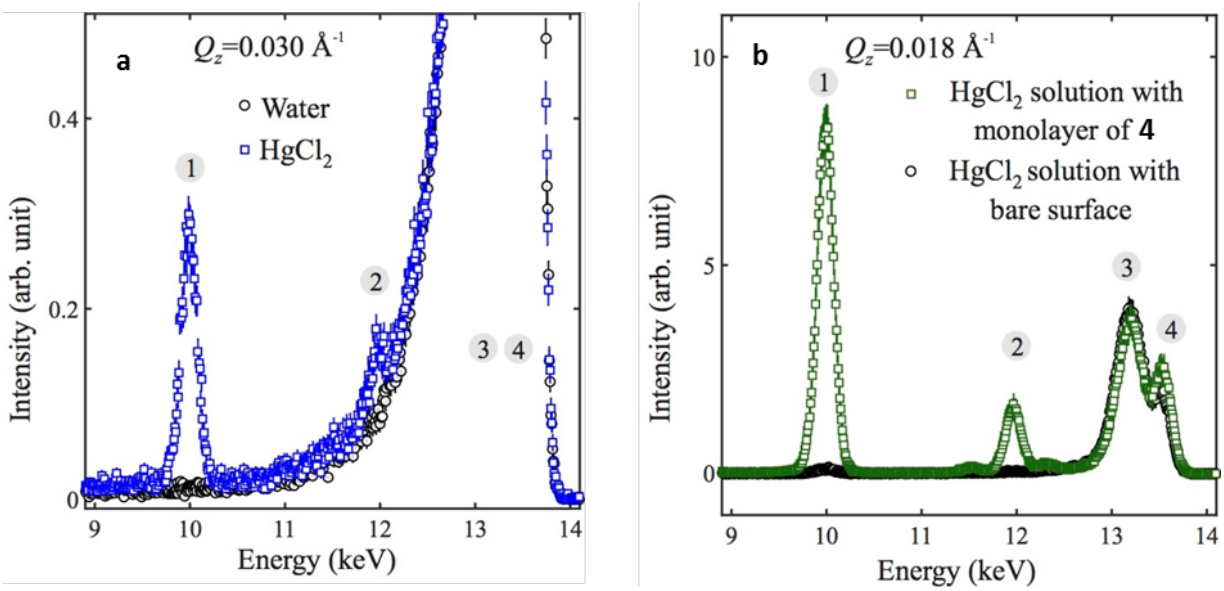

Figure 3.17. Bulk fluorescence spectra for pure water and for a 10^{-3} M aqueous $HgCl_2$ solution (**a**) and surface fluorescence spectrum of the monolayer of **4** on a 10^{-3} M aqueous $HgCl_2$ subphase. In **a** and **b**, the peaks labeled with 1 and 2 are the Hg L_α and L_β characteristic emission lines. Peaks 3 and 4 represent the inelastic and elastic scattering of X-ray from bulk water.

For $\alpha_i < \alpha_c$, the Hg signals are not visible as the X-ray waves interact only with a layer of Hg atoms on the top of the water surface. In the presence of the monolayers of **4**, **5** and **6**, compressed to a surface pressure value of 20 mN m^{-1}, the intensities of the emission lines for Hg atoms are considerably enhanced with respect to that of the primary beam. Quantitative analysis reveals an enrichment of Hg atoms beneath the Langmuir monolayers in the order of **4** > **6** ≥ **5**; the monolayer of **4** binds Hg atoms 4-5 times as much as the monomolecular films of **5** and **6**. The depth of the surface excess ions can be approximated to the vertical length of the

monolayer. This suggests that $HgCl_2$ immediately binds to the monolayers instead of showing a diffusive distribution underneath the monomolecular film. By considering a molecular area value of 115 $Å^2$ $molecule^{-1}$, XNTRF measurements revealed that 2.3 ± 0.2 Hg atoms are bound to one molecule of **4**, 0.47 ± 0.05 Hg atoms to one molecule of **5** and 0.62 ± 0.05 Hg atoms to one molecule of **6**.

XRR measurements demonstrated that the monolayers of **4**, **5** and **6** on a 10^{-3} M aqueous $HgCl_2$ subphase, compressed to a surface pressure value of 20 mN m^{-1}, show enhanced surface electron density and are thickener than the corresponding monolayers on pure water. The higher electron density in the headgroup region is evidence for strong binding of the macrocycles towards $HgCl_2$, cf. Figure 3.18.

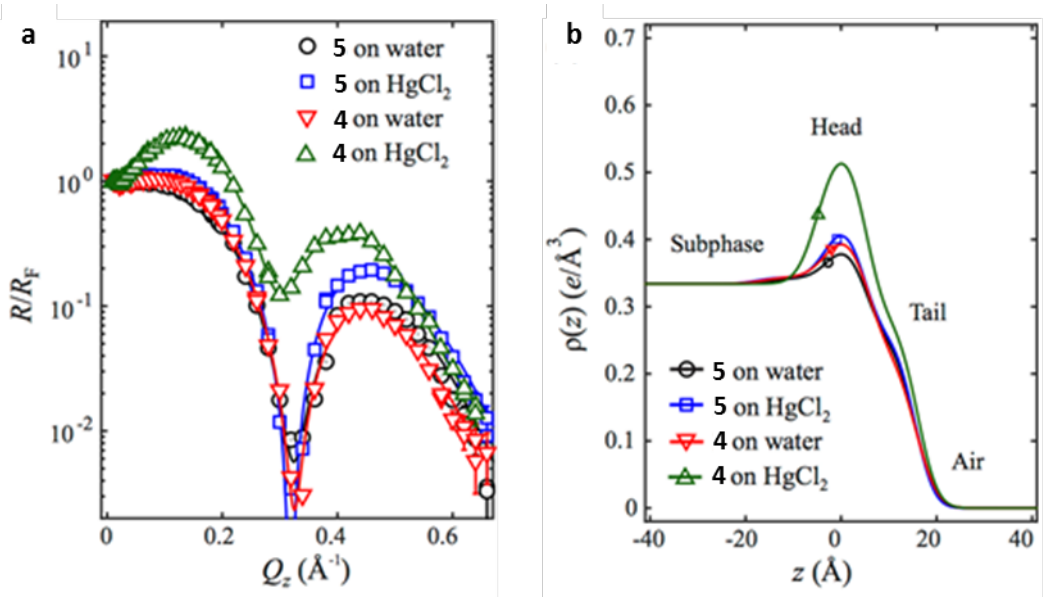

Figure 3.18. R data normalized to the R_F, R/R_F, of the monolayer of **4** and **5** on pure water and on a 10^{-3} M aqueous $HgCl_2$ solution, respectively (**a**), and corresponding best-fit electron density profiles across the interfaces (**b**).

XRR analysis also revealed that 2.4 ± 0.2 Hg atoms are bound to one molecule of **4**, self-assembled as a Langmuir monolayer at the air-water interface, thus confirming the results obtained by XNTRF measurements.

The structures of the monolayers of **4**, **5** and **6** on pure water and on a 10^{-3} M aqueous $HgCl_2$ subphase were investigated by GIXD. The diffraction spectra of the monolayers of **4**, **5** and **6** on pure water revealed the presence of Bragg-reflection-like peaks, indicating that the monomolecular films possess ordered structures, cf. Figure 3.19.

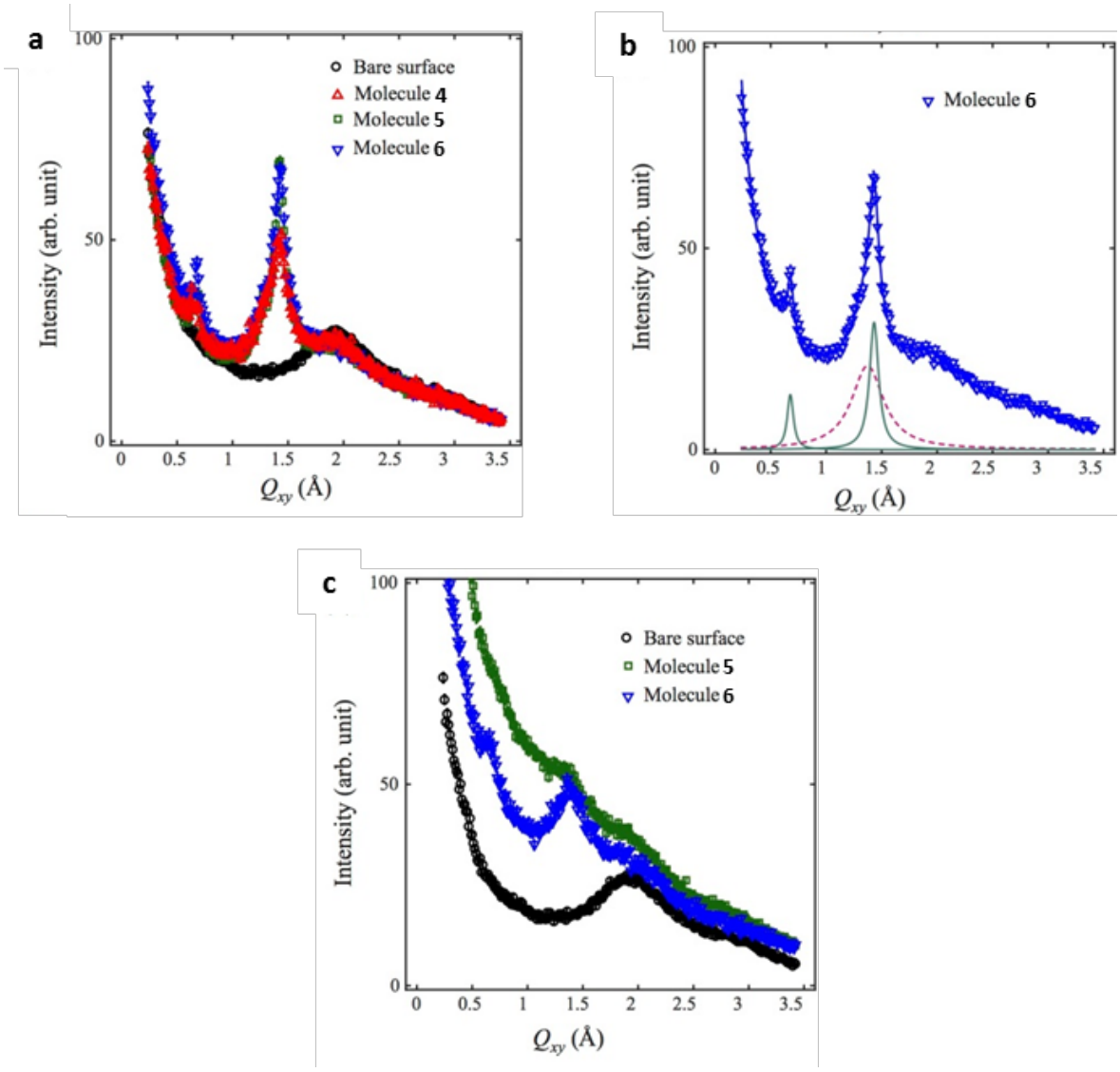

Figure 3.19. GIXD spectra of the monolayers of **4**, **5** and **6** on pure water (**a**), GIXD profile of the monolayer of **6** on pure water showing constituent peaks (**b**) and GIXD spectra of the monolayers of **5** and **6** on a 10^{-3} M aqueous $HgCl_2$ solution compared to that of a water bare surface (**c**).

In the case of the monolayer of **3** on pure water, compressed at a surface pressure value of 20 mN m^{-1}, GIXD measurements demonstrated that the aliphatic chains are organized in a 2D liquid-like phase. In the present case, the Bragg-reflection-like peaks of the monolayers of **4**, **5**

and **6** on pure water, compressed at the same surface pressure value of 20 mN m^{-1}, are sharper than those observed for the monolayer of **3** (Figure 3.19). These results indicate that the amino-substituted calix[4]arenes organize into ordered structures at the air-water interface. The Bragg-reflection-like peaks of the monolayers of **4**, **5** and **6** on pure water are similar (Figure 3.19). These data suggest that the contribution of the amino functions on the lateral packing of **4**, **5** and **6** within the monolayers is negligible. The diffraction spectra of the monolayers of **5** and **6** on pure water show one low-*Q* peak that is associated with the ordering of the amino functions of the macrocycles (Figure 3.19). This peak is related to the headgroups organized in a square lattice with an area value of 85 $Å^2$ $molecule^{-1}$; this value is reasonably in agreement with the Langmuir compression isotherms. The more intense and broader peak of the diffraction spectra of the monolayers of **5** and **6** is attributed to the moderate ordering of the hydrocarbon chains of the macrocycles. The GIXD spectrum of the monolayer of **4** on pure water reveals that the low intensity peak is shifted to lower values of Q_{xy}, i.e. Q_{xy} = 0.65 $Å^{-1}$. This value corresponds to an average molecular area of 100 $Å^2$ $molecule^{-1}$ and it is consistent with the Langmuir compression isotherm results (Figure 3.19). The high intensity peak of the GIXD spectrum of the monolayer of **4** on pure water is ascribed to the short-range order among the aliphatic chains of the macrocycles. The same peak is broader when $HgCl_2$ is added in the aqueous solution at a concentration of 10^{-3} M, indicating that the interaction of the monolayer of **4** with the Hg atoms partially disrupts the order of the hydrophobic chains of the macrocycle. The GIXD spectra of the monolayer of **5** and **6** on a 10^{-3} M aqueous $HgCl_2$ solution show the presence of more intense diffuse scattering so as to overwhelm the Bragg-reflection-like peaks (Figure 3.19). It is likely that the binding of the monolayers of **5** and **6** towards Hg atoms considerably reduces the repulsions among the macrocycle headgroups leading to partially disordered structures.[129]

3.3.4 Conclusions

The self-assembly properties of **4**, **5** and **6** on pure water and on a 10^{-3} M aqueous $HgCl_2$ solution were studied by means of Langmuir compression isotherms. The isotherms demonstrated that the two diamino-substituted and the tetraamino-substituted calix[4]arenes form stable Langmuir monolayers at the air-water interface. When $HgCl_2$ is dissolved in the aqueous subphase, the isotherm profile of **5** is significantly different from that of **6**. This result indicates that, even if the macrocycles have highly similar structures, the monolayers of **5** and **6** show significant differences in their interfacial binding towards $HgCl_2$.

BAM measurements revealed that the monolayer of **4** forms relatively large liquid-condensed domains on a 10^{-3} M aqueous $HgCl_2$ solution already before the isotherm takeoff. This result demonstrates that the monomolecular film of **4** shows high affinity to $HgCl_2$ at relatively low compression states. The monolayers of **5** and **6** appear highly homogeneous at a surface pressure of 1 mN m^{-1}; this value is lower than that on pure water, i.e. π = 5 mN m^{-1}. These results indicate that a relevant interaction of the monolayers of **4**, **5** and **6** with $HgCl_2$ takes place at the air-water interface.

The structure and the binding properties of the monolayers of **4**, **5** and **6** on pure water and on a 10^{-3} M aqueous $HgCl_2$ solution were investigated by means of synchrotron-based X-ray diffraction measurements. XNTRF revealed that the monolayer of **4** binds to $HgCl_2$ approximately 4-5 times as much as the monolayers of **5** and **6**. In addition, it is demonstrated that one molecule of **4** binds 2.3 ± 0.2 Hg atoms, one molecule of **5** to 0.47 ± 0.05 Hg atoms and one molecule of **6** to 0.62 ± 0.05 Hg atoms at the air-water interface. XRR analyses showed that the thickness of the monolayers of **4**, **5** and **6** on the $HgCl_2$ solution is higher than that on pure water. These results confirm the interfacial interaction of the monomolecular films of **4**, **5** and **6** with Hg atoms. GIXD measurements showed that **4**, **5** and **6**, self-assembled as Langmuir monolayers at the air-water interface, are orderly packed on pure water. The coincidence of the

Bragg-reflection-like peaks of the monolayers of **4**, **5** and **6** suggests that the influence of the amino moieties on the lateral packing of the molecules is negligible. The diffraction spectra of the monolayers of **5** and **6** on a 10^{-3} M aqueous $HgCl_2$ solution are characterized by intense diffuse scattering. This result suggests that the binding of the macrocycles with Hg atoms considerably decreases the repulsions among the headgroups so as to lead to a partial molecular disorder.

3.4 Calix[4]arene-based Langmuir monolayers as two-dimensional metal organic networks

3.4.1 Synthesis of 5,11,17,23-tetra-carboxy-25,26,27,28-tetrapropoxycalix[4]arene (7)

The synthesis of 25,26,27,28-tetrapropoxycalix[4]arene was performed as mentioned in chapter 3.1.1, using 1-bromopropane as alkylating agent in the Williamson reaction. The introduction of the formyl functions at the *p*-positions of 25,26,27,28-tetrapropoxycalix[4]arene was conducted by Duff reaction in the presence of hexamine and trifluoroacetic acid (TFA). The oxidation of the formyl groups to carboxylic functions to yield **7** was performed through Pinnick reaction in the presence of sulfamic acid and sodium chlorite. The synthetic route for the synthesis of **7** is shown in Figure 3.20.[113,115,131,132]

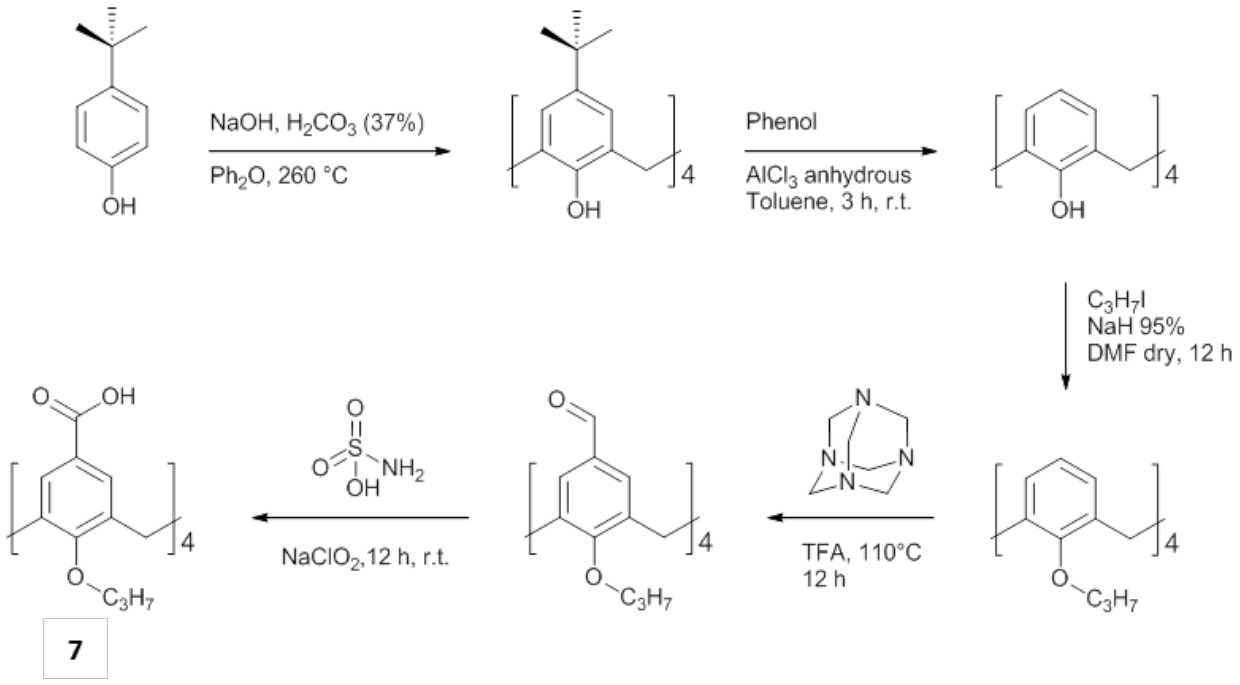

Figure 3.20. Synthetic route of **7**.

3.4.2 Langmuir compression isotherms

The ability of **7** to form stable Langmuir monolayers at the air-water interface was investigated by surface pressure-area compression isotherms. Despite the short length of the alkyl chains, i.e. C_3 chains, the macrocycles self-assemble as highly stable Langmuir monolayers at the air-water interface, cf. Figure 3.21.

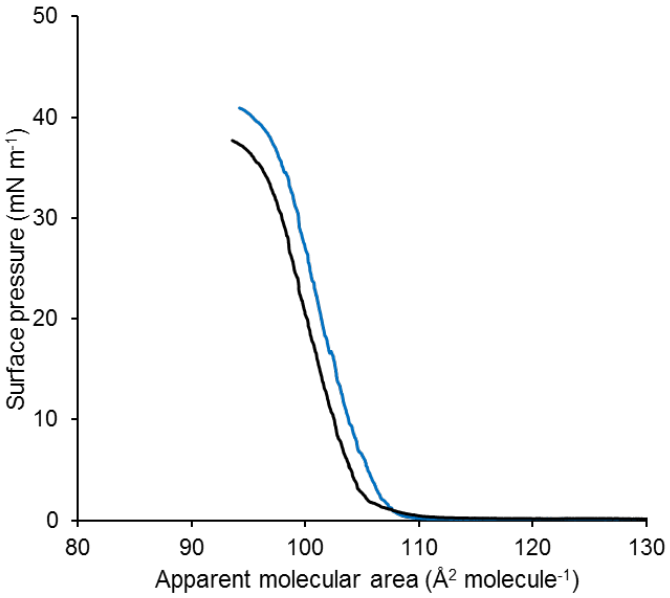

Figure 3.21. Surface pressure-area compression isotherms of the monolayer of **7** on pure water (**–**) and on a 10^{-5} M aqueous $CuCl_2$ solution (–).

Unlike **7**, its corresponding monomer does not self-assemble as a stable Langmuir monolayer at the air-water interface. This indicates that, as shown for **3** in chapter 3.1.2, the macrocyclic backbone plays a crucial role in the interfacial molecular self-assembly of **7**. Langmuir monolayers of surfactants are typically stabilized by van der Waals interactions among hydrocarbon chains and electrostatic interactions (e.g. H-bonding) between the headgroups and water molecules.[97] In the present case, the contribution of the van der Waals interactions to the stabilization of the monomolecular film of **7** is weak, if not negligible, due to the short length of

the alkyl chains of the macrocycle. The high π_c value of 37 ± 1 mN m^{-1} shown by the compression isotherm of **7** on pure water is therefore attributed to the strong π-π interactions among aromatic rings of neighboring amphiphiles. The A_{lim} value of the isotherm of **7** on pure water measures 105 ± 1 $Å^2$ $molecule^{-1}$ (Figure 3.21). This value is consistent with the presence of a calix[4]arene derivative at the air-water interface with the pseudo C_4 symmetry axis orthogonal to the water surface. Shahgaldian et al. investigated the self-assembly behavior of a series of *p*-acyl calix[4]arenes with different chain length at the air-water interface.[54] The apparent molecular area value of 100 $Å^2$ $molecule^{-1}$ shown by the compression isotherms confirmed the parallel orientation of the macrocycles at the interface. The authors found out that the length of the hydrocarbon chains of the *p*-acyl calix[4]arenes does not affect the A_{lim} values of the macrocycle isotherms. In the present case, the limiting area of the isotherm of **7** on pure water is considerably lower than that of the C_{12} structural analogue **3**. The lower value of A_{lim} may be ascribed to the fact that, in the case of **7**, the packing is limited by the size of the aromatic ring while, in the case of **3** the packing is limited by the C_{12} aliphatic chains. In the presence of a 10^{-5} M aqueous $CuCl_2$ subphase, the isotherm of **7** shows an A_{lim} value of 106 ± 1 $Å^2$ $molecule^{-1}$, similar to that measured on pure water (A_{lim} = 105 ± 1 $Å^2$ $molecule^{-1}$). On the other hand, the π_c of the isotherm of **7** on an aqueous 10^{-5} M $CuCl_2$ subphase increases up to 41 ± 1 mN m^{-1} when compared to that on pure water (π_c = 37 ± 1 mN m^{-1}). In addition, the isotherm of **7** on an aqueous 10^{-5} M $CuCl_2$ solution rises more rapidly at the takeoff with respect to that on pure, cf. Figure 3.21, where the modulus of the slope of the isotherm of **7** on pure water at π = 1 mN m^{-1} is 0.3 while that on the aqueous Cu^{2+} ions subphase measures 1.2. This set of results indicates that the amphiphiles, self-assembled as a Langmuir monolayer at the air-water interface, interact with Cu^{2+} ions. The higher value of the modulus of the slope measured on the 10^{-5} M aqueous $CuCl_2$ subphase in comparison with that on pure water strongly suggests that the macrocycles self-assemble into condensed domains prior to compression. In chapter 3.2.1, the binding properties of **3** with a series of divalent cations at the air-water interface have been

discussed. Due to geometric constraints and the limited conformational freedom of the headgroups of **3**, it is expected that the macrocycles, self-assembled as Langmuir monolayers at the air-water interface, bind the cations via a distorted octahedral coordination geometry. In the present case, the structural analogy of **7** with **3** strongly suggests that the short chain calix[4]arene derivative binds Cu^{2+} ions via the same coordination geometry, where the cations are bound by two carboxylic groups of adjacent amphiphiles of **7** and two water molecules, in cis position around the central ion.

Stability tests of the monolayer of **7** on pure water and on a 10^{-5} M aqueous $CuCl_2$ subphase were conducted to gain information on the stability of the monomolecular film in the absence of compression as a function of time, cf. Figure 3.22.

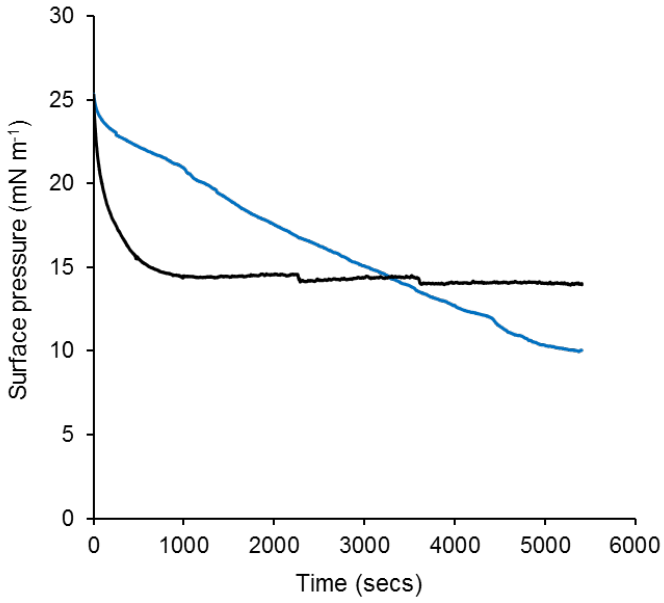

Figure 3.22. Stability test of the monolayer of **7** on pure water (**–**) and on a 10^{-5} M aqueous $CuCl_2$ solution (–).

In these experiments, the monolayer of **7** was compressed to 25 mN m^{-1} and the variation of the surface pressure as a function of time, in the absence of compression, was investigated. The

experiments revealed that the surface pressure of the monolayer of **7** on pure water rapidly decreases from a value of 25 to a value of 15 mN m^{-1} within 15 minutes. After 15 minutes, the surface pressure value of the isotherm of **7** remains constant within the next 75 minutes. These results suggest that the amphiphiles partially reorganize to form the most stable structure at a surface pressure value of 15 mN m^{-1}. On the other hand, when $CuCl_2$ is dissolved in the aqueous subphase at a concentration of 10^{-5} M, the π value of the isotherm of **7** steadily decreases as a function of time. At time t = 15 minutes, the surface pressure value of the isotherm of **7** on pure water is 15 mN m^{-1} while that on the aqueous $CuCl_2$ subphase is 21 mN m^{-1}. The higher value of π measured on the aqueous $CuCl_2$ solution in comparison with that on pure water is attributed to the formation of extended 2D array of noncovalent interactions between the amphiphiles and Cu^{2+} ions at the interface that significantly stabilize the monomolecular film at the interface. At t = 50 minutes, the surface pressure of the monolayer of **7** on the aqueous $CuCl_2$ solution is 15 mN m^{-1} and, at t = 90 minutes, π = 10 mN m^{-1}. The constant decrease of π as a function of time is explained by the fact that the reversible bonds between **7** and Cu^{2+} ions are partially broken in the absence of compression. This causes the amphiphiles to rearrange within the monolayer into a less stable structure.

3.4.3 BAM measurements

The morphology of the monolayer of **7** on pure water and on a 10^{-5} M aqueous $CuCl_2$ subphase was investigated by BAM. It is known from the literature that Langmuir monolayers of amphiphilic calixarenes typically appear homogeneous after the isotherm takeoff, i.e. π = 1-5 mN m^{-1}).[126,127] On the contrary, Langmuir monolayers of **7** on pure water possess a diverse structure (Figure 3.23).

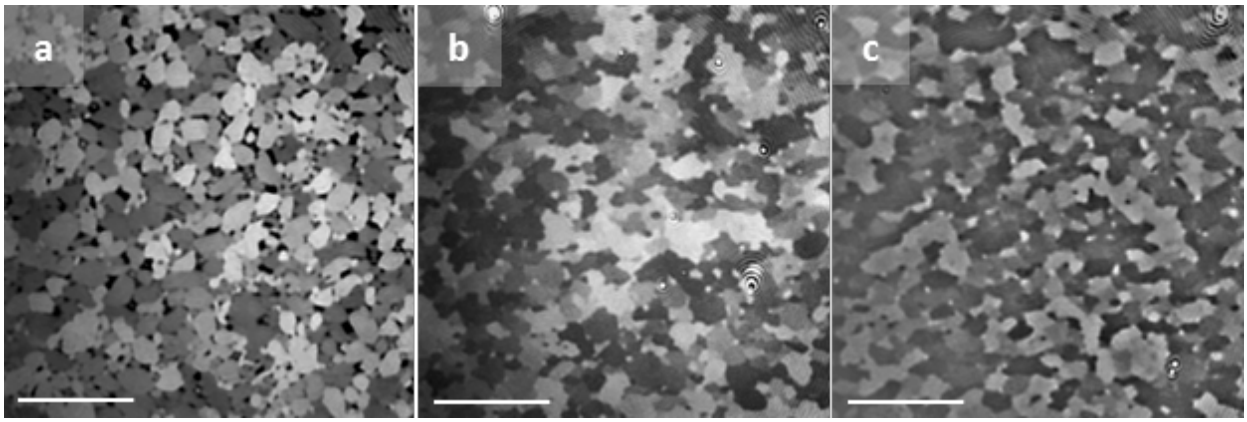

Figure 3.23. BAM micrographs of the monolayer of **7** on pure water compressed at surface pressure values of 0.1 (**a**), 20 (**b**) and 30 (**c**) mN m^{-1}. Scale bar = 100 μm.

Indeed, at the isotherm takeoff (π = 0.1 mN m^{-1}), well-defined domains that possess different contrasts are observed. By further compression, the domains merge with one another and get larger (Figure 3.23). As discussed in chapter 3.4.2, the contribution of the van der Waals interactions of the short C_3 aliphatic chains to the molecular self-assembly of **7** at the air-water interface is weak, if not negligible. The formation of well-organized domains at such low surface pressure values (π = 0.1 mN m^{-1}) is attributed to the strong π-π interactions among aromatic rings of neighboring amphiphiles, thus confirming the observations gained by Langmuir compression isotherms. Domains with different contrasts have been observed in Langmuir monolayers of single and double chain surfactants.[133,134] For example, dipalmitoyl-phosphatidylglycerol molecules, self-assembled as Langmuir monolayers at the air-water interface, form circular domains of distinct contrast on pure water.[133] The authors attributed the difference in the contrast to the molecule azimuthal angle. The amphiphiles possess the same azimuthal angle in one domain but different azimuthal angles in different domains so as to produce different contrast. In the present case, the aliphatic chains of **7** are too short to contribute to the molecular packing. The different contrast of the domains of **7** is therefore ascribed to the anisotropy generated by the directional π stacking among aromatic rings of

neighboring macrocycles. The solid-state structure of **7** reveals that the macrocycle possesses a pinched cone conformation where two distal aromatic rings are parallel to each other while the other two are splayed apart.[117] If the pinched cone conformation is retained at the air-water interface, the pseudo C_4 symmetry of the amphiphile is lost. The pinched cone conformation would therefore allow for the propagation of the anisotropic order of the macrocycle in the two dimensions so as to generate domains of different contrast. In the presence of a 10^{-5} M aqueous $CuCl_2$ solution, the texture of the monolayer of **7** dramatically changes, cf. Figure 3.24.

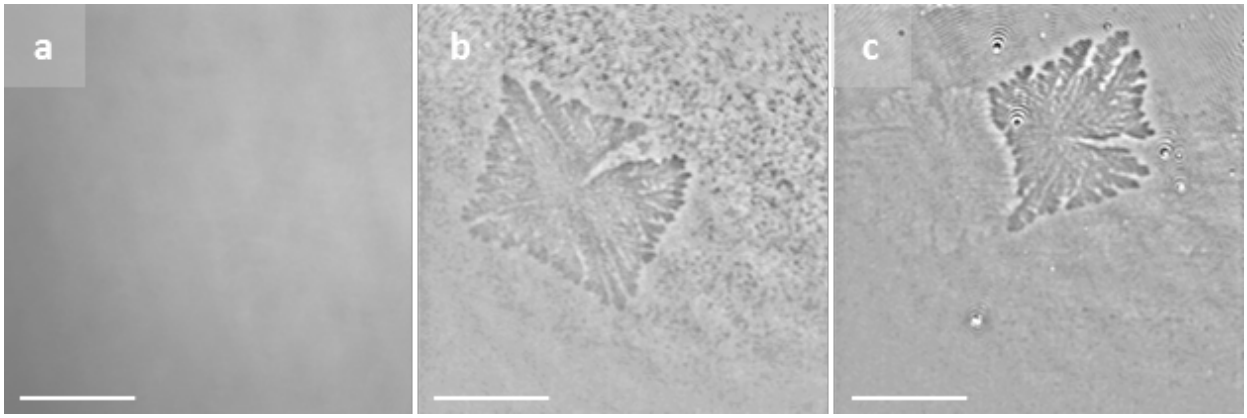

Figure 3.24. BAM micrographs of the monolayer of **7** on a 10^{-5} M aqueous $CuCl_2$ subphase compressed at surface pressure values of 0.1 (**a**), 20 (**b**) and 30 (**c**) mN m^{-1}. Scale bar = 100 μm.

Before the isotherm takeoff (π = 0 mN m^{-1}; A = 115 $Å^2$ $molecule^{-1}$), the monomolecular film of **7** appears homogeneous. This result suggests that Cu^{2+} ions trigger the self-assembly of the amphiphiles at the air-water interface prior to compression, thus in agreement with the Langmuir compression isotherms. The monolayer shows a regular texture until a surface pressure of ca. 15 mN m^{-1}. Remarkably, at π = 20 mN m^{-1}, considerably large crystalline dendritic domains are observed, cf. Figure 3.24. The dendritic domains formed on the 10^{-5} M aqueous $CuCl_2$ solution possess different contrast, suggesting that the amphiphiles are anisotropically ordered at the air-water interface. The dendritic domains are observed until the monolayer collapse. The formation of the dendritic domains is attributed to the interfacial interaction

between the macrocycles and the cations, where two carboxylic groups of adjacent amphiphiles bind one Cu^{2+} ion so as to form COO–Cu–COO bridges. The presence of such supramolecular bridges is expected to favor the generation of two-dimensional extended arrays of noncovalent interactions, that is 2D metal organic networks at the air-water interface.

The effect of Cu^{2+} ions in the aqueous subphase on the texture of the monolayer of **7** was further investigated via the post-injection/compression method. In the previous experiments, appropriate amounts of solutions of **7** in $CHCl_3$ were spread on the surface of a preformed aqueous $CuCl_2$ subphase. In the present case, a specific volume of an aqueous $CuCl_2$ solution is injected into the pure aqueous subphase after spreading and compressing the monolayer of **7** to the desired surface pressure value. In the first experiment, the monolayer of **7** is compressed on pure water to a surface pressure value of 5 mN m^{-1} and kept under pressure control. Subsequently, 200 μL of an 8×10^{-2} M aqueous $CuCl_2$ solution are injected into the pure aqueous subphase. When the aqueous $CuCl_2$ solution is injected from the side of the trough, no change in the morphology of the monolayer is observed within the next two hours. This may be attributed to the fact that the cations slowly diffuse into the subphase causing a local effect on a small portion of the monolayer close to the injection site. On the contrary, when the aqueous $CuCl_2$ solution is injected from the center of the trough, the texture of the monolayer of **7** drastically changes as a function of time, cf. Figure 3.25.

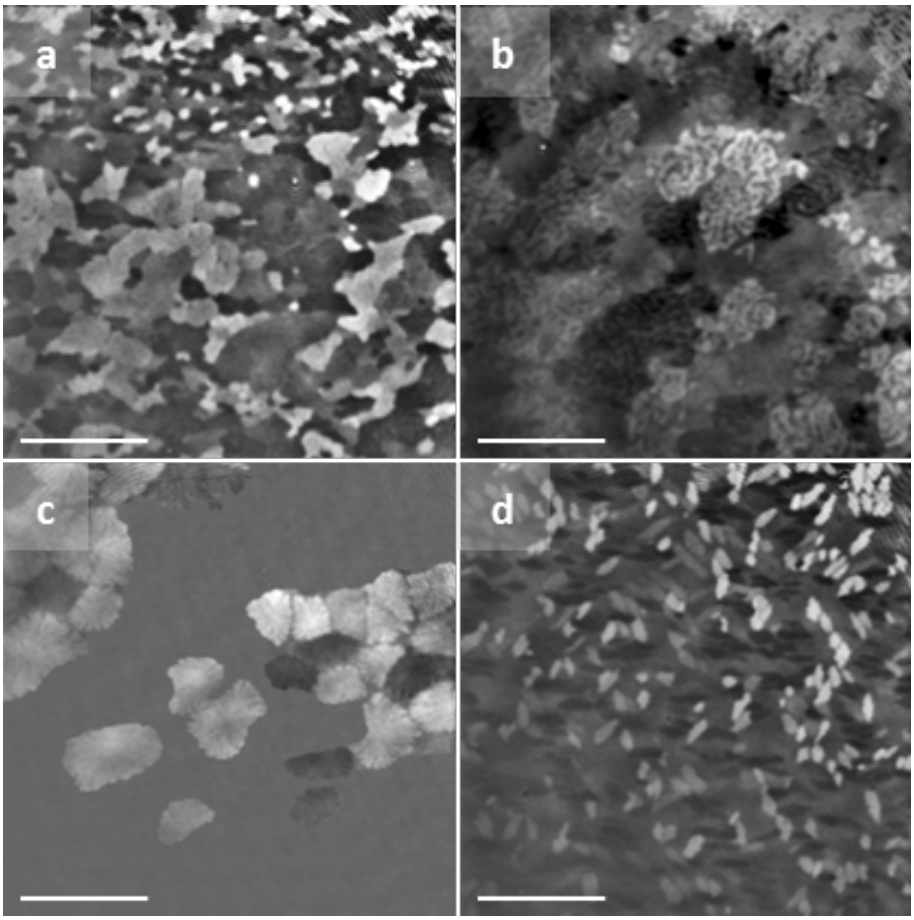

Figure 3.25. BAM micrographs of the monolayer of **7** acquired after compression of the monomolecular film to 5 mN m^{-1} and injection of 200 μL of an 8×10^{-2} M aqueous $CuCl_2$ solution in the pure aqueous subphase (post-injection/compression method), at times equal to 40 (**a**), 50 (**b**), 80 (**c**) and 120 (**d**) minutes. Scale bar = 100 μm.

During the first 40 minutes, the morphology of the monolayer of **7** is identical to that on pure water. After 50 minutes, the morphology of the monomolecular film of **7** rapidly changes. Worm-like structures coexisting with a highly homogeneous phase are observed, indicating that an interaction between the macrocycles and Cu^{2+} ions takes place at the interface. Such structures are maintained for 30 minutes and, right after (t = 80 minutes), dendritic domains of different contrast are observed at the interface, cf. Figure 3.25. These results demonstrate that

the binding of the amphiphiles to Cu^{2+} ions trigger the formation of crystalline dendritic domains of different contrast at the air-water interface. For longer times, i.e. up to 120 minutes, smaller well-defined domains of different contrast coexisting with a regular phase are observed (Figure 3.25). It is expected that these domains derive from the interaction between **7** and the cations, where two carboxylic groups of adjacent amphiphiles bind one Cu^{2+} ion so as to form COO–Cu–COO bridges, but of smaller size than those shown in Figure 3.25 **c**. No changes in the morphology of the monolayer of **7** are observed, during the same amount of time, when 200 μL of pure water were injected into the pure aqueous subphase in the presence of the monolayer of **7** compressed at 5 mN m^{-1}, i.e. control experiment (Figure 3.26).

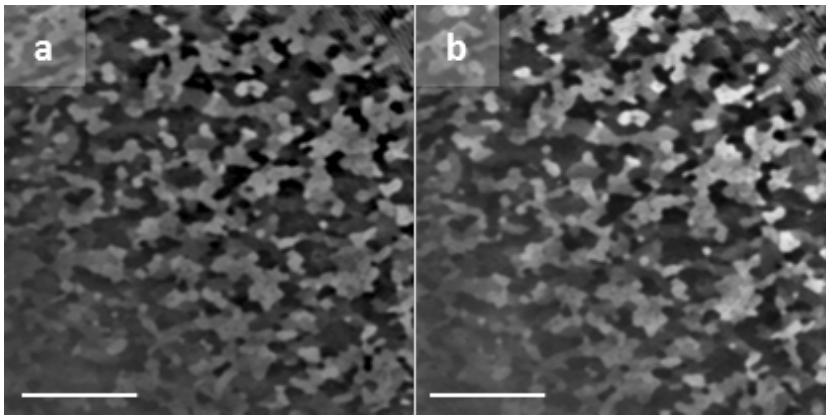

Figure 3.26. BAM micrographs of the monolayer of **7** acquired after compression of the monolayer to 5 mN m^{-1} and injection of 200 μL of pure water in the pure aqueous subphase (post-injection/compression method), at times equal to 60 (**a**) and 120 (**b**) minutes. Scale bar = 100 μm.

The control experiments confirm that Cu^{2+} ions bind to the monolayer of **7** and trigger the formation of crystalline dendritic domains of different contrast at the air-water interface.

The post-injection/compression method was applied to the monomolecular film of **7** compressed to a surface pressure value of 20 mN m^{-1}, i.e. fully compressed monolayer. 200 μL

of an 8×10^{-2} M aqueous $CuCl_2$ solution were added into the pure aqueous solution in the presence of the monolayer of **7**, cf. Figure 3.27.

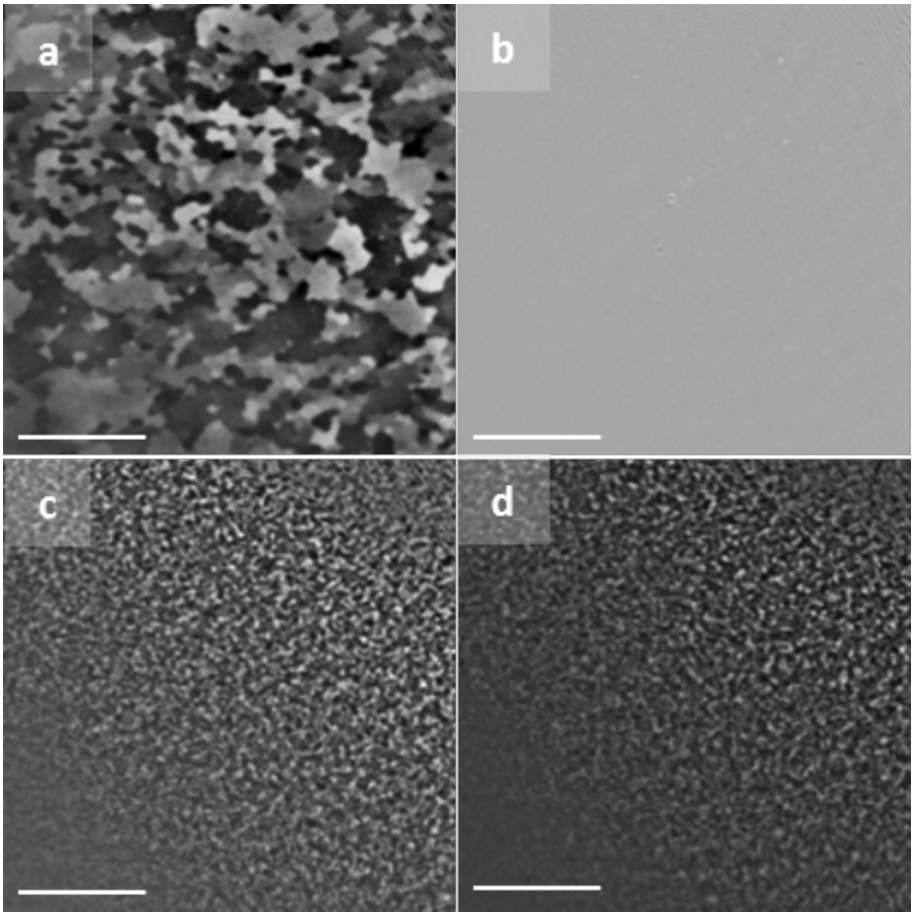

Figure 3.27. BAM micrographs of the monolayer of **7** acquired after compression of the monolayer to 20 mN m^{-1} and injection of 200 μL of an 8×10^{-2} M aqueous $CuCl_2$ solution in the pure aqueous subphase (post-injection/compression method), at times equal to 30 (**a**), 50 (**b**), 80 (**c**) and 120 (**d**) minutes. Scale bar = 100 μm.

During the first 30 minutes, the morphology of the monolayer of **7** appears identical to that on pure water. Within the next 20 minutes (t = 50 minutes), the texture of the monomolecular layer changes from an irregular to a highly homogeneous phase, thus indicating that the cations

interact with the monolayer and cause a change in its morphology. The homogeneous phase of the monolayer is observed for additional 10 minutes (t = 60 minutes). After 60 minutes, a grainy texture becomes visible and such structure is maintained up to 120 minutes (Figure 3.27). Such texture is ascribed to the growth of ordered domains originating from the formation of COO–Cu–COO bridges between adjacent molecules of **7** and the cations. The post injection/compression method indicates that the dendritic structures are grown when the monolayer of **7** is compressed to a surface pressure value of 5 mN m^{-1}, while a grainy texture is observed for the same monolayer compressed to 20 mN m^{-1}. This experimental result might be explained by the fact that, when the monolayer is compressed to π = 5 mN m^{-1}, the distance among the amphiphiles is ideal for binding Cu^{2+} ions so as to generate an extended array of noncovalent interactions at the air-water interface. On the other side, the highly packed state of the monolayer of **7** compressed at 20 mN m^{-1} partially hinders the propagation of such arrays between the macrocycles and the cations and structures of smaller size are formed.

The control experiment, in which 200 μL of pure water are added into the pure aqueous solution in the presence of the monolayer compressed at 20 mN m^{-1}, showed that the texture of the monomolecular film of **7** does not change within the same amount of time (t = 120 minutes), cf. Figure 3.28.

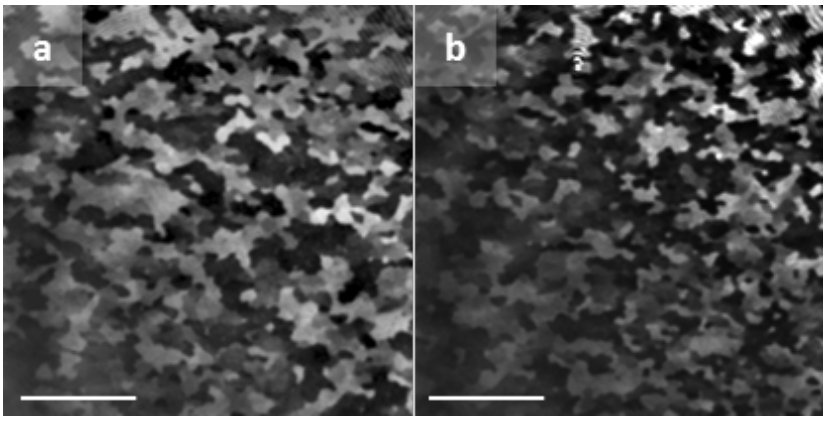

Figure 3.28. BAM micrographs of the monolayer of **7** acquired after compression of the monolayer to 20 mN m^{-1} and injection of 200 μL of pure water in the pure aqueous subphase (post-injection/compression method), at times equal to 60 (**a**) and 120 (**b**) minutes. Scale bar = 100 μm.

The control experiments confirm that Cu^{2+} ions play a crucial role in the change of the morphology of the monolayer of **7**.

The variation of the surface pressure of the monolayer of **7** as a function of time in the absence of compression, i.e. stability test, was monitored in parallel with BAM. The monolayer of **7** on pure water, compressed to π = 25 mN m^{-1}, consists of domains of distinct contrast. After 15 minutes, in the absence of compression, the surface pressure value decreases from to 25 to 15 mN m^{-1} with no changes observed in the monomolecular layer texture. Such morphology is maintained for the next 75 minutes, cf. Figure 3.29.

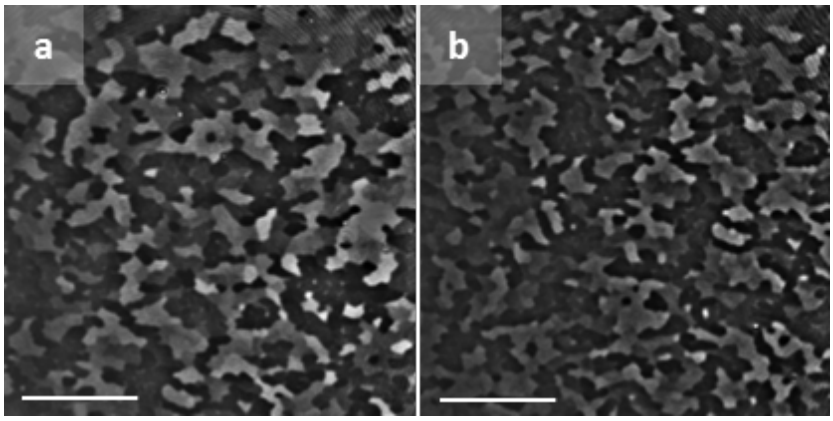

Figure 3.29. BAM micrographs of the monolayer of **7** on pure water. The monomolecular film was compressed to a surface pressure of 25 mN m^{-1} and its texture was investigated in the absence of compression (**a**: π = 25 mN m^{-1}; **b**: π = 15 mN m^{-1}). Scale bar = 100 μm.

In the presence of a 10^{-5} M aqueous $CuCl_2$ solution, the monolayer of **7** consists of dendritic domains that coexist with a homogeneous phase. In the absence of compression, the surface pressure linearly decreases as a function of time and the dendritic structures rapidly disappear. At a surface pressure of 15 mN m^{-1} (t = 50 minutes), the texture of the monolayer of **7** is highly similar to that on pure water. Such morphology is observed until t = 90 minutes, cf. Figure 3.30.

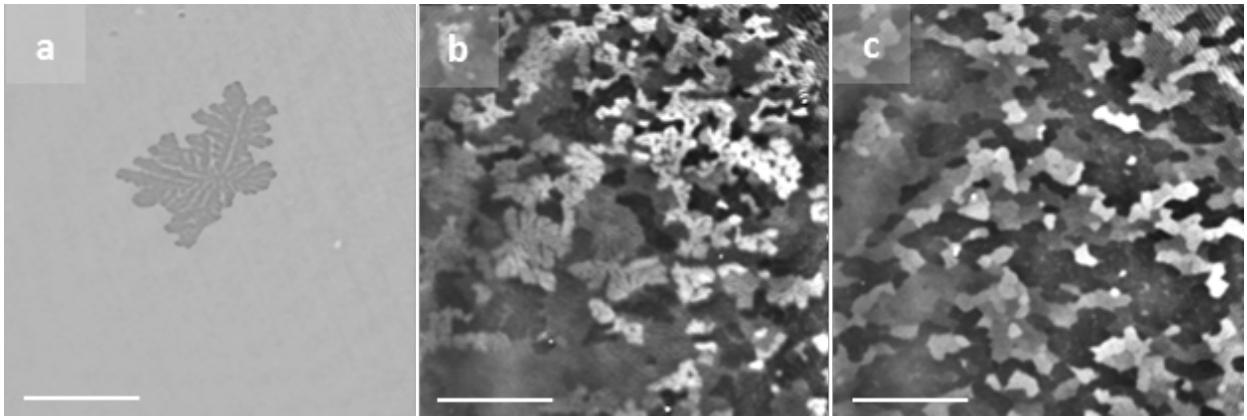

Figure 3.30. BAM micrographs of the monolayer of **7** on a 10^{-5} M aqueous $CuCl_2$ subphase. The monomolecular film was compressed to a surface pressure of 25 mN m^{-1} and its texture was investigated

in the absence of compression (**a**: π = 25 mN m^{-1}; **b**: π = 15 mN m^{-1}; **c**: π = 10 mN m^{-1}). Scale bar = 100 μm.

The fact that the dendritic structures vanish rapidly in the absence of monolayer compression indicates that the COO–Cu–COO bridges formed through the interfacial interaction of the macrocycles with Cu^{2+} ions are partially broken in the absence of compression.

In order to determine the effect of the speed of monolayer compression on the size of the dendritic domains of **7**, BAM experiments were conducted decreasing the speed of compression of the monolayer of **7**. When the monomolecular film of **7** is compressed to a surface pressure value of 20 mN m^{-1} on a 10^{-5} M aqueous $CuCl_2$ solution, at a barrier speed of 20 cm^2 min^{-1}, the micrographs reveal the presence of significantly large dendritic domains, cf. Figure 3.24. Indeed, the dendritic domains formed by **7** have sizes in the range of ca. 200 × 200 μm^2 (scale bar = 100 μm). It is known from the literature that highly ordered structures are typically observed in SAMs of thiolates on gold. Despite that, the size of such crystalline phases is far smaller, typically in the order of nanometers.[135] When the monolayer of **7** is compressed at a lower speed, i.e. 6 cm^2 min^{-1}, the micrographs show the presence of dendritic domains right after the takeoff of the isotherm, i.e. π = 2 mN m^{-1} (Figure 3.31).

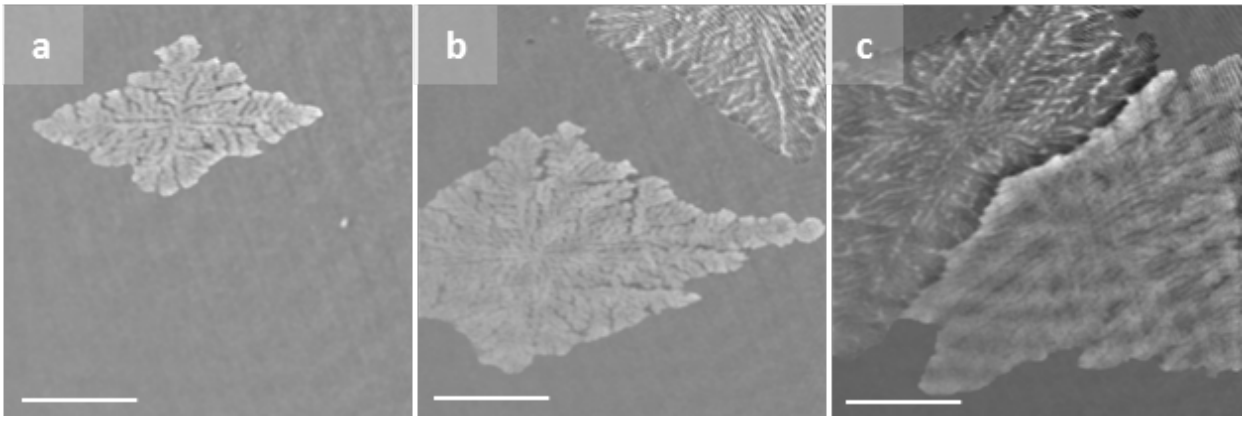

Figure 3.31. BAM micrographs of the monolayer of **7** on a 10^{-5} M aqueous $CuCl_2$ solution compressed at a barrier speed of 6 cm^2 min (**a**: π = 2 mN m^{-1}; **b**: π = 15 mN m^{-1}; **c**: π = 20 mN m^{-1}). Scale bar = 100 μm.

Upon further compression of the monolayer, the size of the dendritic domains steadily increases. At a surface pressure value of 15 mN m^{-1}, highly defined dendritic domains with a dimension significantly larger than that observed at a higher compression speed (barrier speed = 20 cm^2 min^{-1}) are formed (Figure 3.31). The micrographs show that the domains have a size in the range of ca. 400 × 400 μm^2 (scale bar = 100 μm). These results demonstrate that the speed of compression of the monolayer of **7** has a crucial effect on the size of the dendritic domains. The lower speed of compression is expected to favor the ordered aggregation of the amphiphiles around the formed "molecular seeds" instead of producing more nucleation sites so as to promote the formation of larger supramolecular assemblies.

In the presence of a 10^{-5} M aqueous $CuCl_2$ subphase, the macrocycles self-assemble into highly organized dendritic structures that possess different contrast. The different contrast of such structures is ascribed to the anisotropic ordering of the amphiphiles within the single domains. Domains with internal anisotropy have different reflectivity from isotropic regions when the polarizer of the BAM is set away from 0°.[136] The anisotropic domains show different contrast after rotating the polarizer while no changes in the contrast are observed if the domains are isotropic. In order to demonstrate the anisotropy of the dendritic structures, BAM

measurements of the monolayer of **7** on a 10^{-5} M aqueous $CuCl_2$ subphase were conducted. At a surface pressure value of 20 mN m^{-1}, dendritic structures are readily visible at the air-water interface. The micrographs in Figure 3.32 show the dendritic structures before and after rotating the polarizer.

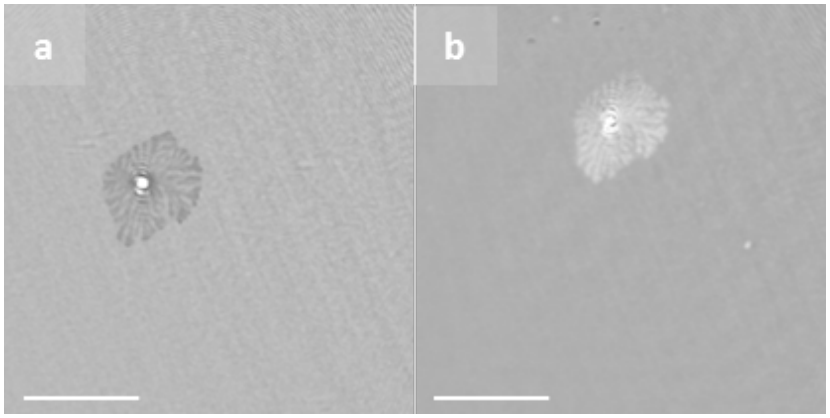

Figure 3.32. BAM micrographs of the monolayer of **7** on a 10^{-5} M aqueous $CuCl_2$ solution, compressed at a surface pressure of 20 mN m^{-1}, before (**a**) and after (**b**) rotating the polarizer. Scale bar = 100 μm.

When the polarizer is set to a value of 10°, the dendritic domain in Figure 3.32 appears dark. After rotating the polarizer to - 10°, the contrast is reversed and the dendritic domain appears bright. This finding undoubtedly demonstrates that the dendritic domains of **7** grown on a 10^{-5} M aqueous $CuCl_2$ solution are monocrystalline, with the amphiphiles anisotropically organized within the single domains. On the other hand, the contrast of the regular phase does not change by rotating the polarizer, therefore suggesting the presence of either an isotropic or an amorphous phase. The same experiment was repeated for the monolayer of **7** on pure water, cf. Figure 3.33.

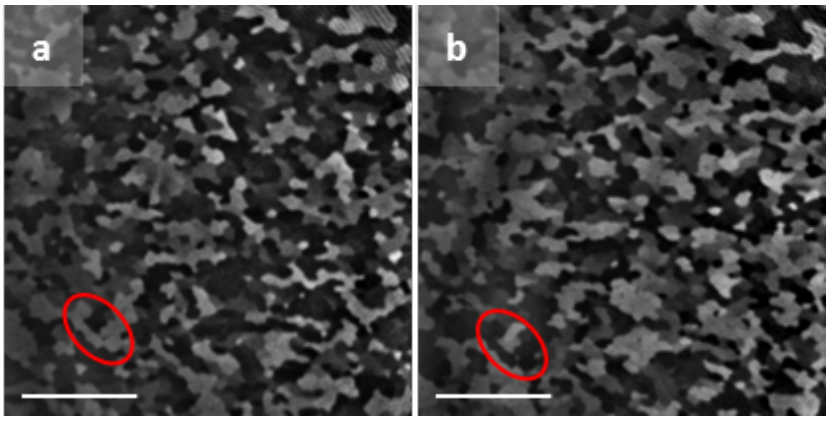

Figure 3.33. BAM micrographs of the monolayer of **7** on pure water, compressed at a surface pressure of 20 mN m^{-1}, before (**a**) and after (**b**) rotating the polarizer. The red circles are added to facilitate the visualization of the contrast change in the domains of **7**. Scale bar = 100 μm.

The micrographs reveal that the domains characterized by optical contrast are anisotropic; by rotating the polarizer, the contrast of such domains changes. The observation of contrast inversion confirms the presence of densely packed anisotropic structures of **7**.

3.4.4 LB transfer and deposition

BAM results strongly suggest that the amphiphiles, self-assembled as Langmuir monolayers at the air-water interface, are stabilized by Cu^{2+} ions. The formation of COO–Cu–COO bridges is expected to generate an extended array of noncovalent interactions, i.e. 2D metal organic networks. The presence of the Cu^{2+} linker is supposed to increase the lateral cohesiveness of the monomolecular film so as to allow its transfer onto hydrophobic substrates with the headgroups of the macrocycles pointing into air. The LB transfer and deposition technique was used to verify this hypothesis. Si(100)/SiO_2 slides (2 cm × 1 cm) were chemically modified with a monolayer of octadecyltrichlorosilane (OTS). The thickness of the OTS monolayer was measured to be 2.7 nm, a value in agreement with that reported in the literature.[137] The transfer of the monomolecular layer of **7** from the air-water interface to the hydrophobic substrate was

conducted as follows. The $CHCl_3$ solution containing the amphiphiles is spread on the water surface. The monolayer is compressed to a surface pressure of 25 mN m^{-1} and, while maintaining the monolayer under compression, the hydrophobic substrate is slowly dipped into the subphase. The solid substrate is kept in the aqueous subphase for 60 minutes, the barriers opened and the substrate rapidly removed from the aqueous subphase. Two compression isotherms, one before and one after dipping the solid substrate into the aqueous subphase, were conducted in order to determine the amount of **7** deposited on the substrate in terms of molecular area. The control experiment, carried out without dipping the substrate into the aqueous subphase, revealed that the monolayer of **7** shows hysteresis; a shift of 2 cm^2 between the two isotherms is observed, cf. Figure 3.34.

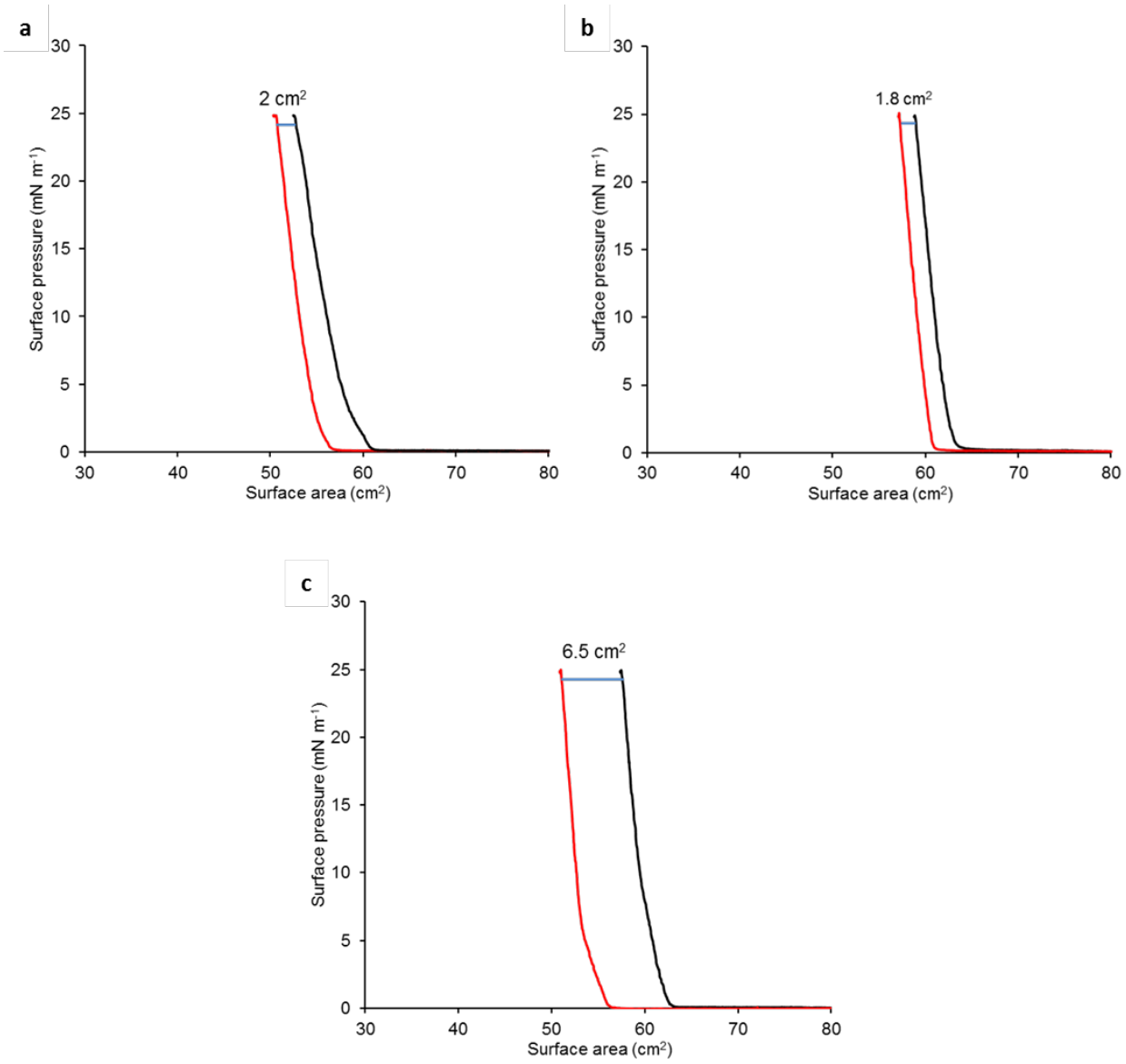

Figure 3.34. Surface pressure vs. surface area compression isotherms of the monolayer of **7** (**a**) on pure water before (**–**) and after (**–**) 60 minutes without dipping the substrate, i.e. control experiment, (**b**) on pure water before (**–**) and after (**–**) dipping the substrate for 60 minutes and (**c**) on a 10^{-5} M aqueous $CuCl_2$ solution before (**–**) and after (**–**) dipping the substrate for 60 minutes.

When the substrate is dipped into the pure aqueous solution, the two isotherms are shifted of a value that is highly similar to that of the control experiment, i.e. 1.8 cm^2. This result indicates

that the monolayer of **7** was not transferred onto the hydrophobic substrate and that the monomolecular film comes back to the air-water interface. In the presence of a 10^{-5} M aqueous $CuCl_2$ subphase, the shift between the two isotherms is of 6.5 cm^2. Taking into consideration the hysteresis of **7** (2 cm^2), the value of 4.5 cm^2 is in reasonable agreement with the transfer of a single layer of the macrocycles on the surface of a hydrophobic substrate that has an area of 4 cm^2, with the polar groups oriented outwards. Surface ellipsometry and contact angle (CA) measurements were conducted in order to confirm the transfer of a monomolecular film of **7** onto a hydrophobic substrate with the aliphatic chains in contact with the substrate. Ellipsometry measurements revealed that, on pure water, the monolayer of **7** is not transferred onto the solid substrate; the measured thickness was 0.2 ± 0.2 nm. This result indicates that the monolayer returns to the interface and therefore confirms the results obtained by Langmuir compression isotherms. On the other hand, in the presence of an aqueous $CuCl_2$ solution at a concentration of 10^{-5} M, the thickness of the transferred film is 1.0 ± 0.2 nm, with a transfer ratio of the downward deposition of 1.0 ± 0.1. The solid-state structure of **7** reveals that the vertical dimension of the macrocycle is 1.0 nm. The measured thickness of 1.0 ± 0.2 nm is therefore in agreement with the successful deposition of a monomolecular layer of **7** onto a hydrophobic substrate with the polar heads, bridged by Cu^{2+} ions, pointing in air.[117] The successful transfer of the monolayer is attributed to the formation of a supramolecular network at the air-water interface that consists of noncovalent interactions between the carboxylic groups of adjacent amphiphiles and Cu^{2+} ions. These interactions favor the lateral cohesion among the macrocycles and stabilize the monolayer so as to prevent it from returning at the interface during the transfer. A bilayer of **7** was transferred onto a hydrophobic substrate in the presence of a 10^{-5} M aqueous $CuCl_2$ solution. After compressing the monolayer to a surface pressure of 25 mN m^{-1}, the solid substrate is immerged into the subphase so as to allow for the transfer of one layer of **7**. The subsequent removal of the substrate is conducted at the same speed of the downward trip and keeping the monolayer compressed at π = 25 mN m^{-1}, so as to

allow for the transfer of the second layer of **7**. The transferred film is a Y-type bilayer, where the monolayer deposits onto the substrate in both up and down directions with the interlayer consisting of headgroups-headgroups interactions. Ellipsometry revealed that the transferred film had a thickness of 2.1 ± 0.2 nm, with a transfer ratio value of 1.0 ± 0.1 for both the downward and upward trips. The measured thickness value of 2.1 nm demonstrates the successful deposition of a double layer on the solid substrate. The fact that the thickness of the transferred bilayer is nearly twice the thickness of the monomolecular layer of **7** further confirms the successful transfer of the monolayer onto the solid substrate with the carboxylic functions pointing in air.

The CA of the OTS monolayer was measured to be 110°; this value is in agreement with that reported in the literature.[138] On the other hand, the CA value of the monolayer of **7** was measured to be 91°. The value of 91° is significantly lower than the CA measured for the OTS layer (CA = 110°), thus confirming the successful transfer of the monomolecular film of **7** on a hydrophobic substrate with the polar functions oriented outwards. Despite that, the value of 91° is slightly higher than that expected for a hydrophilic surface.[139] This might be ascribed to the partial instability of the monolayer of **7** towards interfaces or to a molecular rearrangement of the macrocycles within the single layer.

The monolayer of **7**, deposited onto a hydrophobic substrate with the polar functions pointing in air by the LB method, i.e. vertical transfer, was imaged by means of tapping mode AFM, cf. Figure 3.35.

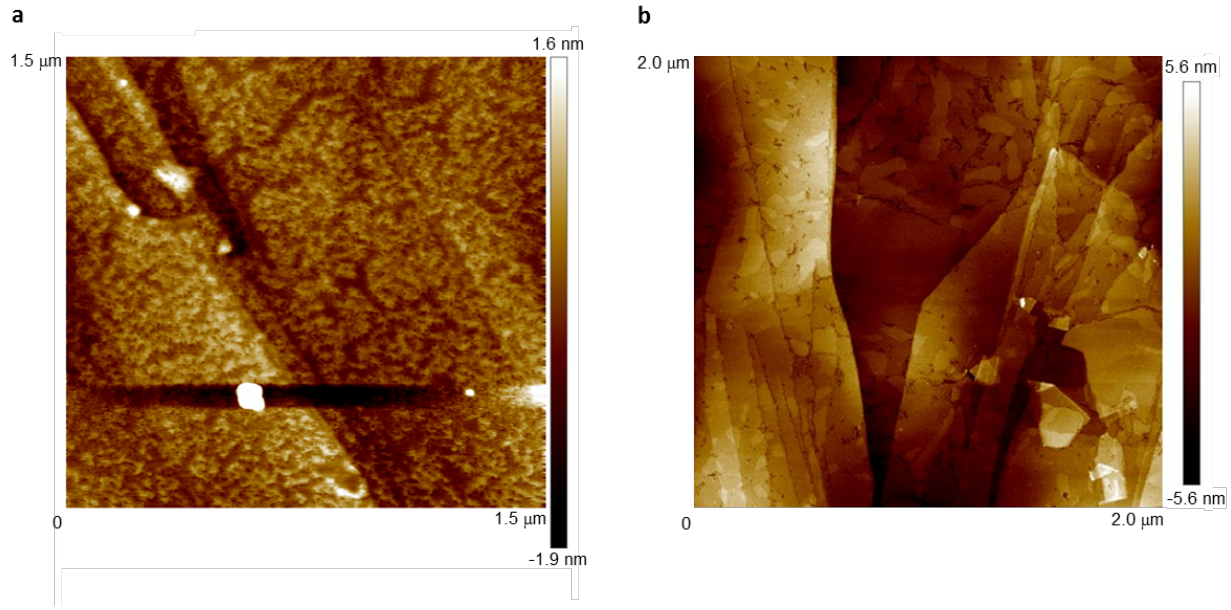

Figure 3.35. AFM micrographs of the monolayer of **7** deposited onto HOPG by the LB (**a**) and Langmuir-Schaefer techniques (**b**).

The micrograph shows that the transferred film has an irregular morphology with the macrocycles assembled in a worm-like structure. The diverse structuring of the film on a solid substrate in comparison with that observed at the air-water interface might be attributed to a partial molecular rearrangement of **7** occurring during the monolayer transfer. The limited flexibility of the headgroups of **7**, along with the loss of water molecules, may cause the macrocycles to adopt more favourable coordination geometry toward the cations. On the other hand, the film transferred onto a solid substrate by the Langmuir-Schaefer (LS) technique, i.e. horizontal deposition, is highly homogeneous (Figure 3.35). This result may be explained by the fact that, during the horizontal transfer, the macrocycles do not undergo a molecular reorganization, as they do not cross any interface. This result confirms the successful transfer and deposition of **7** onto a hydrophobic substrate with the polar functions pointing into air as a monomolecular film.

The presence of the dendritic highly organized domains of the monolayer of **7** on a 10^{-5} M aqueous $CuCl_2$ solution is ascribed to the interfacial formation of COO–Cu–COO bridges among adjacent amphiphiles and the cations. It is expected that the presence of polar heads with some degree of conformational freedom may improve the crystallinity of the corresponding monolayers. Indeed, the conformational freedom of the carboxylic moieties may provide the most stable coordination complex between the macrocycle and Cu^{2+} ions at the air-water interface.

3.4.5 Synthesis of 5,11,17,23-tetra-methylcarboxy-25,26,27,28-tetrapropoxycalix[4]arene (9)

The synthesis of 25,26,27,28-tetrapropoxycalix[4]arene was performed as mentioned in chapter 3.4.1. The introduction of the chloro-methyl functions at the *p*-positions of the alkylated calix[4]arene was conducted in the presence of concentrated HCl in dioxane, as described in the literature.[140] The synthesis of the new 5,11,17,23-tetra-methylcyano-25,26,27,28-tetrapropoxycalix[4]arene (**8**) was accomplished by nucleophilic substitution (S_N2) using NaCN as nucleophilic agent in DMSO. Hydrolysis of the nitrile functions of **8** under basic conditions yielded 5,11,17,23-tetra-methylcarboxy-25,26,27,28-tetrapropoxycalix[4]arene **9** as an off-white powder. The synthetic route of **9** is depicted in Figure 3.36.

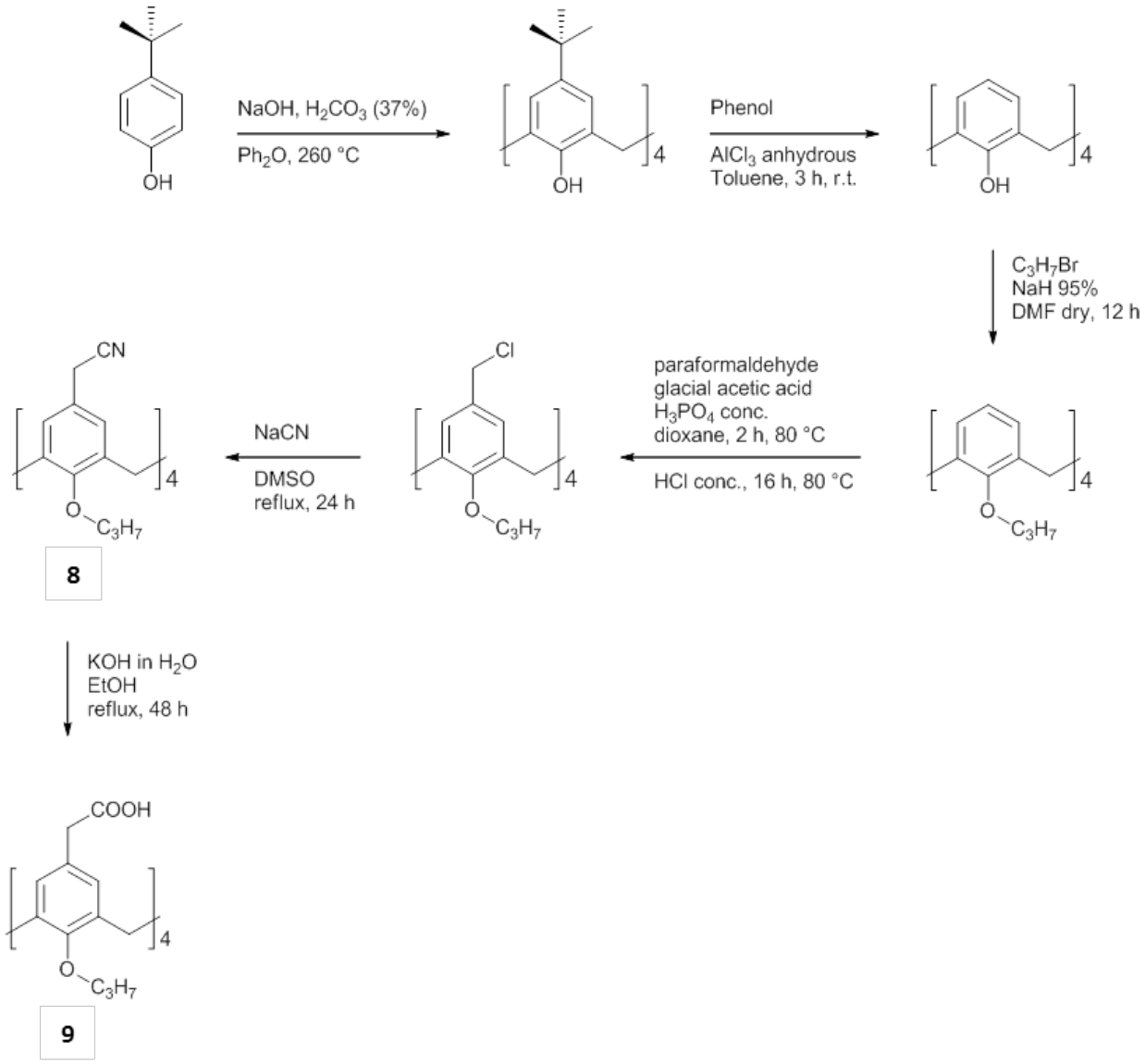

Figure 3.36. Synthetic route of **9**.

3.4.6 Langmuir compression isotherms

The ability of **9** to form stable Langmuir monolayers at the air-water interface was investigated by means of surface pressure-area compression isotherms. As shown by the isotherm of **9** on pure water, cf. Figure 3.37, the macrocycles self-assemble as a Langmuir monolayer at the air-water interface. The isotherm of **9** on pure water shows a π_c of 11 ± 1 mN m^{-1} and A_c, A_{lim} and A_0 values of 89, 100 and 103 ± 1 $Å^2$ $molecule^{-1}$, respectively. In addition, the $|\delta\pi/\delta A|$ measures 1 ± 0.2 mN $m^{-1}/Å^2$ $molecule^{-1}$, cf. Table 3.

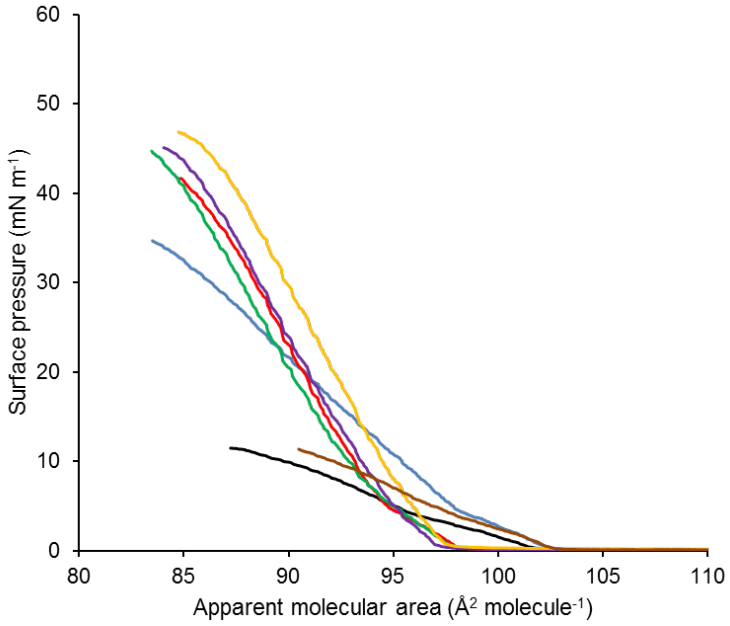

Figure 3.37. Surface pressure-area compression isotherms of the monolayer of **9** on pure water (–) and on 10^{-7} (–), 10^{-6} (–), 10^{-5} (–), 10^{-4} (–), 10^{-3} (–), and 10^{-2} M (–) aqueous $CuCl_2$ solutions.

Table 3. Characteristic values of the isotherms of **9** on pure water and on 10^{-7}, 10^{-6}, 10^{-5}, 10^{-4}, 10^{-3}, and 10^{-2} M aqueous $CuCl_2$ solutions.

Subphase	π_c	A_c	A_{lim}	A_0	$\lvert\delta\pi/\delta A\rvert$
Pure water	11 ± 1	89 ± 1	100 ± 1	103 ± 1	1 ± 0.2
10^{-7} M $CuCl_2$	11 ± 1	91 ± 1	101 ± 1	103 ± 1	1.2 ± 0.2
10^{-6} M $CuCl_2$	34 ± 1	84 ± 1	100 ± 1	103 ± 1	2.2 ± 0.2
10^{-5} M $CuCl_2$	40 ± 1	86 ± 1	96 ± 1	99 ± 1	4.3 ± 0.2
10^{-4} M $CuCl_2$	43 ± 1	84 ± 1	95 ± 1	98 ± 1	4.2 ± 0.2
10^{-3} M $CuCl_2$	45 ± 1	85 ± 1	96 ± 1	98 ± 1	4.2 ± 0.2
10^{-2} M $CuCl_2$	46 ± 1	86 ± 1	97 ± 1	98 ± 1	4.5 ± 0.2

Π_c and A_c represent the maximum values of pressure and area to which, after further compression of the monolayer, the amphiphile is forced out of the interface. A_{lim} is the extrapolation of the linear part of the isotherm on the x-axis. A_0 is the area occupied by one molecule at the isotherm takeoff. $\lvert\delta\pi/\delta A\rvert$ is the modulus of the slope on the steepest part of the monolayer.

The A_{lim} value of 100 ± 1 $Å^2$ $molecule^{-1}$ of the monolayer of **9** on pure water is reasonably in agreement with the presence of a calix[4]arene derivative at the air-water interface with the pseudo C_4 symmetry axis perpendicular to the water surface. The π_c value of the isotherm of **9** on pure water is 11 ± 1 mN m^{-1}. This value is significantly lower than that of its structural analogue **7** (π_c = 37 ± 1 mN m^{-1}), indicating the lower stability of **9**, self-assembled as a Langmuir monolayer at the air-water interface, in comparison with **7**. This may be attributed to the fact that **9** possess a less rigid conformation than **7** as a consequence of the presence of flexible polar functions (CH_2COOH) that partially disrupt the π-π interactions among aromatic rings of neighbouring amphiphiles at the air-water interface.

The variation of the characteristic values of the isotherm of **9** as a function of the concentration of $CuCl_2$ dissolved in the aqueous subphase was investigated. The isotherms revealed that, for a range of aqueous $CuCl_2$ solution concentrations that goes from 10^{-7} to 10^{-2} M, A_{lim} of **9**

fluctuates from a value of 101 to 95 ± 1 $Å^2$ $molecule^{-1}$ while A_c ranges from a value of 91 to 84 ± 1 $Å^2$ $molecule^{-1}$, cf. Figure 3.38.

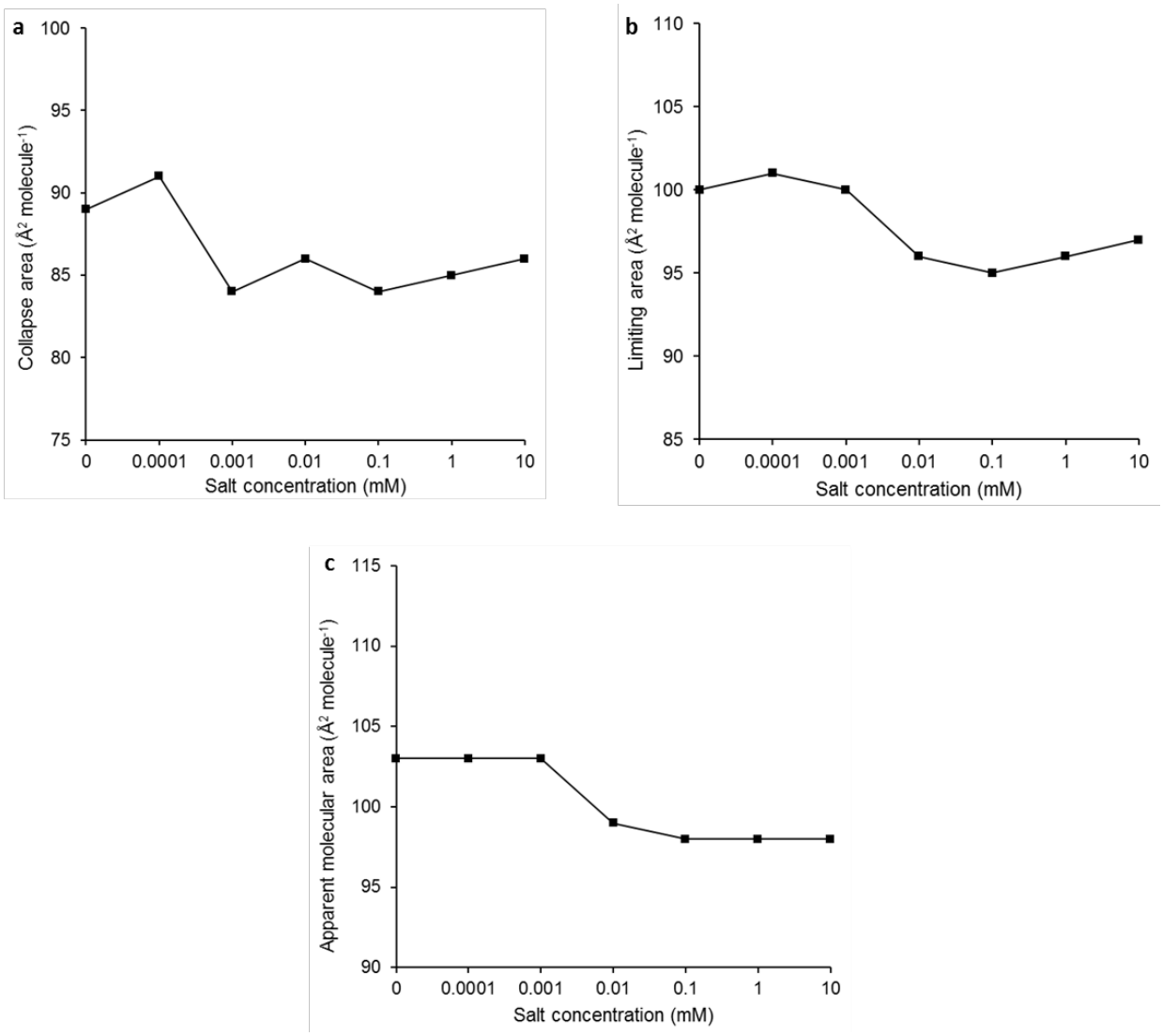

Figure 3.38. Variation of A_c (**a**), A_{lim} (**b**) and A_0 (**c**) values of the isotherms of **9** as a function of the concentration of Cu^{2+} ions in the aqueous solution.

The A_0 of the isotherm of **9** slightly decreases with the increase of the concentration of Cu^{2+} ions, from a value of 103 on a 10^{-6} M aqueous $CuCl_2$ subphase to a value of 98 ± 1 $Å^2$ $molecule^{-1}$ on a 10^{-4} M aqueous $CuCl_2$ subphase (Figure 3.38). This set of results indicates that A_c, A_{lim} and A_0 values of **9** are not affected by the concentration of Cu^{2+} ions in the aqueous solution. In addition, the values of A_c, A_{lim} and A_0 of **9** on the Cu^{2+} ions subphases are similar to those on pure water (A_c = 89 ± 1 $Å^2$ $molecule^{-1}$; A_{lim} = 100 ± 1 $Å^2$ $molecule^{-1}$; A_0 = 103 ± 1 $Å^2$ $molecule^{-1}$). These data indicate that the A_c, A_{lim} and A_0 values are not altered by the interfacial interaction of the monomolecular film of **9** with Cu^{2+} ions. On the other side, the π_c value of the monolayer of **9** significantly increases with the increasing of the cations concentration, as shown in Figure 3.39.

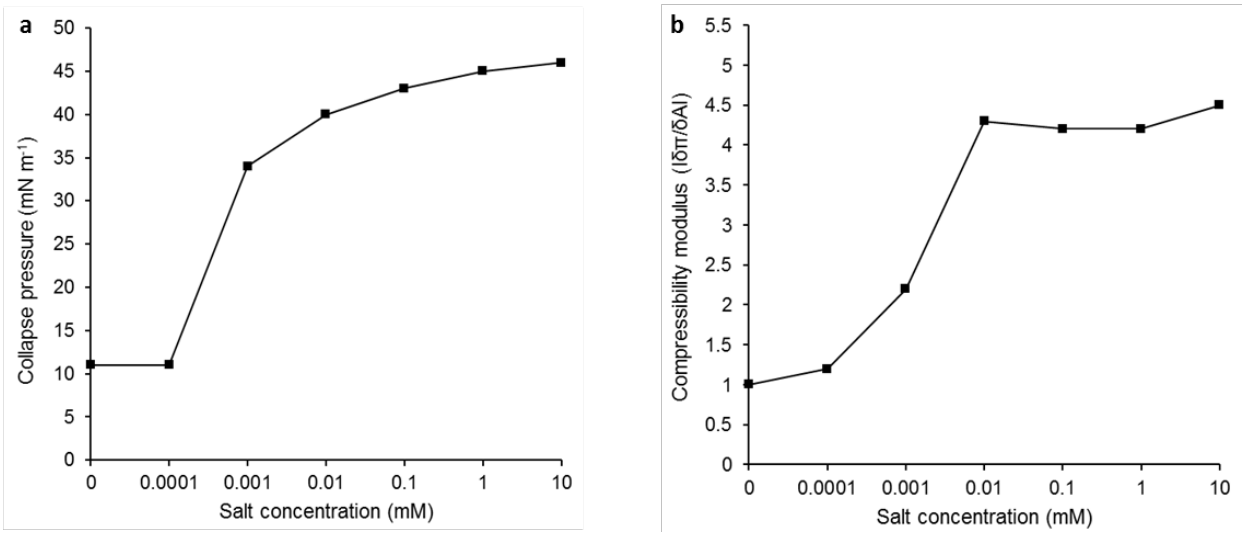

Figure 3.39. Variation of π_c (**a**) and $|\delta\pi/\delta A|$ (**b**) values of the isotherms of **9** as a function of the concentration of Cu^{2+} ions in the aqueous solution.

The π_c value of **9** significantly increases from a value of 11 on pure water to a value of 34 ± 1 mN m^{-1} on an aqueous $CuCl_2$ solution at a relatively low concentration of 10^{-6} M. In addition, the π_c further increases from a value of 34 on a 10^{-6} M aqueous $CuCl_2$ solution to 46 ± 1 mN m^{-1} on a

10^{-2} M aqueous $CuCl_2$ solution (Figure 3.39). These results clearly indicate that the monolayer of **9** shows high interfacial affinity towards Cu^{2+} ions. The evolution of the $|\delta\pi/\delta A|$ values of **9** follows a trend similar to that of π_c, cf. Figure 3.39. $|\delta\pi/\delta A|$ considerably increases from a value of 1 on pure water to 4.3 ± 0.2 mN $m^{-1}/Å^2$ $molecule^{-1}$ on a 10^{-5} M aqueous $CuCl_2$ solution. These results indicate that the increasing concentration of Cu^{2+} ions in the aqueous solution contributes to the formation of a more condensed monolayer phase. In addition, from a Cu^{2+} ions concentration of 10^{-5} to 10^{-2} M, the $|\delta\pi/\delta A|$ value slightly increases from 4.3 to 4.5 suggesting that the monolayer of **9** is approaching cation binding saturation (Figure 3.39).

3.4.7 BAM measurements

The morphology of the monolayer of **9** on pure water and on a 10^{-5} M aqueous $CuCl_2$ subphase was investigated by BAM. The micrographs revealed that the macrocycles self-assemble on pure water in the form of relatively large liquid-expanded domains before the isotherm takeoff, i.e. A = 105 $Å^2$ $molecule^{-1}$ (Figure 3.40).

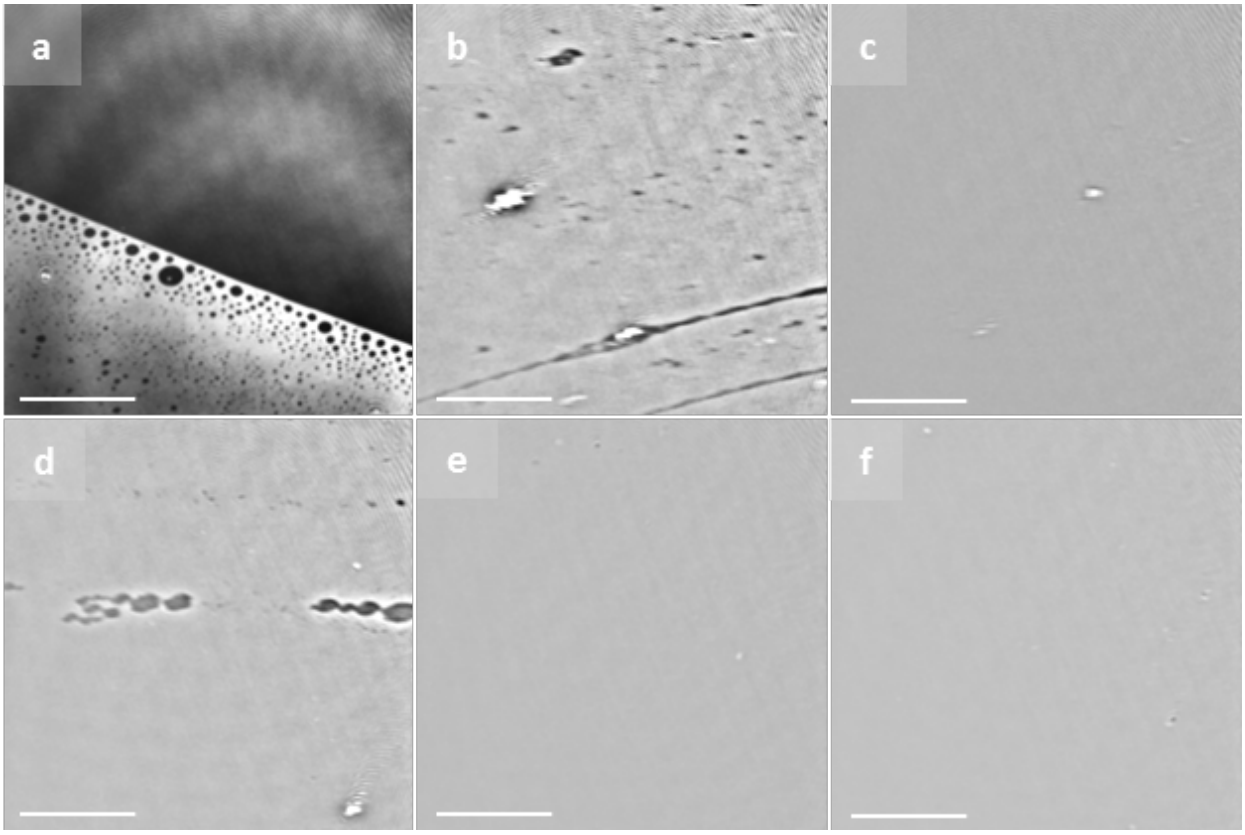

Figure 3.40. BAM micrographs of the monolayer of **9** on pure water (**a**: π = 0 mN m^{-1}; **b**: π = 0.1 mN m^{-1}; **c**: π = 3 mN m^{-1}) and on a 10^{-5} M aqueous $CuCl_2$ solution (**d**: π = 0 mN m^{-1}; **e**: π = 0.1 mN m^{-1}; **f**: π = 3 mN m^{-1}).

At the isotherm takeoff, i.e. π = 0.1 mN m^{-1}, the monomolecular film of **9** appears highly regular and, at π = 3 mN m^{-1}, homogeneous. The monolayer remains highly homogeneous until the

collapse. The texture of the monolayer of **9** significantly differs from that of its structural analogue **7** which consists of anisotropically ordered domains of different contrast. This may be ascribed to the minor contribution of the π stacking to the interfacial self-assembly of **9** in comparison with that of **7**, thus consistent with the Langmuir compression experiments.

In the presence of a 10^{-5} M aqueous $CuCl_2$ solution, the monolayer of **9** appears highly homogeneous before the isotherm takeoff, i.e. A = 104 $Å^2$ $molecule^{-1}$ (Figure 3.40). The micrographs reveal that, at the isotherm takeoff, the monolayer possesses a homogeneous texture that is maintained until the collapse of the monomolecular film. These results indicate that the macrocycles, self-assembled as a Langmuir monolayer at the air-water interface, interact with Cu^{2+} ions at a relatively low compression state.

3.4.8 Conclusions

The short chain C_3 calix[4]arene **7** was demonstrated to self-assemble as a stable Langmuir monolayer at the air-water interface. The high surface pressure value shown by the compression isotherm of **7** is attributed to the strong π-π interactions among aromatic rings of neighboring macrocycles. The π stacking is expected to compensate the weak or negligible contribution of the van der Waals interactions among the alkyl chains of **7**. In the presence of a 10^{-5} M aqueous $CuCl_2$ solution, the profile of the isotherm of **7** differs from that on pure water, thus indicating that the monolayer interacts with Cu^{2+} ions at the air-water interface.

The morphology of the monomolecular film of **7** on pure water and on a 10^{-5} M aqueous $CuCl_2$ solution was investigated by BAM. The micrographs revealed that the monolayer of **7** on pure water is not homogeneous; well-defined domains of different contrast are formed at the isotherm takeoff, i.e. π = 0.1 mN m^{-1}. By further compression, the domains get coarser and larger. The anisotropic domains generated by **7** have distinct reflectivity and therefore show different contrast in the BAM micrograph. Remarkably, the morphology of the monolayer of **7**

drastically changes when $CuCl_2$ is dissolved in the aqueous subphase at a concentration of 10^{-5} M. At the isotherm takeoff, the monolayer appears highly homogeneous. At higher surface pressure values, i.e. 15 mN m^{-1}, significantly large crystalline dendritic domains of different contrast grow at the air-water interface. The growth of such domains is attributed to the binding of the amphiphiles to Cu^{2+} ions so as to produce highly ordered and extended 2D arrays of noncovalent interactions at the air-water interface, namely 2D metal organic networks. These results highlight the influence of the molecular design of the organic building block on the fabrication of molecularly thin crystalline films at the air-water interface. While the interfacial self-assembly of **3** is mainly driven by van der Waals interactions among aliphatic chains that generate partially disordered structures, the self-assembly of **7** is mainly driven by π-π interactions among aromatic rings of neighboring macrocycles so as to produce highly organized structures. The anisotropy of the dendritic domains of **7** is unambiguously proved by rotating the polarizer away from 0° during BAM measurements. It is shown that, after rotating the polarizer, the contrast of the dendritic structures is reversed. This result therefore demonstrates that the dendritic domains of **7** are monocrystalline and that the macrocycles are anisotropically organized within the single domains.

The transfer of the monolayer of **7** onto a hydrophobic substrate with the polar groups pointing in air was performed by the LB technique. Ellipsometry measurements revealed that, in the presence of a 10^{-5} M aqueous $CuCl_2$ solution, the transferred film has a thickness of 1.0 ± 0.2 nm. This value is consistent with the vertical length of the solid-state structure of the macrocycle, thus demonstrating the successful transfer of a single layer of **7** onto a hydrophobic substrate with the polar functions pointing in air. The successful transfer of the monolayer of **7** is attributed to the stabilization effect caused by Cu^{2+} ions. Each cation is expected to interact with two carboxylic groups of adjacent amphiphiles so as to increase the lateral cohesion among the macrocycles at the interface. AFM images revealed that the monolayer transferred onto the hydrophobic substrate by the LB technique, i.e. vertical deposition, is irregular. On the other

hand, the monomolecular film of **7** transferred onto the hydrophobic substrate by the LS technique, i.e. horizontal deposition, appears highly homogeneous. Unlike the horizontal deposition, molecular reorganization of **7** may occur when the monolayer, deposited onto the substrate by the LB technique and immerged into the aqueous subphase, is pulled out from water and crosses the water-air interface.

The synthesis of a new amphiphilic calix[4]arene derivative **9** was accomplished. The macrocycle was proven, by surface pressure-area compression isotherms, to form less stable Langmuir monolayers than those of its structural analogue **7**. This is attributed to the minor contribution of the π-π interactions among aromatic rings of neighboring macrocycles of **9** to the self-assembly process at the air-water interface. When $CuCl_2$ is added in the aqueous subphase at a relatively low concentration of 10^{-6} M, the collapse pressure of the monolayer of **9** significantly increases in comparison with that on pure water, thus indicating that a relevant interaction between the amphiphiles and Cu^{2+} ions takes place.

4 Conclusions and future directions

Solid-state polymorphism is a matter of great importance for the pharmaceutical industry. Distinct polymorphs of the same API may possess different physicochemical properties, which can significantly affect the formulation and bioavailability of the final drug. The findings reported in this manuscript show that, for the first time, Langmuir monolayers of a *p*-carboxycalix[4]arene derivative **3** induce the crystal growth of GBP, an API used to relieve neuropathic pain, at the air-water interface, with a control over its polymorphism. While the polar functions of the macrocycle act as recognition units for the interfacial nucleation of GBP, the packing density of the amphiphiles exert a control over the polymorphism of the pharmaceutical. Single crystal X-ray diffraction and IR spectroscopy unambiguously revealed that the fully compressed monolayer of **3** kicks off the crystallization of GBP polymorphic form α while the partially compressed monolayer of **3** induces the crystallization of GBP polymorphic form γ. Remarkably, in the absence of the monolayer, the hydrate form of GBP grows at the interface and in the bulk solution. As of today, the limited number of water soluble APIs that show polymorphism prevented us from investigating the template effect of calix[4]arene-based Langmuir monolayers on other pharmaceuticals. As a future perspective, the ability of calix[4]arene-based LB films to trigger the crystallization of APIs in organic solvents may be investigated.

Langmuir monolayers of amphiphilic calixarenes show good recognition properties towards ions at the air-water interface. This is mainly due to the presence of a rigid cavity, which give a best-fit with the target ion. The findings reported in this manuscript give new insight into the interfacial binding properties of calix[4]arenes monolayers towards divalent cations. Calix[4]arenes possess multiple polar functions that can bind more than one ion at the air-water interface. The multivalency of amphiphilic calix[4]arenes is exploited to generate highly ordered and extended 2D arrays of noncovalent interactions with divalent cations at the interface, that

is two-dimensional metal organic networks. It is demonstrated that the molecular structure of the calix[4]arene plays a crucial role in the fabrication of such two-dimensional networks. While Langmuir monolayers of the long chain *p*-carboxycalix[4]arene **3** interact with Cu^{2+} ions generating a disordered phase, the binding of the monomolecular film of its short chain C_3 structural analogue **7** to Cu^{2+} ions produces highly ordered crystalline dendritic structures. BAM measurements unambiguously demonstrated that the dendritic domains of **7**, formed on a 10^{-5} M aqueous $CuCl_2$ subphase, are monocrystalline and anisotropic. The so-produced monolayers represent the first example of molecularly thick 2D films at the air-water interface possessing a lateral size in the range of micrometres that consist of an intrinsically 3D building block.

The introduction of flexible polar functions at the *p*-positions of the short chain C_3 macrocycle might contribute to increase the degree of crystallinity of the corresponding calix[4]arene-based monolayers. The conformational freedom of the polar arms of the macrocycle is indeed expected to provide the most stable coordination complex between the ligands and Cu^{2+} ions at the interface. To confirm this assumption, the new calix[4]arene derivative **9** has been synthesised and its self-assembly properties at the air-water interface investigated. Langmuir compression isotherms revealed that the monolayer of **9** interacts with Cu^{2+} ions at a relatively low concentration of 10^{-6} M the air-water interface. BAM measurements indicated that the monolayer of **9** appears highly homogeneous both on pure water and on a 10^{-5} M aqueous $CuCl_2$ subphase. Further investigations, e.g. X-ray diffraction measurements on liquid and solid surfaces, are currently ongoing to determine the effect of Cu^{2+} ions on the structure of the monomolecular film of **9** at the air-water interface.

This manuscript proved that the proper design of the organic building block plays a crucial role in the fabrication of two-dimensional, considerably large and highly ordered metal organic networks at the air-water interface. Such crystalline domains may be exploited to trigger the crystal growth of calix[4]arene-based MOFs at the air-water interface. The **7**-based metal

organic networks are expected to consist of Cu^{2+} ions that present available coordination sites weakly bound to water molecules. Additional carboxylate ligands, belonging to water-soluble calix[4]arene derivatives that are structural analogues of **7**, may bind to the available coordination sites of the cations possibly forming the most stable "paddle-wheel" Cu_2 clusters. The presence of a solute in the aqueous subphase with same structure and size of the amphiphile that self-assembles as a Langmuir monolayer at the air-water interface would represent a perfect fit for lattice matching epitaxial growth. The propagation of the network in the axial direction with respect to the water surface is expected to generate three-dimensional surface-grown calix[4]arene-based MOFs.

5 Experimental methods

5.1 General

All chemicals were purchased from Sigma-Aldrich and used without further purification. ^{1}H and ^{13}C NMR spectra (300 and 75 MHz, respectively) were recorded on Bruker spectrometer in $CDCl_3$. Mass spectra were recorded in ESI mode on a Finnigan LCQ Deca instrument. Elemental analyses were measured on a Leco CHN-900 microanalyser (C-, H-, N-detection) and are reported in mass per cent. Thin layer chromatography (TLC) was performed on silica-coated plates with a UV_{254} indicator and column chromatography on 230−400 mesh Merck 60 silica gel. Compounds **3** and **7** were synthesised as previously described in the literature.[116,132] The analytical data are in perfect agreement with that reported. Others in our group have synthesized compounds **4**, **5** and **6**.[129] Analytical grade chloroform, dichloromethane, methanol and pyridine were purchased from Sigma-Aldrich and used without further purification. Nanopure water (resistivity ≥ 18 MΩ × cm) was produced with a Millipore Synergy purification system. Gabapentin was purchased from AK Scientific and used without further purification. Copper chloride dihydrate ($CuCl_2$), cobalt chloride hexahydrate ($CoCl_2$), nickel chloride hexahydrate ($NiCl_2$), manganese chloride tetrahydrate ($MnCl_2$) and mercury chloride ($HgCl_2$) were purchased from Sigma-Aldrich and used without further purification. Aqueous $CuCl_2$, $CoCl_2$, $NiCl_2$, $MnCl_2$ and $HgCl_2$ solutions at concentrations of 10^{-5} and 10^{-3} M were prepared extemporaneously by dissolving appropriate amounts of the substances in nanopure water. Infrared (IR) spectra were collected in attenuated total reflection (ATR) using a single reflection diamond ATR device (Golden Gate) and a Varian 670-IR spectrometer.

5.2 Synthesis

5,11,17,23-tetra-methylcyano-25,26,27,28-tetrapropoxycalix[4]arene (8). 5,11,17,23-tetrakis(chloromethyl)-25,26,27,28-tetrapropoxycalix[4]arene (1 g, 1.27 mmol) was dissolved in

DMSO (150 mL) and NaCN (0.37 g, 6 eq.) was subsequently added to the solution. The mixture was allowed to stir at 80 °C under N_2 atmosphere for 3 hours. The pale yellow solution was cooled down to room temperature, added to 400 mL of ice/water and acidified with a 2 M HCl solution with the formation of a white precipitate. The precipitate was filtered off and recrystallized twice from methanol to obtain **8** as thin plate-like crystals with a yield of 45%.

^{1}H NMR ($CDCl_3$-d, 300 MHz) δ_H = 6.63 (s, 8 H, Ar*H*), 4.44 (d, J = 13.3 Hz, 4 H, ArC*H*$_2$Ar), 3.85 (t, J = 13.3 Hz, 8 H, OC*H*$_2$CH$_2$CH$_3$), 3.51 (s, 8 H, ArC*H*$_2$CN), 3.15 (d, J = 13.5 Hz, 4 H, ArC*H*$_2$Ar), 1.93 (sxt, J = 7.5 Hz, 8 H, OCH$_2$C*H*$_2$CH$_3$), 1.00 ppm (t, J = 7.4 Hz, 12 H, OCH$_2$CH$_2$C*H*$_3$). ^{13}C NMR ($CDCl_3$-d, 75 MHz) δ_C = 156.2, 135.4, 127.8, 123.5, 118.4, 77.2, 30.84, 23.2, 22.9, 10.2 ppm. MS (ESI) m/z: [M + Na]$^+$ cald for $C_{48}H_{52}N_4O_4$ 771.9; found 771.1; [M]$^+$ cald for $C_{48}H_{52}N_4O_4$, 747.9; found 747.4. Elemental analysis (%); cald. C: 76.98, H: 7.00, N: 7.48; found C: 76.52, H: 7.29, N: 7.45.

5,11,17,23-tetra-methylcarboxy-25,26,27,28-tetrapropoxycalix[4]arene (9). 5,11,17,23-tetra-methylcyano-25,26,27,28-tetrapropoxycalix[4]arene (0.5 g, 0.67 mmol) was dissolved in EtOH (50 mL) and a solution of KOH (1000 eq.) in H_2O (50 mL) was subsequently added to the solution. The mixture was allowed to stand under stirring at 80 °C for 48 hours. The mixture was allowed to cool down to room temperature and concentrated HCl was added with the formation of a brownish precipitate. The precipitate was filtered off, dissolved in methanol and precipitated with water. Column chromatography (CH_2Cl_2/MeOH 5%/FA 3%) yielded **9** pure with a yield of 60%.

^{1}H NMR ($CDCl_3$-d, 300 MHz) δ_H = 6.55 (br. s., 7 H, Ar*H*), 4.39 (d, *J* = 12.9 Hz, 4 H, ArC*H*$_2$Ar), 3.82 (br. s., 8 H, OC*H*$_2$CH$_2$CH$_3$), 3.18 (br. s., 8 H, ArC*H*$_2$COOH), 3.11 (d, *J* = 13.1 Hz, 4 H, ArC*H*$_2$Ar), 1.94 (sxt, *J* = 7.40 Hz, 8 H, OCH$_2$C*H*$_2$CH$_3$), 1.01 ppm (t, *J* = 7.31 Hz, 12 H, OCH$_2$CH$_2$C*H*$_3$). ^{13}C NMR ($CDCl_3$-d, 75 MHz) δ_C = 179.1, 155.61, 134.97, 129.46, 126.82, 76.85, 40.55, 30.48, 23.30, 10.32 ppm. MS (ESI) m/z: [M + Na]$^+$ cald for $C_{48}H_{56}O_{12}$ 847.9; found 847.7; [M + 2Na]$^+$ cald for

$C_{48}H_{56}O_{12}$ 870.9; found 869.3; $[M + K]^+$ cald for $C_{48}H_{56}O_{12}$ 864.1; found 863.9. Elemental analysis (%); cald. C: 69.88, H: 6.84; found C: 68.74, H: 7.12.

5.3 Surface pressure-area compression isotherms

Surface pressure-area compression isotherms were carried out using a Nima 112D system. The Langmuir trough was cleaned with analytical grade chloroform in order to remove potential organic impurities and thoroughly rinsed with nanopure water prior to use. Solutions of **3** and **7** were prepared by dissolving the appropriate amount of the amphiphiles in chloroform (5 and 20% methanol, respectively) at the concentration of 1 g L^{-1}. Solutions of **4**, **5**, **6** and **9** were prepared by dissolving the appropriate amount of the macrocycles in chloroform at the concentration of 1 g L^{-1} for **4**, **5** and **6** and 0.5 g L^{-1} for **9**. 10 µL of the solutions of **3**, **4**, **5** and **6**, 7 µL of **7** and 13 µL of **9** were spread on the water surface using a Hamilton microsyringe. Monolayers were allowed to stand for 15 minutes to allow for solvent evaporation and stabilization of the amphiphiles at the interface. Symmetric compression of the monolayers was performed at a speed of 5 cm^2 min^{-1}.

5.4 Brewster angle microscopy

Micrographs were acquired by using a Nanofilm_ep3 system (Accurion) equipped with an internal, solid-state laser at a wavelength of 658 nm. The images were acquired using a CCD camera (768 × 562 pixels) and a 10× objective, equipped with an automatic focus scanner. The lateral resolution was 1 µm. 80 µL of solutions of **3**, **4**, **5**, **6** and **7** and 110 µL of a solution of **9** were spread at the surface of water. The monolayers were allowed to stand for 20 minutes for the evaporation of the solvent and the stabilization of the macrocycles at the interface. Symmetric compression of the monolayers was performed at a speed of 15 cm^2 min^{-1} for **3**, **4**, **5** and **6**, at speeds of 20 and 6 cm^2 min^{-1} for **7** and at a speed of 10 cm^2 min^{-1} for **9**. The micrographs of **7** and **9** were high-pass filtered to remove a low spatial frequency artefact from

the data. The filtering was chosen such that the artefact remains visible, but can be recognized at the same time with the fine structure of the molecular layer.

5.5 Spectroscopic imaging ellipsometry

Ellipsometry measurements were carried out using a Nanofilm_ep3 system (Accurion) equipped with an internal, solid-state laser at a wavelength of 658 nm in a nulling PCSA (polarizer-compensator-sample-analyser) set-up. The linear polarizer (P) and the quarter-wave plate (C) yielded an elliptically polarized incident beam that was reflected off as linearly polarized to the analyser (A). The variation of the angles for P and A while keeping C constant allowed fulfilling the nulling conditions for the analysed samples. The data were converted into the ellipsometric angles Δ (phase shift of *p*- and *s*-polarized components of light upon reflection off the sample) and Ψ (ratio of amplitude change for the *p* and *s* components). The measurements were conducted at an incident angle of 42° with diverse wavelengths (k = 629.1, 710.2, 791.2, 880.7, 1000.8 nm). The optical model allowed determining the thickness of the LB films as a function of the measured ellipsometric angles.

5.6 Langmuir-Blodgett transfer and deposition

The Langmuir-Blodgett (LB) transfer and deposition process was carried out using a vertical system dipping. Silicon wafers were used as solid substrates for the LB transfer. The substrates (2 × 1 cm) were pre-cleaned with soap and thoroughly rinsed with nanopure water, acetone and methanol respectively. They were dried with a nitrogen flow and placed in a UV-O_3 chamber for 20 min and subsequently rinsed with methanol. The substrates were placed in a 4.4 g L^{-1} OTS solution in dry heptane for 90 minutes and rinsed with heptane and chloroform respectively. The monolayer of **7** was spread on the water surface and, after 15 min of equilibration time, compressed to a surface pressure of 25 mN m^{-1}. The hydrophobic substrate was dipped into the aqueous solution at a speed of 5 mm min^{-1}. After 60 minutes of equilibration time, the barriers

were opened and the solid substrate removed from the aqueous solution (speed rate of 60 mm min^{-1}).

5.7 Crystallization experiments

The crystallization experiments were performed in scintillation vials spreading appropriate volumes of solutions of **3** at the surface of supersaturated aqueous solutions of GBP. The saturation point of the GBP solution was measured at 22 °C by adding small amounts of the API to the solution and corresponded to 143 g L^{-1}. Each condition was repeated ten times to ensure the reproducibility of the experiments. Two controls were used; one spreading only chloroform at the surface in order to ensure that the crystal growth was not dependent on the endothermic evaporation of the solvent and the other one having only the supersaturated aqueous GBP solution. The so-prepared solutions were allowed to stand at 22 °C and after 14 days, millimetre- to centimetre-sized crystals were present in all the crystallization vials where **3** was spread on the aqueous solution surface, strictly confined to the air-liquid interface.

5.8 Single crystal X-ray diffraction

Anhydrous gabapentin polymorphic forms α and ɣ and hydrate gabapentin polymorphic forms were identified by determination of the unit cell parameters on a Bruker KappaAPEX diffractometer using the APEX2 data collection software.[141]

Single crystals of **3** were crystallized from pyridine. A suitable crystal was measured on a SuperNova, Dual, Cu at zero, Atlas diffractometer using mirror monochromatized CuK_α (λ = 1.5418 Å) radiation at a temperature of 120.01(10) K. The structure was solved with the olex2.solve structure solution program (Charge Flipping) in Olex2 software,[142] and refined with the XL refinement[143] package using Least Squares minimization and SHELX-97 package. The hydrogen atoms were calculated to their idealized positions with isotropic temperature factors

(1.2 or 1.5 times the C temperature factor) and refined as riding atoms, except OH hydrogen atoms, which were located from the electron density map and restrained using DFIX 0.82. One of the carboxylic acid groups was disordered (C80, O11, O12; site occupancies 0.68:0.32) and OH of the less occupied site was calculated to the idealized position on O12B. OH on O6 was disordered over two positions H6:H5 (0.5:0.5). Two of the dodecyl chains were modelled as disordered over two positions: C29-C32 with site occupancies of 0.78:0.22, and C65, C68 and C70 with site occupancies of 0.53:0.47. Restrains SADI, DELU and SIMU, and EADP constrain were used, when necessary. Residual electron density (0.84 e $Å^{-3}$) was located at 0.97 Å from C65 causing a B-level alert in checkcif. For C72-C76 vibration perpendicular to chain axis induced elongated ellipsoids and shorter C-C bond lengths than expected, regardless of DFIX 1.54 restrain (B- and C-level errors in checkcif). Three disordered pyridine moieties were located from the electron density with site occupancies N100-C105:N104-C109, 0.5:0.5; N124-C129:N118-C123, 0.63:0.37; N130-C135:N136-C140, 0.73:0.27. The pyridine moieties were restrained using FLAT, SADI, DELU and SIMU, or constrained using AFIX 66 or EADP, when necessary. Building a disorder model for pyridine C112-C117 was attempted but it did not improve the structure. In addition, continuous electron density corresponding approximately to one pyridine moiety was included between layers of **3**. No reasonable disorder model was found for this electron density, and it was removed from the later stage of refinement using solvent mask option in Olex2 (see checkcif). Crystallographic data (excluding structure factors) for the structures have been deposited with the Cambridge Structural Data Center as supplementary publication no. CCDC973532.

5.9 Synchrotron-based X-ray reflectivity, X-ray near-total-reflection fluorescence and grazing incidence X-ray diffraction

Synchrotron-based X-ray reflectivity (XRR), X-ray near-total-reflection fluorescence (XNTRF) and grazing incidence X-ray diffraction (GIXD) of monolayers of **3**, **4**, **5** and **6** were carried out on the

liquid surface spectrometer (LSS) using synchrotron radiation (X-ray energy $E = 13.474$ keV, wavelength $\lambda = 0.9201$ Å) at sector 9ID-C, Advanced Photon Source (APS), Argonne National Laboratory. Solutions of **3**, **4**, **5** and **6** were spread at the water surface and compressed on a Teflon Langmuir trough contained in an airtight canister that was purged with water-saturated helium.[144] The scattering vector (wavevector transfer), **Q**, is defined as $k_f - k_i$, where k_i and k_f represent the wavevectors of the incident and scattered beam, respectively. In reflectivity measurements, the incident angle (α) and the exit angle (β) of the beam with respect to the liquid surface are set equal and the azimuthal angle $\phi_{xy} = 0$ (ϕ_{xy} defined as the in-plane angle between the projection of the exit beam on the liquid surface and the incident plane). The reflectivity, *R*, is a function of the *z*-component of **Q**, Q_z ($Q_z = 4\pi\sin(\alpha)\lambda^{-1}$), and is related to the electron density (ED), $\rho(z)$, across the interface along the *z*-axis along the surface normal.[144] A parameterized multi-slab model using Parratt's recursive method[145] is used to extract the ED from the reflectivity data. The fluorescence measurements are conducted near the critical angle for total reflection, α_c (its corresponding Q_z, denoted as Q_c), using an energy dispersive detector (EDD, silicon drift X-ray detector, Vortex-90EX) that subtended the illuminated surface area with a collimator (angular resolution ~ 1°) in the front end of the probe. Various attenuation levels for the incident beam are used depending on the Q_z-range scanned. For a full Q_z-range scan, where α_i varied from below to above the critical angle, the incident beam is attenuated more (to avoid saturation of the EDD) at α_i greater than α_c as a result of intense scattering of the primary beam from bulk solution. The GIXD is used to determine the two-dimensional (2D) in-plane ordering and correlations in the monolayer.[144] The GIXD measurements were conducted with a vertically mounted position sensitive detector (PSD), as the function of the in-plane component of **Q**, Q_{xy} ($Q_{xy} \sim 4\pi \sin(\phi_{xy} 2^{-1}) \lambda^{-1}$.[144] In this study, the incident angle α was kept at 0.065° that is below the critical angle for total reflection, α_c ($\alpha_c = 0.091°$), which corresponds to a penetration depth of X-ray ~ 50-100 Å normal to the surface. More experimental details can be found elsewhere.[144-146]

5.10 Contact angle

The contact angle was measured using a commercial Krüss EasyDrop optical system (Krüss, GmbH, Germany). 5 µL drops of nanopure water were placed on the strips so as to measure static water contact angle. To ensure reproducibility, the measurements were repeated at 6 different positions of each sample.

5.11 Atomic force microscopy

Solid substrates were imaged by atomic force microscopy in tapping mode using a Multimode 5 instrument (Bruker AXS) equipped with a Nanoscope IIIa controller; MicroMash NSC15 silicon tips were used.

6 Acknowledgements

My heartfelt thank goes to my mentor Prof. Dr. Patrick Shahgaldian. He passed on me the knowledge and the passion for science becoming a key figure in my professional life. He thought me that there is always room for improvement, always a better way. It is thanks to him that I am a better scientist today.

I would like to thank my doctor father Prof. Dr. Wolfgang Meier for the support and the freedom he gave me during my PhD.

I am deeply grateful to the members of my committee, Prof. Dr. Thomas A. Jung and Prof. Dr. Scott J. Dalgarno, for the time and the effort they put in evaluating my thesis. Moreover, I am thankful to Prof. Dr. Thomas A. Jung for the collaboration on structural evaluation of calixarene-based monolayers on solid substrates and for the many challenging scientific discussions.

Sincere thanks go to Prof. Dr. David Vaknin and Dr. Wenjie Wang for the hard work on the structural characterization of calixarene-based monolayers at the air-water interface and for the productive collaboration. I would like to thank the technical support of Dr. Ivan Kuzmenko and William Lindemann.

I am grateful to Dr. Markus Neuburger and Dr. Kaisa Helttunen for their work on crystal structures determination.

I would like to thank the group of Prof. Dr. Uwe Pieles for providing me with constant availability on laboratory facilities and instruments issues.

My special thanks goes to my current and former colleagues. A puzzle is made of many small pieces, each of them playing an important role in the final outcome. Each of you guys is a small piece that deeply contributed to make me feel essential part of a special group.

The financial support from the Swiss Nanoscience Institute (SNI), Swiss National Science Foundation (SNSF) and U.S. Department of Energy, Basic Energy Sciences, Office of Science is gratefully acknowledged.

I would not be here writing my thesis without my parents and without the most extraordinary person I have ever met in my life, Olesia. Thank you for your love.

7 References

1. Steed, J. W.; Atwood, J. L.; Gale, P. A., Definition and Emergence of Supramolecular Chemistry. In *Supramolecular Chemistry: From Molecules to Nanomaterials*; John Wiley & Sons, Ltd: 2012.
2. Lehn, J.-M. Supramolecular Chemistry—Scope and Perspectives Molecules, Supermolecules, and Molecular Devices (Nobel Lecture). *Angew. Chem. Int. Ed. Engl.* **1988,** *27*, 89-112.
3. Izatt, R. M. Charles J. Pedersen: Innovator in macrocyclic chemistry and co-recipient of the 1987 Nobel Prize in chemistry. *Chem. Soc. Rev.* **2007,** *36*, 143-147.
4. Dyadin, Y. A.; Terekhova, I. S.; Rodionova, T. V.; Soldatov, D. V. Half-century history of clathrate chemistry. *J. Struct. Chem.* **1999,** *40*, 645-653.
5. Fischer, E. Einfluss der Configuration auf die Wirkung der Enzyme. *Ber.* **1894,** *27*, 2985-2993.
6. Kaufmann, G. B., *Alfred Werner: Founder of Coordination Chemistry*. Springer Verlag: Berlin and New York, 1966.
7. Lehn, J.-M. Toward complex matter: Supramolecular chemistry and self-organization. *Proc. Natl. Acad. Sci. U.S.A.* **2002,** *99*, 4763-4768.
8. Ercolani, G. Physical Basis of Self-Assembly Macrocyclizations. *J. Phys. Chem. B* **1998,** *102*, 5699-5703.
9. Whitesides, G. M.; Grzybowski, B. Self-Assembly at All Scales. *Science* **2002,** *295*, 2418-2421.
10. Geer, M. F.; Shimizu, L. S., Self-Assembly and Self-Organization. In *Supramolecular Chemistry: From Molecules to Nanomaterials*; John Wiley & Sons, Ltd: 2012.
11. Philp, D.; Stoddart, J. F. Self-Assembly in Natural and Unnatural Systems. *Angew. Chem. Int. Ed. Engl.* **1996,** *35*, 1154-1196.
12. Klug, A. From Macromolecules to Biological Assemblies (Nobel Lecture). *Angew. Chem. Int. Ed. Engl.* **1983,** *22*, 565-582.
13. Chakrabarty, R.; Mukherjee, P. S.; Stang, P. J. Supramolecular Coordination: Self-Assembly of Finite Two- and Three-Dimensional Ensembles. *Chem. Rev.* **2011,** *111*, 6810-6918.
14. Meissner, R. S.; Rebek, J.; de Mendoza, J. Autoencapsulation Through Intermolecular Forces: A Synthetic Self-Assembling Spherical Complex. *Science* **1995,** *270*, 1485-1488.
15. Meissner, R.; Garcias, X.; Mecozzi, S.; Rebek, J. Synthesis and Assembly of New Molecular Hosts: Solvation and the Energetics of Encapsulation. *J. Am. Chem. Soc.* **1997,** *119*, 77-85.
16. Rebek, J. Reversible Encapsulation and Its Consequences in Solution. *Acc. Chem. Res.* **1999,** *32*, 278-286.
17. Szabo, T.; Hilmersson, G.; Rebek, J. Dynamics of Assembly and Guest Exchange in the Tennis Ball. *J. Am. Chem. Soc.* **1998,** *120*, 6193-6194.
18. Dalgarno, S. J.; Thallapally, P. K.; Barbour, L. J.; Atwood, J. L. Engineering void space in organic van der Waals crystals: calixarenes lead the way. *Chem. Soc. Rev.* **2007,** *36*, 236-245.
19. MacGillivray, L. R.; Atwood, J. L. A chiral spherical molecular assembly held together by 60 hydrogen bonds. *Nature* **1997,** *389*, 469-472.

20. Gellert, M.; Lipsett, M. N.; Davies, D. R. Helix Formation by Guanylic Acid. *Proc. Natl. Acad. Sci. U. S. A.* **1962,** *48*, 2013-2018.

21. Davis, J. T.; Spada, G. P. Supramolecular architectures generated by self-assembly of guanosine derivatives. *Chem. Soc. Rev.* **2007,** *36*, 296-313.

22. Rivera-Sánchez, M. d. C.; Andújar-de-Sanctis, I.; García-Arriaga, M.; Gubala, V.; Hobley, G.; Rivera, J. M. Walking a Supramolecular Tightrope: A Self-Assembled Dodecamer from an 8-Aryl-2′-deoxyguanosine Derivative. *J. Am. Chem. Soc.* **2009,** *131*, 10403-10405.

23. Palmer, L. C.; Stupp, S. I. Molecular Self-Assembly into One-Dimensional Nanostructures. *Acc. Chem. Res.* **2008,** *41*, 1674-1684.

24. Zubarev, E. R.; Pralle, M. U.; Sone, E. D.; Stupp, S. I. Self-Assembly of Dendron Rodcoil Molecules into Nanoribbons. *J. Am. Chem. Soc.* **2001,** *123*, 4105-4106.

25. Butler, H., *Poucher's Perfumes, Cosmetics and Soaps*. Springer Netherlands: 2000.

26. Toedt, J.; Koza, D.; Van Cleef-Toedt, K., *Chemical Composition of Everyday Products*. Greenwood Press: 2005.

27. Whitesides, G. M.; Boncheva, M. Beyond molecules: Self-assembly of mesoscopic and macroscopic components. *Proc. Natl. Acad. Sci. U. S. A.* **2002,** *99*, 4769-4774.

28. Kellermann, M.; Bauer, W.; Hirsch, A.; Schade, B.; Ludwig, K.; Böttcher, C. The First Account of a Structurally Persistent Micelle. *Angew. Chem. Int. Ed.* **2004,** *43*, 2959-2962.

29. Romsted, L. S., Introduction to Surfactant Self-Assembly. In *Supramol Chem*; John Wiley & Sons, Ltd: 2012.

30. Lowik, D. W. P. M.; van Hest, J. C. M. Peptide based amphiphiles. *Chem. Soc. Rev.* **2004,** *33*, 234-245.

31. Ulijn, R. V.; Smith, A. M. Designing peptide based nanomaterials. *Chem. Soc. Rev.* **2008,** *37*, 664-675.

32. Li, L.-s.; Stupp, S. I. One-Dimensional Assembly of Lipophilic Inorganic Nanoparticles Templated by Peptide-Based Nanofibers with Binding Functionalities. *Angew. Chem. Int. Ed.* **2005,** *44*, 1833-1836.

33. Zhao, X.; Pan, F.; Xu, H.; Yaseen, M.; Shan, H.; Hauser, C. A. E.; Zhang, S.; Lu, J. R. Molecular self-assembly and applications of designer peptide amphiphiles. *Chem. Soc. Rev.* **2010,** *39*, 3480-3498.

34. Li, L.-s.; Jiang, H.; Messmore, B. W.; Bull, S. R.; Stupp, S. I. A Torsional Strain Mechanism To Tune Pitch in Supramolecular Helices. *Angew. Chem. Int. Ed.* **2007,** *46*, 5873-5876.

35. Egli, S.; Nussbaumer, M. G.; Balasubramanian, V.; Chami, M.; Bruns, N.; Palivan, C.; Meier, W. Biocompatible functionalization of polymersome surfaces: a new approach to surface immobilization and cell targeting using polymersomes. *J. Am. Chem. Soc.* **2011,** *133*, 4476-83.

36. Boerakker, M. J.; Hannink, J. M.; Bomans, P. H. H.; Frederik, P. M.; Nolte, R. J. M.; Meijer, E. M.; Sommerdijk, N. A. J. M. Giant Amphiphiles by Cofactor Reconstitution. *Angew. Chem. Int. Ed.* **2002,** *41*, 4239-4241.

37. Velonia, K.; Rowan, A. E.; Nolte, R. J. M. Lipase Polystyrene Giant Amphiphiles. *J. Am. Chem. Soc.* **2002,** *124*, 4224-4225.

38. Le Droumaguet, B.; Mantovani, G.; Haddleton, D. M.; Velonia, K. Formation of giant amphiphiles by post-functionalization of hydrophilic protein-polymer conjugates. *J. Mater. Chem.* **2007,** *17*, 1916-1922.

39. Reynhout, I. C.; Cornelissen, J. J. L. M.; Nolte, R. J. M. Synthesis of Polymer−Biohybrids: From Small to Giant Surfactants. *Acc. Chem. Res.* **2009,** *42*, 681-692.

40. Hannink, J. M.; Cornelissen, J. J. L. M.; Farrera, J. A.; Foubert, P.; De Schryver, F. C.; Sommerdijk, N. A. J. M.; Nolte, R. J. M. Protein–Polymer Hybrid Amphiphiles. *Angew. Chem. Int. Ed.* **2001,** *40*, 4732-4734.

41. Kang, Y.; Liu, K.; Zhang, X. Supra-Amphiphiles: A New Bridge Between Colloidal Science and Supramolecular Chemistry. *Langmuir* **2014,** *30*, 5989-6001.

42. Liu, K.; Yao, Y.; Wang, C.; Liu, Y.; Li, Z.; Zhang, X. From Bola-amphiphiles to Supra-amphiphiles: The Transformation from Two-Dimensional Nanosheets into One-Dimensional Nanofibers with Tunable-Packing Fashion of n-Type Chromophores. *Chem. Eur. J.* **2012,** *18*, 8622-8628.

43. Li, F.; Song, Q.; Yang, L.; Wu, G.; Zhang, X. Supra-amphiphiles formed by complexation of azulene-based amphiphiles and pyrene in aqueous solution: from cylindrical micelles to disklike nanosheets. *Chem. Commun.* **2013,** *49*, 1808-1810.

44. Chi, X.; Ji, X.; Xia, D.; Huang, F. A Dual-Responsive Supra-Amphiphilic Polypseudorotaxane Constructed from a Water-Soluble Pillar[7]arene and an Azobenzene-Containing Random Copolymer. *J. Am. Chem. Soc.* **2015,** *137*, 1440-1443.

45. Wang, C.; Wang, Z.; Zhang, X. Amphiphilic Building Blocks for Self-Assembly: From Amphiphiles to Supra-amphiphiles. *Acc. Chem. Res.* **2012,** *45*, 608-618.

46. Wang, C.; Yin, S.; Chen, S.; Xu, H.; Wang, Z.; Zhang, X. Controlled Self-Assembly Manipulated by Charge-Transfer Interactions: From Tubes to Vesicles. *Angew. Chem. Int. Ed.* **2008,** *47*, 9049-9052.

47. Gutsche, C. D. Calixarenes: An Introduction, 2nd Edition. *Monogr Supramol Chem* **2008**, 1-276.

48. Gutsche, C. D.; Muthukrishnan, R. Calixarenes. 1. Analysis of the product mixtures produced by the base-catalyzed condensation of formaldehyde with para-substituted phenols. *J. Org. Chem.* **1978,** *43*, 4905-4906.

49. Mandolini, L.; Ungaro, R., *Calixarenes in action*. Imperial College Press: London, 2000.

50. Asfari, Z.; Böhmer, V.; Harrowfield, J.; Vicens, J., *Calixarenes 2001*. Kluwer Academic Publishers: Dordrecht ; Boston, 2001.

51. Vicens, J.; Baklouit, L.; Harrowfield, J., *Calixarenes in the Nanoworld*. Springer Netherlands: 2006.

52. Baldini, L.; Sansone, F.; Casnati, A.; Ungaro, R., Calixarenes in Molecular Recognition. In *Supramolecular Chemistry: From Molecules to Nanomaterials*; John Wiley & Sons, Ltd: 2012.

53. Helttunen, K.; Shahgaldian, P. Self-assembly of amphiphilic calixarenes and resorcinarenes in water. *New J. Chem.* **2010,** *34*, 2704-2714.

54. Shahgaldian, P.; Coleman, A. W.; Kalchenko, V. I. Synthesis and properties of novel amphiphilic calix-[4]-arene derivatives. *Tetrahedron Lett.* **2001,** *42*, 577-579.

55. Gutsche, C. D.; Pagoria, P. F. Calixarenes. 16. Functionalized calixarenes: the direct substitution route. *J. Org. Chem.* **1985,** *50*, 5795-5802.

56. Gutsche, C. D.; Dhawan, B.; Levine, J. A.; Hyun No, K.; Bauer, L. J. Calixarenes 9 : Conformational isomers of the ethers and esters of calix[4]arenes. *Tetrahedron* **1983,** *39*, 409-426.

57. Iwamoto, K.; Araki, K.; Shinkai, S. Syntheses of all possible conformational isomers of O-alkyl-p-t-butylcalix[4]arenes. *Tetrahedron* **1991,** *47*, 4325-4342.

58. Groenen, L. C.; Ruël, B. H. M.; Casnati, A.; Timmerman, P.; Verboom, W.; Harkema, S.; Pochini, A.; Ungaro, R.; Reinhoudt, D. N. syn-1,2-dialkylated calix[4]arenes : general intermediates in the NaH/DMF tetraalkylation of calix[4]arenes. *Tetrahedron Lett.* **1991,** *32*, 2675-2678.

59. Shinkai, S.; Araki, K.; Tsubaki, T.; Arimura, T.; Manabe, O. New syntheses of calixarene-p-sulphonates and p-nitrocalixarenes. *J. Chem. Soc., Perkin Trans. 1* **1987**, 2297-2299.

60. Dondoni, A.; Marra, A.; Scherrmann, M.-C.; Casnati, A.; Sansone, F.; Ungaro, R. Synthesis and Properties of O-Glycosyl Calix[4]Arenes (Calixsugars). *Chem. Eur. J.* **1997,** *3*, 1774-1782.

61. Düker, M. H.; Gómez, R.; Vande Velde, C. M. L.; Azov, V. A. Upper rim tetrathiafulvalene-bridged calix[4]arenes. *Tetrahedron Lett.* **2011,** *52*, 2881-2884.

62. Almi, M.; Arduini, A.; Casnati, A.; Pochini, A.; Ungaro, R. Chloromethylation of calixarenes and synthesis of new water soluble macrocyclic hosts. *Tetrahedron* **1989,** *45*, 2177-2182.

63. Markowitz, M. A.; Bielski, R.; Regen, S. L. Perforated monolayers: porous and cohesive monolayers from mercurated calix[6]arenes. *J. Am. Chem. Soc.* **1988,** *110*, 7545-7546.

64. Nakamoto, Y.; Kallinowski, G.; Boehmer, V.; Vogt, W. Langmuir monolayers of p-octadecylcalix[4]arene. *Langmuir* **1989,** *5*, 1116-1117.

65. Shahgaldian, P.; Coleman, A. W. Miscibility Studies on Amphiphilic Calix[4]arene−Natural Phospholipid Mixed Films. *Langmuir* **2003,** *19*, 5261-5265.

66. He, W.; Vollhardt, D.; Rudert, R.; Zhu, L.; Li, J. Phase Transition and Domain Morphology in Langmuir Monolayers of a Calix[4]arene Derivative Containing No Alkyl Chain. *Langmuir* **2003,** *19*, 385-392.

67. Strobel, M.; Kita-Tokarczyk, K.; Taubert, A.; Vebert, C.; Heiney, P. A.; Chami, M.; Meier, W. Self-Assembly of Amphiphilic Calix[4]arenes in Aqueous Solution. *Adv. Funct. Mater.* **2006,** *16*, 252-259.

68. Van der Heyden, A.; Regnouf-de-Vains, J.-B.; Warszyński, P.; Dalbavie, J.-O.; Żywociński, A.; Rogalska, E. Probing Inter- and Intramolecular Interactions of Six New p-tert-Butylcalix[4]arene-Based Bipyridyl Podands with Langmuir Monolayers. *Langmuir* **2002,** *18*, 8854-8861.

69. Vollhardt, D.; Gloede, J.; Weidemann, G.; Rudert, R. Characteristic features of amphiphilic p-functionalized calixarene monolayers at the air/water interface. *Langmuir* **2003,** *19*, 4228-4234.

70. Moridi, N.; Elend, D.; Danylyuk, O.; Suwinska, K.; Shahgaldian, P. Amidophenol-Modified Amphiphilic Calixarenes: Synthesis, Interfacial Self-Assembly, and Acetaminophen Crystal Nucleation Properties. *Langmuir* **2011,** *27*, 9116-9121.

71. Shahgaldian, P.; Cesario, M.; Goreloff, P.; Coleman, A. W. Para-acyl calix[4]arenes: amphiphilic self-assembly from the molecular to the mesoscopic level. *Chem. Commun.* **2002**, 326-327.

72. Lonetti, B.; Lo Nostro, P.; Ninham, B. W.; Baglioni, P. Anion effects on calixarene monolayers: A Hofmeister series study. *Langmuir* **2005,** *21*, 2242-2249.

73. Capuzzi, G.; Fratini, E.; Dei, L.; LoNostro, P.; Casnati, A.; Gilles, R.; Baglioni, P. Counterion complexation of calixarene ligands in monolayers and micellar solutions. *Colloid Surface A* **2000,** *167*, 105-113.

74. Supian, F. L.; Richardson, T. H.; Deasy, M.; Kelleher, F.; Ward, J. P.; McKee, V. Interaction between Langmuir and Langmuir-Blodgett Films of Two Calix[4]arenes with Aqueous Copper and Lithium Ions. *Langmuir* **2010,** *26*, 10906-10912.

75. Houel, E.; Lazar, A.; Da Silva, E.; Coleman, A. W.; Solovyov, A.; Cherenok, S.; Kalchenko, V. I. Interfacial interactions of cations with amphiphilic dihydroxyphosphonyl-calix-[4]-arene mesosystems. *Langmuir* **2002,** *18*, 1374-1379.

76. Korchowiec, B.; Orlof, M.; Sautrey, G.; Ben Salem, A.; Korchowiec, J.; Regnouf-de-Vains, J. B.; Rogalska, E. The Mechanism of Metal Cation Binding in Two Nalidixate Calixarene Conjugates. A Langmuir Film and Molecular Modeling Study. *J. Phys. Chem. B* **2010,** *114*, 10427-10435.

77. Shahgaldian, P.; Pieles, U.; Hegner, M. Enantioselective recognition of phenylalanine by a chiral amphiphilic macrocycle at the air-water interface: A copper-mediated mechanism. *Langmuir* **2005,** *21*, 6503-6507.

78. Sugden, M. W.; Richardson, T. H.; Davis, F.; Higson, S. P. J.; Faul, C. F. J. Langmuir and LB properties of two calix[4]resorcinarenes: Interactions with various analytes. *Colloid Surface A* **2008,** *321*, 43-46.

79. Guo, X.; Lu, G. Y.; Li, Y. Interaction between calix[4]arene derivative bearing adenino units and complementary nucleosides at the air-water interface. *Thin Solid Films* **2004,** *460*, 264-268.

80. Liu, F.; Lu, G. Y.; He, W. J.; Liu, M. H.; Zhu, L. G.; Wu, H. M. Molecular recognition of nucleotides by a calix[4]arene derivative with two alkyl guanidinium groups at the air water interface. *New J. Chem.* **2002,** *26*, 601-606.

81. Weis, M.; Janicek, R.; Cirak, J.; Hianik, T. Study of the calix[4]resorcinarene-dopamine interactions in monolayers by measurement of pressure-area isotherms and Maxwell displacement currents. *J. Phys. Chem. B* **2007,** *111*, 10626-10631.

82. Zadmard, R.; Arendt, M.; Schrader, T. Multipoint recognition of basic proteins at a membrane model. *J. Am. Chem. Soc.* **2004,** *126*, 7752-7753.

83. Zadmard, R.; Schrader, T. Nanomolar protein sensing with embedded receptor molecules. *J. Am. Chem. Soc.* **2005,** *127*, 904-915.

84. Shahgaldian, P.; Sclotti, M. A.; Pieles, U. Amino-substituted amphiphilic calixarenes: Self-assembly and interactions with DNA. *Langmuir* **2008,** *24*, 8522-8526.

85. Rullaud, V.; Moridi, N.; Shahgaldian, P. Sequence-Specific DNA Interactions with Calixarene-Based Langmuir Monolayers. *Langmuir* **2014,** *30*, 8675-8679.

86. Brittain, H. G., *Polymorphism in Pharmaceutical Solids, Second Edition*. Taylor & Francis: 2009.

87. Hilfiker, R.; Blatter, F.; Raumer, M. v., Relevance of Solid-state Properties for Pharmaceutical Products. In *Polymorphism: in the Pharmaceutical Industry*; Wiley-VCH Verlag GmbH & Co. KGaA: 2006; pp 1-19.

88. Bernstein, J., Polymorphism and Patents from a Chemist's Point of View [1]. In *Polymorphism: in the Pharmaceutical Industry*; Wiley-VCH Verlag GmbH & Co. KGaA: 2006; pp 365-384.

89. Bučar, D.-K.; Lancaster, R. W.; Bernstein, J. Disappearing Polymorphs Revisited. *Angew. Chem. Int. Ed.* **2015,** *54*, 6972-6993.

90. Hilfiker, R.; De Paul, S. M.; Szelagiewicz, M., Approaches to Polymorphism Screening. In *Polymorphism: in the Pharmaceutical Industry*; Wiley-VCH Verlag GmbH & Co. KGaA: 2006; pp 287-308.

91. Foster, J. A.; Piepenbrock, M. O. M.; Lloyd, G. O.; Clarke, N.; Howard, J. A. K.; Steed, J. W. Anion-switchable supramolecular gels for controlling pharmaceutical crystal growth. *Nat. Chem.* **2010,** *2*, 1037-1043.

92. Mann, S.; Heywood, B. R.; Rajam, S.; Birchall, J. D. Controlled Crystallization of Caco3 under Stearic-Acid Monolayers. *Nature* **1988,** *334*, 692-695.

93. Mann, S.; Heywood, B. R.; Rajam, S.; Birchall, J. D. Interfacial Control of Nucleation of Calcium-Carbonate under Organized Stearic-Acid Monolayers. *Proc. R. Soc. London A* **1989,** *423*, 457-&.

94. Volkmer, D.; Fricke, M.; Vollhardt, D.; Siegel, S. Crystallization of (012) oriented calcite single crystals underneath monolayers of tetra(carboxymethoxy)calix[4] arenes. *J. Chem. Soc., Dalton Trans.* **2002**, 4547-4554.

95. Volkmer, D.; Fricke, M.; Agena, C.; Mattay, J. Interfacial electrostatics guiding the crystallization of CaCO3 underneath monolayers of calixarenes and resorcarenes. *J. Mater. Chem.* **2004,** *14*, 2249-2259.

96. Brezesinski, G.; Mohwald, H. Langmuir monolayers to study interactions at model membrane surfaces. *Adv. Colloid Interface Sci.* **2003,** *100*, 563-584.

97. Kaganer, V. M.; Mohwald, H.; Dutta, P. Structure and phase transitions in Langmuir monolayers. *Rev. Mod. Phys.* **1999,** *71*, 779-819.

98. Kuzmenko, I.; Rapaport, H.; Kjaer, K.; Als-Nielsen, J.; Weissbuch, I.; Lahav, M.; Leiserowitz, L. Design and Characterization of Crystalline Thin Film Architectures at the Air−Liquid Interface: Simplicity to Complexity. *Chem. Rev.* **2001,** *101*, 1659-1696.

99. Kmetko, J.; Datta, A.; Evmenenko, G.; Dutta, P. The effects of divalent ions on Langmuir monolayer and subphase structure: A grazing-incidence diffraction and Bragg rod study. *J. Phys. Chem. B* **2001,** *105*, 10818-10825.

100. Leveiller, F.; Jacquemain, D.; Lahav, M.; Leiserowitz, L.; Deutsch, M.; Kjaer, K.; Alsnielsen, J. Crystallinity of the Double-Layer of Cadmium Arachidate Films at the Water-Surface. *Science* **1991,** *252*, 1532-1536.

101. Schwartz, D. K.; Garnaes, J.; Viswanathan, R.; Zasadzinski, J. A. N. Surface Order and Stability of Langmuir-Blodgett-Films. *Science* **1992,** *257*, 508-511.

102. Schwartz, D. K. Langmuir-Blodgett film structure. *Surf. Sci. Rep.* **1997,** *27*, 245-334.

103. Ishikawa, Y.; Kunitake, T.; Matsuda, T.; Otsuka, T.; Shinkai, S. Formation of calixarene monolayers which selectively respond to metal ions. *J. Chem. Soc., Chem. Commun.* **1989**, 736-738.

104. LoNostro, P.; Casnati, A.; Bossoletti, L.; Dei, L.; Baglioni, P. Complexation properties of calixarenes in Langmuir films at the water-air interface. *Colloids Surfaces A: Physicochem. Eng. Aspects* **1996,** *116*, 203-209.

105. Shahgaldian, P.; Coleman, A. W. Anion and cation interactions with p-dodecanoylcalix[4]arene monolayers at the air-water interface. *Langmuir* **2001,** *17*, 6851-6854.

106. Govindaraju, T.; Avinash, M. B. Two-dimensional nanoarchitectonics: organic and hybrid materials. *Nanoscale* **2012,** *4*, 6102-6117.

107. Ulman, A. Formation and structure of self-assembled monolayers. *Chem. Rev.* **1996,** *96*, 1533-1554.

108. Love, J. C.; Estroff, L. A.; Kriebel, J. K.; Nuzzo, R. G.; Whitesides, G. M. Self-assembled monolayers of thiolates on metals as a form of nanotechnology. *Chem. Rev.* **2005,** *105*, 1103-1169.

109. Makiura, R.; Konovalov, O. Interfacial growth of large-area single-layer metal-organic framework nanosheets. *Sci. Rep.* **2013,** *3*.

110. Makiura, R.; Motoyama, S.; Umemura, Y.; Yamanaka, H.; Sakata, O.; Kitagawa, H. Surface nano-architecture of a metal-organic framework. *Nat. Mater.* **2010,** *9*, 565-571.

111. Bauer, T.; Zheng, Z. K.; Renn, A.; Enning, R.; Stemmer, A.; Sakamoto, J.; Schluter, A. D. Synthesis of Free-Standing, Monolayered Organometallic Sheets at the Air/Water Interface. *Angew. Chem. Int. Ed.* **2011,** *50*, 7879-7884.

112. Moridi, N.; Danylyuk, O.; Suwinska, K.; Shahgaldian, P. Monolayers of an amphiphilic para-carboxy-calix[4]arene act as templates for the crystallization of acetaminophen. *J. Colloid Interface Sci.* **2012,** *377*, 450-455.

113. Gutsche, C. D.; Dhawan, B.; No, K. H.; Muthukrishnan, R. Calixarenes. 4. The synthesis, characterization, and properties of the calixarenes from p-tert-butylphenol. *J. Am. Chem. Soc.* **1981,** *103*, 3782-3792.

114. Gutsche, C. D.; Levine, J. A. Calixarenes .6. Synthesis of a Functionalizable Calix[4]Arene in a Conformationally Rigid Cone Conformation. *J. Am. Chem. Soc.* **1982,** *104*, 2652-2653.

115. Gutsche, C. D.; Pagoria, P. F. Calixarenes .16. Functionalized Calixarenes - the Direct Substitution Route. *J. Org. Chem.* **1985,** *50*, 5795-5802.

116. Sasine, J. S.; Brewster, R. E.; Caran, K. L.; Bentley, A. M.; Shuker, S. B. Heterodimerization studies of calix[4]arene derivatives in polar solvents. *Org. Lett.* **2006,** *8*, 2913-2915.

117. Kennedy, S.; Teat, S. J.; Dalgarno, S. J. Versatile assembly of p-carboxylatocalix[4]arene-O-alkyl ethers. *Dalton Trans.* **2010,** *39*, 384-387.

118. Vaknin, D.; Dahlke, S.; Travesset, A.; Nizri, G.; Magdassi, S. Induced Crystallization of Polyelectrolyte-Surfactant Complexes at the Gas-Water Interface. *Phys. Rev. Lett.* **2004,** *93*, 218302/1-4.

119. Lee, A. G. The Physical-Chemistry of Lipids - from Alkanes to Phospholipids - Handbook of Lipid Research, Vol 4 - Small,Dm. *Nature* **1987,** *328*, 486-486.

120. Hsu, C. H.; Ke, W. T.; Lin, S. Y. Progressive Steps of Polymorphic Transformation of Gabapentin Polymorphs Studied by Hot-stage FTIR Microspectroscopy. *J. Pharm. Pharmaceut. Sci.* **2010,** *13*, 67-77.

121. Tulli, L. G.; Moridi, N.; Wang, W.; Helttunen, K.; Neuburger, M.; Vaknin, D.; Meier, W.; Shahgaldian, P. Polymorphism control of an active pharmaceutical ingredient beneath calixarene-based Langmuir monolayers. *Chem. Commun.* **2014,** *50*, 3938-3940.

122. Ye, B. H.; Tong, M. L.; Chen, X. M. Metal-organic molecular architectures with 2.2 '-bipyridyl-like and carboxylate ligands. *Coord. Chem. Rev.* **2005,** *249*, 545-565.

123. Plater, M. J.; Foreman, M. R. S.; Howie, R. A.; Skakle, J. M. S.; Slawin, A. M. Z. Hydrothermal synthesis of polymeric metal carboxylates from benzene-1,2,4,5-tetracarboxylic acid and benzene-1,2,4-tricarboxylic acid. *Inorg. Chim. Acta* **2001,** *315*, 126-132.

124. Eremenko, I. L.; Nefedov, S. E.; Sidorov, A. A.; Golubnichaya, M. A.; Danilov, P. V.; Ikorskii, V. N.; Shvedenkov, Y. G.; Novotortsev, V. M.; Moiseev, I. I. Bi- and mononuclear nickel(II) trimethylacetate complexes with pyridine bases as ligands. *Inorg. Chem.* **1999,** *38*, 3764-3773.

125. Liu, G. F.; Ye, B. H.; Ling, Y. H.; Chen, X. M. Interlocking of molecular rhombi into a 2D polyrotaxane network via pi-pi interactions. Crystal structure of [Cu-2(bpa)(2)(phen)(2)(H2O)](2)center dot 2H(2)O (bpa(2-) = biphenyl-4,4 '-dicarboxylate, phen=1,10-phenanthroline). *Chem. Commun.* **2002**, 1442-1443.

126. Gonzalez-Delgado, A. M.; Giner-Casares, J. J.; Brezesinski, G.; Regnouf-de-Vains, J. B.; Camacho, L. Langmuir Monolayers of an Inclusion Complex Formed by a New Calixarene Derivative and Fullerene. *Langmuir* **2012,** *28*, 12114-12121.

127. Shahgaldian, P.; Coleman, A. W.; Kuduva, S. S.; Zaworotko, M. J. Amphiphilic behavior of an apparently non-polar calixarene. *Chem. Commun.* **2005**, 1968-70.

128. Tulli, L. G.; Wang, W.; Lindemann, W. R.; Kuzmenko, I.; Meier, W.; Vaknin, D.; Shahgaldian, P. Interfacial binding of divalent cations to calixarene-based Langmuir monolayers. *Langmuir* **2015,** *31*, 2351-9.

129. Tulli, L. G.; Wang, W.; Rullaud, V.; Lindemann, W. R.; Kuzmenko, I.; Vaknin, D.; Shahgaldian, P. *submitted*.

130. Delaigue, X.; Harrowfield, J. M.; Hosseini, M. W.; De Cian, A.; Fischer, J.; Kyritsakas, N. Exoditopic receptors I: synthesis and structural studies on p-tert-butyltetramercaptocalix[4]arene and its mercury complexes. *J. Chem. Soc., Chem. Commun.* **1994**, 1579-1580.

131. Dondoni, A.; Marra, A.; Scherrmann, M. C.; Casnati, A.; Sansone, F.; Ungaro, R. Synthesis and properties of O-glycosyl calix[4]arenes (calixsugars). *Chem. Eur. J.* **1997,** *3*, 1774-1782.

132. Sansone, F.; Barboso, S.; Casnati, A.; Fabbi, M.; Pochini, A.; Ugozzoli, F.; Ungaro, R. Synthesis and structure of chiral cone calix[4]arenes functionalized at the upper rim with L-alanine units. *Eur. J. Org. Chem.* **1998**, 897-905.

133. Vollhardt, D.; Fainerman, V. B.; Siegel, S. Thermodynamic and textural characterization of DPPG phospholipid monolayers. *J. Phys. Chem. B* **2000,** *104*, 4115-4121.

134. Johann, R.; Symietz, C.; Vollhardt, D.; Brezesinski, G.; Mohwald, H. Influence of cholesterol on domain shape and lattice structure in arachidic acid monolayers at high pH. *J. Phys. Chem. B* **2000,** *104*, 8512-8517.

135. Caldwell, W. B.; Campbell, D. J.; Chen, K. M.; Herr, B. R.; Mirkin, C. A.; Malik, A.; Durbin, M. K.; Dutta, P.; Huang, K. G. A Highly Ordered Self-Assembled Monolayer Film of an Azobenzenealkanethiol on Au(111) - Electrochemical Properties and Structural Characterization by Synchrotron in-Plane X-Ray-Diffraction, Atomic-Force Microscopy, and Surface-Enhanced Raman-Spectroscopy. *J. Am. Chem. Soc.* **1995,** *117*, 6071-6082.

136. Stine, K. J., Brewster Angle Microscopy. In *Supramolecular Chemistry: From Molecules to Nanomaterials*; Gale, P. A.; Steed, J. W., Eds. John Wiley & Sons, Ltd: 2012.

137. Wasserman, S. R.; Whitesides, G. M.; Tidswell, I. M.; Ocko, B. M.; Pershan, P. S.; Axe, J. D. The Structure of Self-Assembled Monolayers of Alkylsiloxanes on Silicon - a Comparison of Results from Ellipsometry and Low-Angle X-Ray Reflectivity. *J. Am. Chem. Soc.* **1989,** *111*, 5852-5861.

138. Wang, Y. L.; Lieberman, M. Growth of ultrasmooth octadecyltrichlorosilane self-assembled monolayers on SiO2. *Langmuir* **2003,** *19*, 1159-1167.

139. Li, J. W.; Janout, V.; Regen, S. L. Gluing Langmuir-Blodgett monolayers onto hydrocarbon surfaces. *J. Am. Chem. Soc.* **2006,** *128*, 682-683.

140. Duker, M. H.; Gomez, R.; Velde, C. M. L. V.; Azov, V. A. Upper rim tetrathiafulvalene-bridged calix[4]arenes. *Tetrahedron Lett.* **2011,** *52*, 2881-2884.

141. Apex 2: Version 2 User Manual, M86-E01078. *Bruker Analytical X-ray Systems* **2006**.

142. Dolomanov, O. V.; Bourhis, L. J.; Gildea, R. J.; Howard, J. A. K.; Puschmann, H. OLEX2: a complete structure solution, refinement and analysis program. *J. Appl. Cryst.* **2009,** *42*, 339-341.

143. Sheldrick, G. M. A short history of SHELX. *Acta Crystallogr., Sect. A: Found. Crystallogr.* **2008,** *64*, 112-122.

144. Vaknin, D., X-Ray Diffraction and Spectroscopic Techniques for Liquid Surfaces and Interfaces. In *Characterization of Materials*; John Wiley & Sons, Inc.: 2002.

145. Als-Nielsen, J.; McMorrow, D., Refraction and reflection from interfaces. In *Elements of Modern X-ray Physics*; John Wiley & Sons: 2011; pp 69-112.

146. Wang, W.; Murthy, N. S.; Kuzmenko, I.; Anderson, N. A.; Vaknin, D. Structure of Biodegradable Films at Aqueous Surfaces: X-ray Diffraction and Spectroscopy Studies of Polylactides and Tyrosine-Derived Polycarbonates. *Langmuir* **2013,** *29*, 11420-11430.